Sonogenetic stimulation for vision restoration.

Sara Cadoni

THÈSE DE DOCTORAT DE SORBONNE UNIVERSITÉ

Spécialité: Neurosciences

École Doctorale Cerveau Cognition Comportement

---

realisée

à l'Institut de la Vision - Département: Transmission de l'information visuelle

presentée par

SARA CADONI

SONOGENETIC STIMULATION FOR VISION RESTORATION

Membres du Jury:

Serge Picaud (Directeur de Thèse)
Emilie Franceschini (Rapportrice)
Botond Roska (Rapporteur)
Marie Vidailhet
Mickael Tanter
Charlie Demené

19 Novembre 2020

ABSTRACT

A current challenge for neuroscience is the development of new brain machine interfaces for various neurological diseases and sensory restoration requiring a high spatiotemporal resolution. In the case of visual restoration at the cortical level, visual prostheses generating direct cortical stimulations have proved able to elicit some form vision in blind patients but only for few months. Penetrating electrodes were found to require smaller currents for a higher spatial resolution but at the cost of invasiveness. Ultrasound (US) waves are well known for imaging purposes but can also be used to modulate neural activity. However, they suffer from a major drawback: higher spatial resolution requires greater acoustic intensity and causes potential side effects such as heating. To overcome this disadvantage, a recently developed strategy, *Sonogenetic Therapy*, has been proposed to increase neuronal sensitivity to US stimulation by expressing US sensitive proteins on cell membrane. Unfortunately, all *in vivo* attempts have, to date, failed to provide a high spatiotemporal resolution.

The objective of this thesis is to investigate the potential of Sonogenetics as a neuro-stimulation strategy for vision restoration. In this work we identified a mechano-sensitive ion channel that can be expressed efficiently in retinal ganglion cells and in neurons of the visual cortex thanks to AAV viral vector gene delivery. The bacterial MscL channel (Mechano-sensitive channel of large conductance) opens rapidly when mechanical stress is applied to the cell membrane and is therefore likely to open in response to the cell membrane's mechanical deformation induced by US pressure waves. Efficacy of the ultrasound activation has been investigated on the isolated rat retina. Optimal US stimulation parameters have been identified for the direct depolarization of MscL expressing retinal ganglion cells showing precise spatio-temporal features. We then expressed the same channel in neurons of the primary visual cortex to determine whether high frequency US was able to depolarize those cells *in vivo*. When neurons expressed the MscL channel, US was again able to directly activate neurons with the same spatio-temporal kinetics as retinal ganglion cells. We were able to target tiny

cortical areas (0.35 mm^2) providing a resolution of at least 0.4 mm. According to our thermal model, the temperature increase associated with the used acoustic parameters is negligible, indicating the safety of the technique. No US-evoked response was detected in cortical neurons from non-transfected animals. These results provide the proof of concept that this sonogenetic strategy offers a potential tool with adequate spatio-temporal resolution for vision restoration at the cortical level. Moreover, this strategy will likely spur the developement of a new form of brain machine interfaces to treat a wide range of neurological disorders.

Keywords: Ultrasound, Vision, Brain, Cortex, Retina, Brain-machine interface.

RESUMÉ

Un défi majeur des Neurosciences est le développement d'une interface cerveau-machine efficace pour diverses maladies neurologiques et la restauration sensorielle. Dans le cas de la restauration visuelle, des prothèses stimulant électriquement les aires visuelles corticales ont démontré chez les patients aveugles la possibilité de voir des formes mais uniquement pendant quelques mois. L'utilisation d'électrodes pénétrantes pour la stimulation permet d'obtenir une résolution spatiale plus élevée avec une injection de courant plus faible, mais cette stratégie devient très invasive. Les ondes ultrasonores sont bien connues pour leur application en imagerie mais peuvent également être utilisées pour moduler l'activité neurale de manière non invasive. Cependant, elles présentent un inconvénient majeur : il n'est pas possible d'obtenir une résolution spatiale élevée sans augmenter l'intensité acoustique et provoquer d'éventuels effets secondaires comme l'échauffement des tissus ciblés. Pour remédier à cet inconvénient, une stratégie récente appelée *Thérapie Sonogénétique* a été proposée pour augmenter la sensibilité neuronale à la stimulation ultrasonore en exprimant des protéines sensibles aux ultrasons. Malheureusement, toutes les tentatives d'appliquer cette stratégie in vivo n'ont pas permis, pour le moment, d'obtenir une résolution spatiotemporelle élevée.

L'objectif de cette thèse est d'étudier le potentiel de la sonogénétique comme stratégie de neurostimulation pour la restauration visuelle. Dans ce travail, nous avons identifié un canal ionique mécano-sensible qui peut s'exprimer efficacement dans les cellules ganglionnaires de la rétine et dans les neurones du cortex visuel par le biais d'une thérapie génique utilisant des vecteurs viraux AAV. Le canal bactérien MscL (canal mécanosensible de grande conductance) s'ouvre rapidement lorsqu'une tension mécanique est appliquée à la membrane cellulaire et est donc susceptible de s'ouvrir également en cas de déformation mécanique de la membrane cellulaire induite par des ondes de pression ultrasonores. L'efficacité de la stimulation ultrasonore a été explorée sur des rétines *ex vivo*. Les paramètres optimaux de la stimulation ultrasonore ont été définis pour induire une dépolarisation des cellules ganglionnaires de la rétine exprimant

le canal MscL avec une grande précision spatiotemporelle. Nous avons ensuite exprimé le même canal dans les neurones du cortex visuel primaire afin de déterminer si des ondes ultrasonores à haute fréquence étaient susceptibles de dépolariser directement les neurones corticaux. Lorsque les neurones corticaux exprimaient le canal MscL, les ultrasons étaient capables d'activer directement les neurones avec une cinétique temporelle à la milliseconde. De plus, il était possible de cibler de très petites zones corticales ($0,35$ mm^2) procurant ainsi une résolution d'au moins $0,4$ mm. De plus, selon notre modèle thermique, l'augmentation de température associée aux paramètres acoustiques utilisés est négligeable, ce qui indique la sécurité de la stimulation. Aucune réponse ultrasonore n'a été détectée dans les neurones corticaux d'animaux non transfectés. Ces résultats apportent la preuve que la stratégie sonogénétique proposée offre une résolution spatio-temporelle adéquate pour la restauration de la vision au niveau cortical. De plus, cette stratégie ouvre de nouvelles perspectives pour développer une nouvelle forme d'interface cerveau-machine et traiter un large éventail de troubles neurologiques.

Mots clés : Ultrasons, Vision, Cortex, Rétine, Interface cerveau machine

CONTENTS

LIST OF FIGURES

LIST OF TABLES

ACRONYMS

US Ultrasound

LGN Lateral Geniculate Nucleus

SC Superior Colliculus

V1 Primary Visual Cortex

ONL Outer Nuclear Layer

INL Inner Nuclear Layer

GCL Ganglion Cell Layer

OPL Outer Plexiform Layer

IPL Inner Plexiform Layer

RGCs Retinal Ganglion Cells

RPE Retinal Pigment Epithelium

AMD Age-related Macular Degeneration

RDs Retinal Distrophies

DR Diabetic retinopathy

LCA Leber Congential Amaurosis

AAVs Adeno-Associated Virus

TI Thermal Index

MI Mechanical Index

ARF Acoustic Radiation Force

BBB Blood-Brain Barrier

MscL Mechano-sensitive channel of Large conductance

MscS Mechano-sensitive channel of Small conductance

MS Mechano-Sensitive

WT Wild-Type

Part I

Introduction
Ultrasound waves for vision restoration

1

INTRODUCTION

FOREWORDS

Ultrasound (US) represents today one of the world's leading medical imaging techniques, on account of its non-invasiveness and ability to penetrate deep into tissue while retaining spatial and temporal coherence. US can also be used for other therapeutic purposes, such as neural stimulation. Ultrasonic stimulation appears as a promising strategy for direct stimulation of the visual cortex in the context of vision restoration. The coupling of gene therapy for expressing ultrasound-sensitive actuators on neurons with US stimulation, in other words *Sonogenetics*, might be even more effective in reaching high-quality vision restoration.

The aim of this introduction is to provide an overview of the visual system, related blinding diseases and the state of the art of existing vision restoration techniques. There follows a brief description of medical ultrasound: physics, bio-effects and applications like US neuromodulation. Next, the concept of Sonogenetics is presented with an overview of the mechano-sensitive ion channels that can be used for this purpose.

1.1 THE VISUAL SYSTEM

1.1.1 *General structure*

The visual system has the incredible task of converting the light that is reflected by the objects that surround us into visual perception. This task starts in the eye, the sensory organ of the visual system, where photons are converted into electrical potentials in the retina, and ends in the brain, in the visual cortex, where the information is further processed and sent to other areas of our brain to build the perception of the outer world.

The main components of the visual system of mammals are outlined in Figure 1. Briefly, visual information passes from

the eyes via the optic nerve to the lateral geniculate nucleus and the superior colliculus and from there to the visual cortex. In primates, the visual field of each eye overlaps and the half of each retina receives information about the right and left visual field. At the optic chiasm, the axons arriving from the eye decussate and projections coming from each nasal hemi-retina are sent to the contro-lateral hemisphere: information from the right visual field projects to the left cortex and vice versa (Prasad and Galetta, 2011).

The perception of visual space starts from the sensory organ that interfaces with the outside world, the eye. The outermost layer of the eye is the sclera (Figure 2); this includes the cornea, which is located in the frontal part of the eye and allows the light to enter inside the eye. Under the sclera, the choroid is found where all the vessels that supply all the structures of the eye are regrouped. The iris, in the frontal portion of the eye, controls the aperture of the pupil through which passes the light. After entering through the cornea and the iris, the lens refracts the incident light through the vitreous humor into a small image and projects it into the retina that lines the back of the eye. The retina has then the role of transducing the image of the visual field into electrical pulses and to perform the first stages of image processing before sending these inputs to the visual centres in the brain where they will be further processed (Tovée, 2008). Further details on how retina is organized, how it converts light into electrical pulses and pre-processes this information before sending it to the brain are given in subsubsection 1.1.1.1.

The retina sends the information of the visual scene through the optic nerve to the brain. The fibres of the optic nerve come together and decussate in the optic chiasm where they branch and terminate in different subcortical structures in the brain that process and transmit different information and features about the visual space (e. g. location, color or motion) and other information that does not play a direct role in image formation but supports sight indirectly (e. g. pupil reflexes) or acts in other physiological functions that are modulated by light, such as the circadian rhythms. Almost 90 % of nerve fibres coming from the eye end in the Lateral Geniculate Nucleus (LGN) in the thalamus, which pre-processes the information coming from the retina before sending it to the primary visual cortex. Other nerve fibres branch to the Superior Colliculus (SC) in the mid brain, which is

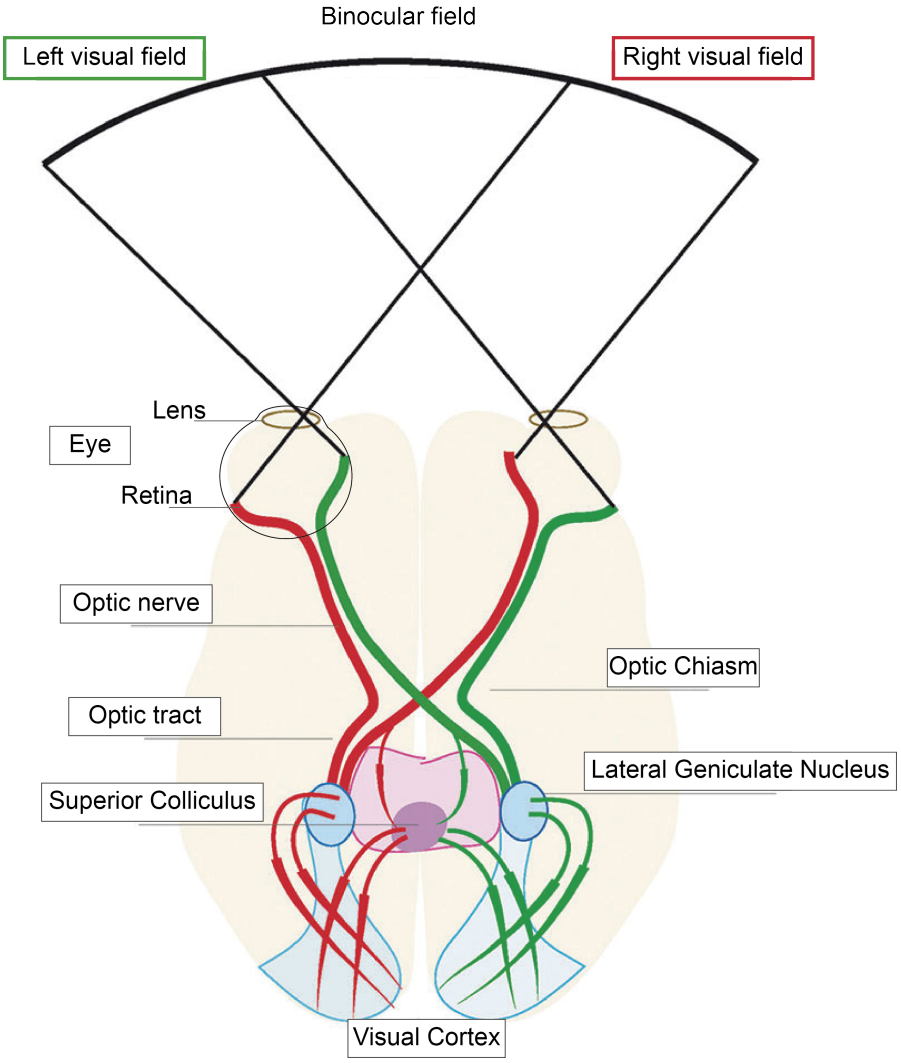

Figure 1: **Simplified diagram of the primate visual pathway.**The visual cortex of each hemisphere receives inputs from the superior collicus and the later geniculate nucleus. These two structures receive visual information from the retina in the eye. The left halves of each retina (red) receive visual information about the right visual field, while the right halves of the retinas (green) receive information about the left visual field. Axons that originate from the left half of each retina terminate in the left hemisphere and vice versa via the optic chiasm. Adapted from (Herrera and Mason, 2007; Larsson, 2015)

connected to the cortex through other intermediate circuits (such as the lateral posterior nucleus or the LGN) and is responsible for eye movements and other motor movements. The remaining fibres branch to other brain structures that control secondary non-image forming mechanisms.

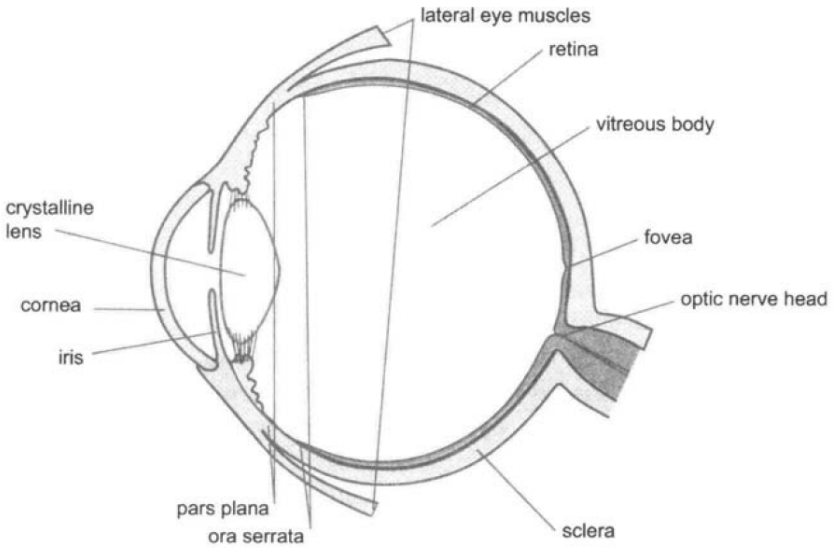

Figure 2: **Schematic drawing of a horizontal cross-section of a human eye.** Source: (Gislin and Eyal, 2004)

Ultimately, the Primary Visual Cortex (V1), located in the occipital lobe of the cortex, plays a critical role in visual information processing before sending information to the rest of the visual cortex. V1 organization and structure is further described in subsubsection 1.1.1.2.

1.1.1.1 *The retina*

The perception of the visual scene starts from photo-reception in the retina. The retina is a well-organized structure, organized in different functional layers which have the task of preprocessing visual information before sending it to the brain.
The retinas of all vertebrates have the same layered organization: three nuclear layers, the Outer Nuclear Layer (ONL), the Inner Nuclear Layer (INL) and the Ganglion Cell Layer (GCL), with two synaptic layers, the Outer Plexiform Layer (OPL) and the Inner Plexiform Layer (IPL), which contain the synapses made by axons and dendrites. Retinal neurons can be classified into the following principal categories: photoreceptors, horizontal, bipolar, amacrine, and ganglion cells (Figure 3) (Demb and Singer, 2015). The cell bodies of photoreceptors are located in the ONL, while the horizontal, bipolar, amacrine and interplexiform cell bodies are located in the INL. Retinal Ganglion Cells (RGCs) constitute most of the proximal layer, the ganglion cell layer, with displaced amacrine cells. Muller cells are the predominant type

of glial cells found in the retinas of vertebrates together with microglial cells and astrocytes; they extend vertically through the entire retina.

Briefly, photoreceptors convert light energy into changes in their membrane potential, which modulate synaptic transmission to second-order neurons, namely bipolar and horizontal cells. These second-order neurons are organized into multiple parallel circuits that converge onto RGCs and amacrine cells. RGCs receive inputs from different inter-neurons pathways and then send their response to the higher visual centres in the brain (Masland, 2012).
In the following subsections a brief description of each retinal neuronal class is given.

PHOTORECEPTOR CELLS Photoreceptors, which convert photons into electrical signals, are divided in two types: rods and cones. Rods operate best in dim light conditions while cones operate best in bright light conditions and are responsible for colour vision. Most species have different types of cones with different spectral sensitivities. These various types of cones have different photo-pigments in their outer segment, which absorb the most in a certain region of the spectrum (Brown and Wald, 1963). Rods and cones are distributed across the retina with very different profiles (Curcio et al., 1987). The density of rods is much greater than cones throughout most of the retina. However, this changes in the fovea, the area of the retina capable of producing the highest visual acuity, where cones are very densely packed in the absence of rods (Schultze, 1886). Unlike most sensory receptor cells, where the appropriate stimulus causes cell membrane depolarization resulting in spike generation, photoreceptors are continuously depolarized in the dark releasing glutamate at their synaptic terminals to second-order neurons. When photoreceptors absorb photons, their photopigments undergo conformational changes, triggering an enzymatic cascade ending in photoreceptor hyperpolarisation and a reduction in the rate of transmitter release onto postsynaptic neurons (Purves et al., 2001).

RETINAL GANGLION CELLS RGCs are the final output neurons of the retina: they receive their input from amacrine and bipolar cells and send their output to the brain in the form of action potentials through the optic nerve. RGCs produce action

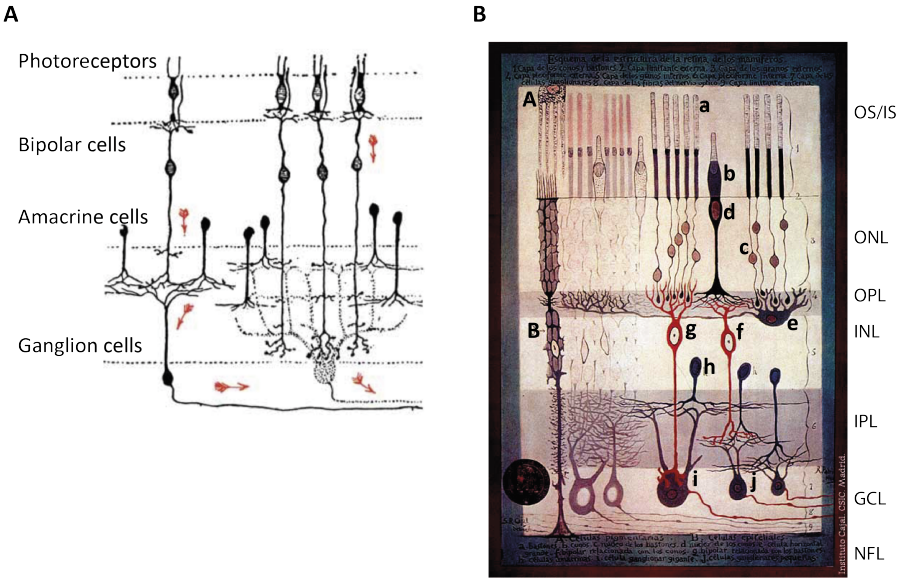

Figure 3: **Structure and connections of the mammalian retina.** Mammalian retina hand painted by Santiago Ramón y Cajal (1893).(A) Photoreceptors connect to bipolar cells, which in turn connect to retinal ganglion cells whose axons constitute the optic nerve. Horizontal cells and Amacrine cells connect predominantly horizontally with photoreceptors, bipolar and ganglion cells. In red, Ramón y Cajal identifies the direction of the signals as they pass from the photoreceptors to the optic nerve. (B) Cellular organization of the retina. Following the original indexation: (A) Pigmentary cells: (a) rods, (b) outer segment of cones (OS), (c) rods and (d) inner segment of cones (IS) which are located in the ONL, (B) Epithelial cells :(e) horizontal cell, (f) bipolar cell related to cones, (g) bipolar cell related to rods, (h) amacrine cells, (i) giant ganglion cell, (j) small ganglion cells in the GCL. OPL stands for outer plexiform layer, INL for inner nuclear layer, IPL inner plexiform layer ad NFL is the optic nerve fibre layer.

potentials as their output, the visual information being contained in the spiking frequency. These cells can be classified into various types according to their dendritic morphology, extent, stratification levels in the inner plexiform layer and electrophysiological properties (Rodieck, 1998). In the mouse retina, more than 30 types of RGCs with different functions have been identified (Baden et al., 2016).

Retinal ganglion cells are also classified according to their physiological responses to light as ON, ON-OFF or OFF- type cells. These types of cells respond to the onset and/or offset of the

light stimulus respectively. RGCs respond to illumination of a restricted but relatively large region of the retina, the receptive field. This organization means that many photoreceptors and inter-neurons contribute to the response of a single retinal ganglion cell. The receptive fields of adjacent retinal ganglion cells overlap partially. Receptive fields are approximately circular and two distinct concentric regions can be identified: centre and surround. When these two regions are stimulated, opposite and antagonistic effects on cell activity are produced. RGCs are divided into ON and OFF-centre cells. ON-centre cells respond best when the centre of the receptive field is illuminated. When the antagonistic surround of the receptive field is illuminated, the RGC is inhibited and a sustained response is generated when the light is turned off. When both regions are illuminated, only a weak response occurs. The opposite occurs for OFF-centre cells (Figure 4). RGCs can be further classified into ON-OFF centre. When random areas of the receptive fields of this type of cell are illuminated they respond to the onset and the offset of the illumination (Dowling, 1987).

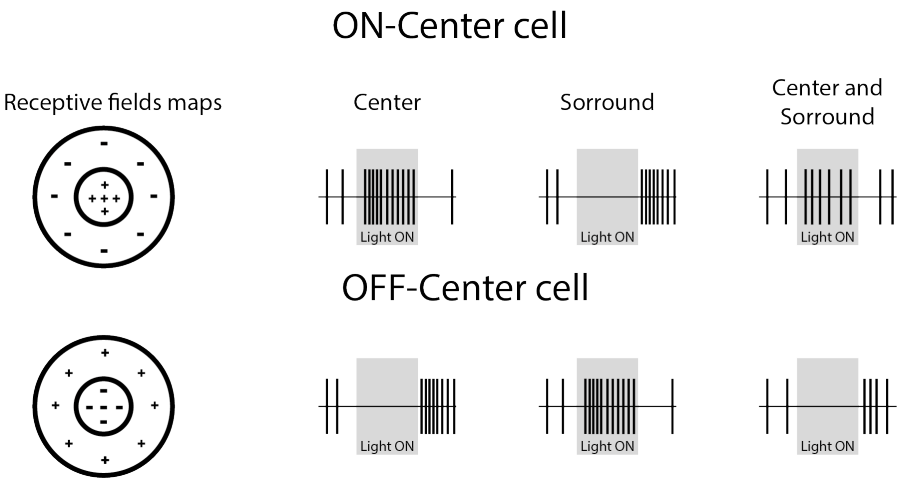

Figure 4: **Responses and receptive fields of ON and OFF-Centre retinal ganglion cells.** (Left) Receptive fields of ON and OFF retinal ganglion cells: + symbol represents an increase in the firing rate of the cell when stimulated, - symbol a decrease. (Right) Responses to a light stimulus in the centre, surround or both regions of the receptive fields.

1.1.1.2 *The primary visual cortex*

The part of the visual cortex that receives inputs directly from the LGN and distributes information to other cortical areas

involved in vision is the primary visual cortex V1 (also called striate cortex). After processing by V1, information flows for further analysis to other extra-striate areas of the visual cortex, such as V2, V3, V4 and V5. These areas process different types of low-level feature information (e.g. orientation, colour or motion). As information passes through different areas, the complexity of neural representation increases. Connections between different visual areas are both of the feed-forward and feedback type, indicating a high degree of interactive processing with each other instead of a cascade process (Tong, 2003). V1 also receives feedback projections from other areas to which it does not project directly (e. g. auditory cortex, frontal eye fields) suggesting how complex the task of visual perception is.

Anatomically, the primary visual cortex resides in the posterior pole of the occipital cortex in both hemispheres. V1 of the left hemisphere receives inputs form the left LGN and inversely V1 of the right hemisphere from the right LGN. The two portions of V1 are connected through the corpus callosum. The primary visual cortex is traditionally divided into 6 different horizontal layers according to Brodmann's scheme (Figure 5). These different layers can be divided anatomically and perform different functions. V1 is also called striate cortex because layer 4 has heavily myelinated stripes, the stria of Gennari, due to the high density of LGN projections. These layers contain three basic types of neurons: spiny pyramidal cells, spiny stellate cells and smooth interneurons.

In primates, cells in the LGN project mainly to layer 4 of V1 and those inputs are sent to other cortical layers that perform different functions in the decoding of visual information (Figure 5). Feedback inputs from other cortical layers reach V1, mostly in the more superficial layers. Projections to other cortical areas, to the thalamus and other sub-cortical regions depart from layer 2/3, 6 and 5 respectively. In primates, layer 4 can be further subdivided into sublayers: 4A, 4B, 4Cα and 4Cβ (Figure 5) (Lund, 1973; Polyak, 1957). Inputs from the LGN arrive principally in layer 4C. This anatomical organization and sensory coding, that defines how a specific subset of neurons responds to a specific stimulus, allows the efficient processing of incoming information through several stages.

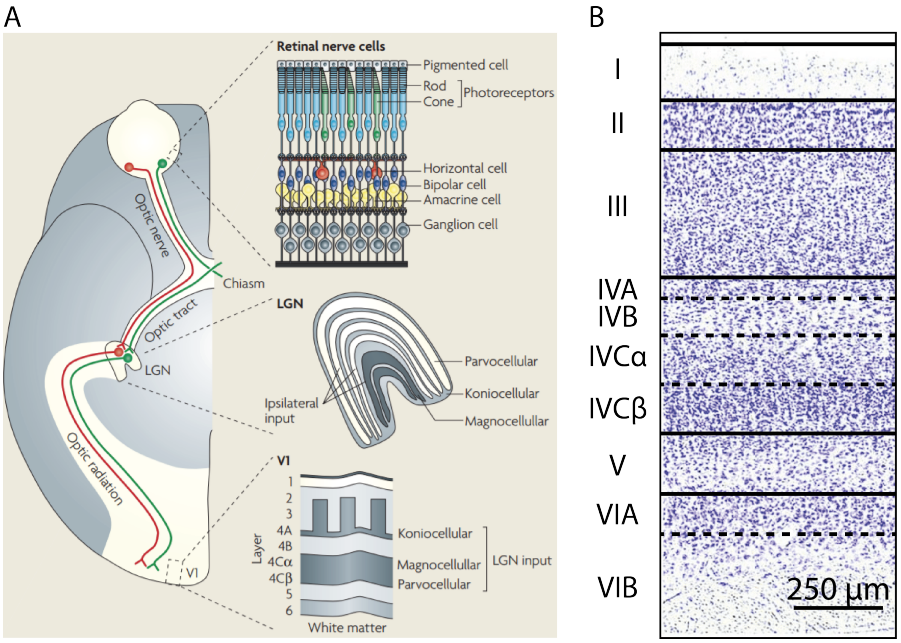

Figure 5: **V1 connections and layers according to Brodmann's nomenclature.** (A) Schematic drawing of the pathway from the retina to V1 through the LGN of the thalamus. The axons of LGN neurons project almost exclusively to V1, where they terminate primarily in layer 4 and form ocular dominance columns. The termination site within layer 4 depends on the layer in which the LGN neuron is found: parvocellular (P) cells project mainly to layer 4Cβ, magnocellular (M) to layer 4Cα, and koniocellular (K) cells to layer 4A and lower layer 3. (B) Two section of macaque V1 stained with Cresyl violet for Nissl substance staining of neurons. Adapted from: (Oga, Okamoto, and Fujita, 2016; Solomon and Lennie, 2007)

The primary visual cortex has a retinotopic organization, meaning that neighboring neurons are stimulated by adjacent regions of the visual space. Therefore, it contains a complete map of the visual field. This retinotopy is continuous: closely spaced points in the visual space correspond to closely spaced points in the cortical map. However, it also presents distortions, such as magnification, which favours the central visual field over the periphery, or geometrical distortions, which transform concentric and radial features into vertical and horizontal lines of activity in V1 (Figure 6).

V1 neurons have elongated receptive fields and, according to Hubel and Wiesel's classification, can be divided into two types: complex and simple. Simple neurons have receptive fields

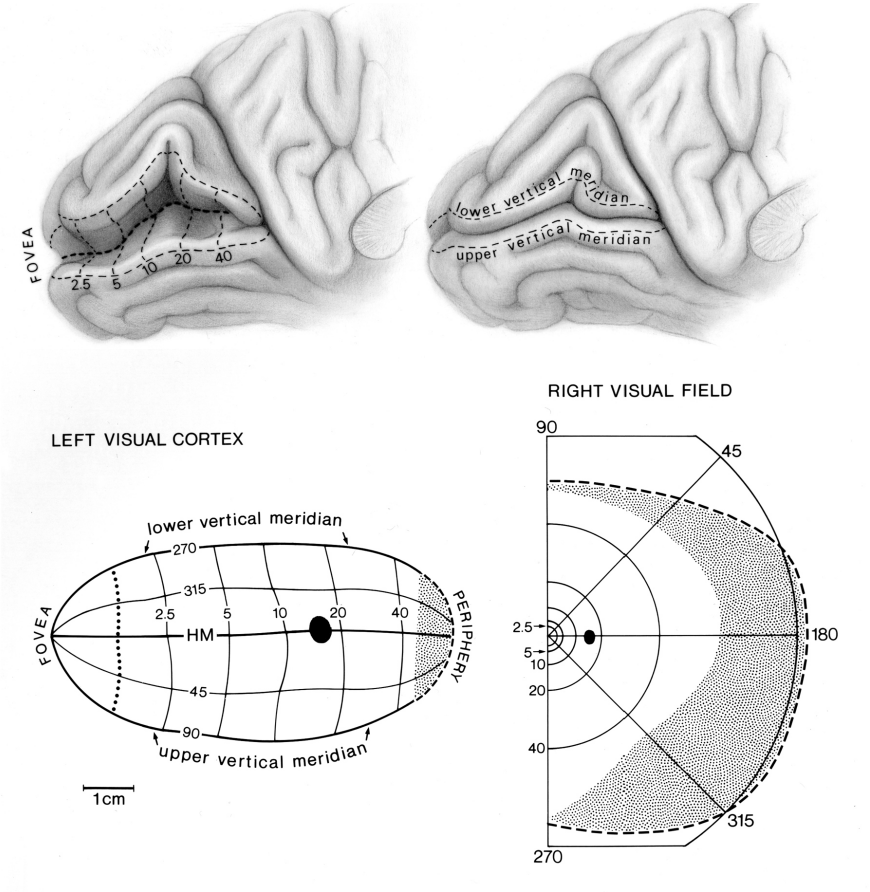

Figure 6: **Retinotopic map of human V1.** The upper right image shows the occipital lobe, with most of V1 buried in the calcarine fissure. In the upper left image, the fissure is opened, with the distance (eccentricity) from the fovea marked in degrees. The lower left image shows the retinotopic map of the left visual cortex flattened artificially. The lower right image shows the corresponding right visual field. Note the magnification of central vision. Dark oval: blind spot. Source: (Horton and Hoyt, 1991).

that are organized into two distinct antagonistic ON and OFF elongated subregions. The spatial organization of these subregions determines the response of the neuron to different stimuli. Simple cells are selective to spatial frequency and orientation of the stimulus. In complex neurons, the ON and OFF receptive field regions are superimposed. Complex neurons are still selective to the spatial frequency and orientation of the stimulus but are invariant to the position and contrast of the stimulus in the receptive field (Hubel and Wiesel, 1962). In addition to being sensitive to the position of the stimulus, V1 neurons also respond to other attributes such as orientation, direction of mo-

tion, spatial and temporal frequency and colour. Many of the forms of selectivity exhibited by V1 neurons are not inherited from the LGN. However the mechanisms and circuits creating this selectivity are in most cases not known.

Besides retinotopic organization, another fundamental feature of V1 neurons is their spatial grouping according to selectivity maps for different stimulus attributes such as orientation selectivity or ocular dominance. V1 neurons with similar properties are grouped together into *cortical columns* that span multiple cortical layers. *Ocular dominance cortical columns* are groups of neurons that respond preferentially to the input from one eye. Visual cortical neurons also respond only to a small range of stimulus orientations, and neighboring neurons tend to have similar orientation preferences forming the so-called *orientation columns* (Hubel and Wiesel, 1962).

1.1.2 *Blinding retinal diseases*

Most visual diseases causing visual impairment and blindness are caused by pathologies affecting the retina. While at present diseases of the lens or the cornea can be effectively treated with surgical procedures, those affecting retinal neurons still cause blindness in millions of people worldwide and are more difficult to treat.
The retinal cells most affected by blinding retinal diseases are photoreceptors and retinal ganglion cells. A brief summary of the most common diseases affecting these cells is presented below. In Figure 7, a human retina is showed and the areas and cell types affected by different retinal diseases are highlighted.

In Age-related Macular Degeneration (AMD), photoreceptors in the macular area degenerate progressively, probably because of the dysfunction and loss of the choroids and the Retinal Pigment Epithelium (RPE), the pigmented cell layer that lies between the retina and the choroids and sustains photoreceptor cells. AMD can be categorized into two types: wet AMD when choroidal neovascularization forms in the macular area and dry AMD, the non-neovascular form that manifests with drusen at the macula (build-up of extracellular material between the RPE and the innermost layer of the choroid) and with RPE changes that lead to progressive photoreceptor loss (Ambati and Fowler, 2012). Photoreceptor degeneration can also occur in Retinal

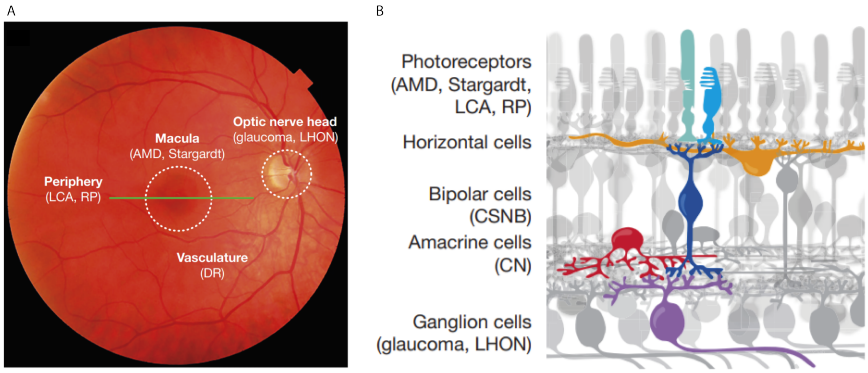

Figure 7: **Retinal diseases.** (A) Image of a human retina seen with an ophthalmoscope. The central region of the retina (the macula) is affected by age-related macular degeneration (AMD), while the periphery of the retina is affected by retinitis pigmentosa (RP). The vasculature is affected by diabetic retinopathy (DR). The optic nerve is affected by glaucoma. (B) Retinal cell types affected by retinal diseases. Photoreceptors (rods in cyan and cones in light blue) are affected by AMD and RP. Retinal ganglion cells (in purple) are affected by glaucoma. Source: (Roska and Sahel, 2018).

Distrophies (RDs) which result from mutations affecting photoreceptors and /or RPE cell function . Common symptoms include night or colour blindness, tunnel vision and progressive vision loss leading to blindness. More than 120 genes are known to be associated with RDs (Nash et al., 2015; *Summaries of Genes and Loci Causing Retinal Diseases, https://sph.uth.edu/retnet/sum-dis.htm*) . Retinitis pigmentosa is one example of RDs that starts with night blindness and evolves to tunnel vision and ultimately blindness. It leads to both rod and cone apoptosis and is characterized by high genetic and clinical heterogeneity.

Glaucoma is a degenerative neuropathy that leads to retinal ganglion cell damage. The irreversible damage to the optic nerve fibres can lead to the complete loss of transmission of visual information to the brain. Elevated intra-ocular pressure is an important risk factor and is also considered as one of the causative factors of glaucoma (Kwom et al., 2009). This elevated intra-ocular pressure originates from reduced aqueous humour outflow from the irido-corneal angle, which can be caused by its closure. As a consequence, glaucoma is classified according to the angle between the iris and the cornea where the aqueous humour, produced by the ciliary body, circulates and is drained. The most common type of glaucoma is open-angle glaucoma,

where the irido-corneal angle remains open.
In Diabetic retinopathy (DR), the weakening of blood vessels caused by diabetes can lead to leakage in the central retina and proliferation of abnormal new vessel. Diabetic macular edema, an important manifestation of DR, originates from the breakdown of the blood-retinal barrier and consequent leakage of fluids into the retina, leading to retinal thickening and cystoid macular edema (Duh, Sun, and Stitt, 2017). Edema is the most common cause of vision loss in DR. A form of glaucoma is often associated with DR.

1.1.3 *Vision restoration techniques*

In the last two decades, major progress has been made in vision restoration for specific types of retinal diseases causing blindness. While several promising approaches have been developed for diseases leading to photoreceptors degeneration, there is still little that can be done for diseases involving retinal ganglion cells damage as is the case for glaucoma.

To counter photoreceptors loss, the most successful approach is to use **retinal prosthetic devices** to provide electrical stimulation to the remaining bipolar or ganglion cells. The visual scene is captured by a camera and is then converted into an electronic stimulation pattern that is transmitted to the prosthesis, implanted in the retina, to stimulate the remaining retinal cells. Retinal electrical stimulation led to visual perceptions and form vision (Yue et al., 2016). These techniques are limited by the low visual acuity and the limited visual field that can be attempted because of the current technological limitations of the stimulating electrodes (low density and number of electrodes) (Cruz et al., 2016). A novel photovoltaic retinal prosthesis has recently shown to provide a visual acuity close to the threshold defined for legal blindness: 1/20 (Palanker et al., 2020). These retinal prostheses require that at least RGCs and the optic nerve are intact so that information can flow to higher visual areas in the brain.

For patients that have lost RGCs, visual prostheses stimulating more central visual structures such as the LGN and the visual cortex have been proposed. **Cortical implants** offer today the most promising alternative for patients suffering from diseases affecting RGCs. These implants stimulate the surface of the pri-

mary visual cortex and have been tested in humans (Fernández and Normann, 2017). Although they can restore form vision in patients who have lost the eye-to-brain connection, the resolution remains too low for complex tasks such as navigation and face recognition (Beauchamp et al., 2020). The use of penetrating electrodes was found in primates to require less current and provide a greater resolution (Tehovnik and Slocum, 2007), such penetrating electrodes are now in clinical trials (NCT02983370). Loss of efficacy with long-term use has also been reported for both surface and penetrating electrodes (Dobelle, 2000; Fernandez et al., 2014). Other visual prostheses stimulating other areas of the visual pathway (e. g. the LGN (Panetsos et al., 2011)) have also been investigated but are limited by the difficulty of accessing these structures. **Deep brain stimulation** has been used to stimulate directly the LGN . Stimulating the thalamus in proximity of the LGN resulted in reports of visual sensations (Marg and Dierssen, 1965), and micro-stimulation of the LGN has been investigated in animal models based on visual saccades (Panetsos et al., 2011). However, the LGN's small size and difficult accessibility makes its direct electric stimulation a challenging approach for vision restoration.

Cell therapy aims to provide retinal repair through cell transplantation to replace damaged cells. Cell transplantation has been investigated particularly for photoreceptors and RPE replacement. Cells are derived from embryonic cell lines or from induced pluripotent stem cells. In mice, transplanted photoreceptor precursor cells derived from embryonic retinas or stem cells were able to integrate into the diseased retina and appeared to be functional. However, it has recently been observed that rather than integrating, transplanted cells pass material to remaining photoreceptor cells and help them to recover function (Pearson et al., 2016). RPE cells have also been transplanted in a few patients with AMD or Stargardt disease, leading to improvements in vision (Schwartz et al., 2015). Photoreceptor cell therapy appears to be more complex because, in order to be functional, transplanted cells need to migrate to the correct location and make efficient synaptic connections with other neurons. RPE cells, on the contrary, do not need to form synaptic connections.

Gene therapy has also been developed to treat photoreceptors degeneration. These techniques aim to replace the abnormal gene causing the degeneration by injecting a viral construct into

the eye. Adeno-Associated Virus (AAVs) are the preferred viral vectors for delivering genes to retinal cells, because they diffuse easily through the tissue and have low toxicity (Ali et al., 1998). For Leber Congential Amaurosis (LCA), a rare type of retinitis pigmentosa where the gene that is required to form the chromophore of visual pigments in photoreceptors is muted, gene therapy has been successful (Garafalo et al., 2020). Gene therapy is feasible in diseases like LCA because the genetic defect is monogenic and because many photoreceptors remain alive even if compromised by the genetic defect.

Optogenetic therapy also offers an alternative approach for restoring vision in patients that have lost photoreceptors. A light-sensitive ion channel (opsin) is introduced into non-light-sensitive retinal cells via gene therapy (Bi et al., 2006; Busskamp et al., 2010; Lagali et al., 2008). A monochromatic light can therefore stimulate the induced light-sensitive cells. The major advantage of this technique is the cell-specificity and the high spatial resolution. However, cells expressing these opsins require bright light stimuli to be activate and do not adapt (Busskamp et al., 2012). In diseases such as AMD, photoreceptors degenerate only in the macular region and the periphery of the retina remains light-sensitive calling into question the possibility of using bright light for optogenetic stimulations. This approach is currently in clinical trials for patients with retinal dystrophies (NCT02556736, NCT03326336, NCT04278131). Optogenetics has been proposed also for cortical stimulation (Jazayeri, Lindbloom-Brown, and Horwitz, 2012; Ju et al., 2018). The major drawback is the invasiveness of the technique: because light is highly scattered and absorbed into brain tissue, efficient stimulation in deeper neuronal layers is not possible without removing the dura and implanting invasive optical fibers (McAlinden et al., 2019).

1.2 ULTRASOUND WAVES FOR NEUROMODULATION

There are some approaches that directly stimulate the cortical neurons non-invasively by means of stimuli that penetrate the skull and brain tissue, such as transcranial magnetic field stimulation (Dayan et al., 2013) and transcranial electric stimulation (Polanía, Nitsche, and Ruff, 2018). Although both approaches are able to stimulate deep brain regions, their variable effects on neurons and limited penetration and spatial resolution make

them difficult to use for vision restoration. US waves represent an interesting tool able to overcome these limitations. US neuromodulation has been shown to be able to modulate neuronal activity in a variety of preparations, ranging from humans to mice (Legon et al., 2014; Tufail et al., 2011) and could become a promising stimulation strategy for vision restoration.
To better understand the underlying mechanisms that make neurons sense US energy and convert it into an electric response, in the following sections an overview of basic ultrasonic physics and US-tissue interaction mechanisms is provided. There follows a comprehensive review of the state of the art of US Neuromodulation.

1.2.1 *Basic Ultrasound physics*

WHAT ARE ULTRASOUNDS? Sound is the rapid motion of molecules. These molecular vibrations transport energy from a transmitter, a sound source such as our voice, to a receiver such as our ear. When the molecules are forced to get closer together, compression occurs; conversely, when they are allowed to expand, rarefaction happens. This rapid, back and forth mechanical motion is the basis for calling sound a mechanically propagated wave. There are sound frequencies below and above the human auditory range. Audible sound is what human beings hear and has an approximate frequency range between 20 Hz and 20 kHz. The ultrasound frequency range starts at a frequency of about 20 kHz. Most medical ultrasound equipment for imaging purposes operates in the ultrasonic frequency range between 1 and 15 MHz (Figure 8). On the other hand, therapeutic ultrasound applications (physical therapy, high-frequency focused ultrasound and ablation) operate typically around 1 MHz.

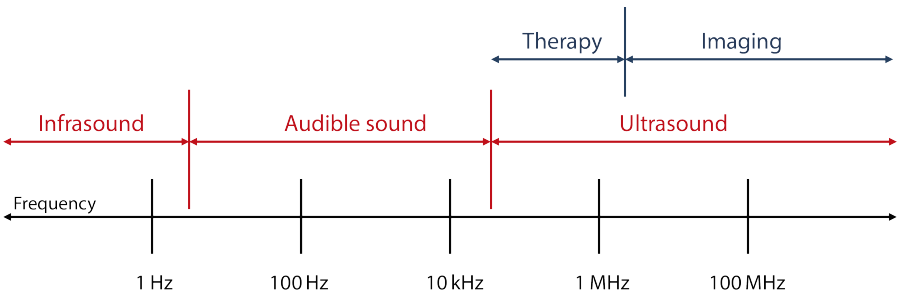

Figure 8: **Acoustic and medical ultrasound spectrum.**

1.2.1.1 *Acoustic waveforms*

Ultrasound travels in the form of a wave, similar to the way light travels. However, unlike light waves, which can travel in a vacuum, US requires an elastic medium such as a liquid or a solid. When these waves travel in some physical medium, pressure is alternately higher and lower and the medium will be respectively compressed or rarefied. The peak compressional and rarefactional values are represented in Figure 9 as the high crest and low troughs of the wave.
The number of cycles completed in one second is called frequency f and is measured in Hertz (Hz). The relation between frequency and the period T in a continuous wave is given by $f = 1/T$. The speed of ultrasound c in a perfectly elastic material at a given temperature and pressure is constant ($c = \sqrt{1/\kappa\rho}$, κ: compressibility, ρ: density) and is related to the frequency f and the wavelength λ: $\lambda = c/f$. For medical applications, the propagation speed c in tissue is typically assumed to be constant at 1540 m/s. The actual velocities in specific tissues vary around this average. For example, the sound speeds of fat, amniotic fluid, kidney, muscle and skull bone are about 1450, 1540, 1565, 1600, and 4080 m/s, respectively (Zagzebski, 1996).

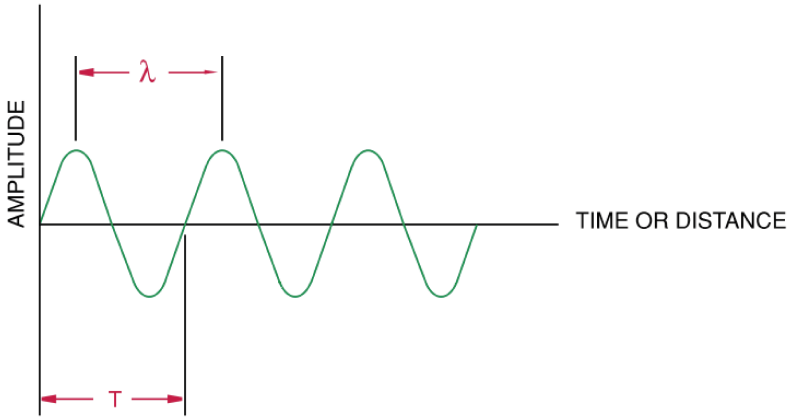

Figure 9: **Schematic representations of an acoustic waveform.**

1.2.1.2 *Wave Propagation and Particle Motion*

US waves propagate in a medium in an oscillatory manner in different operating modes. They are classified according to the direction of the oscillatory motion of the particles within the medium relative to the direction of wave propagation.

A *longitudinal wave* occurs when the particles move backwards and forwards in the same direction as the wave is travelling; this is basically a compressional wave. These waves correspond to regions in the medium where pressure is alternately higher and lower than resting pressure. Where pressure is high, the medium is squeezed or compressed; where pressure is low, the medium is stretched or rarefied. In this condition, each small element of the medium moves back and forth around its resting location but does not undergo any net motion as the wave propagates (Figure 10). Propagated longitudinal waves travel through all kinds of materials: gases, liquids and solids (O'Brien Jr., 2007).
A *shear wave* occurs when the particle motion is perpendicular to the direction of wave propagation, as shown in Figure 10. In this case, the particles move vertically up and down, while the wave energy moves horizontally. Shear waves exist only in solid materials, not in fluids. Shear waves do not exist in soft tissues because soft tissues can be approximated as liquids. Shear waves do, however, travel in harder biological materials such as bone tissue. As these transverse waves are rapidly attenuated in tissue, they do not play a direct role in US medical imaging and therapy (O'Brien Jr., 2007); only longitudinal waves are relevant.

When an US wave encounters an object, its particles tend to resist to the displacement induced by the sound wave. The magnitude of this resistance depends on the *acoustic impedance* Z of the given material. Z is a property of the medium and can be defined in a simplified manner as $Z = \rho c$, where ρ is the density of the medium and c the acoustic speed of the wave (Szabo, 2004). This impedance is measured in rayl (kg/m^2s).
When the medium is a biological medium, it is typically composed of tissues with different physical properties, which therefore have different acoustic impedance. The boundary between two tissues with different acoustic impedance is called acoustic interface. Similarly to optics when light encounters a surface with a different refraction index, when an US wave encounters an impedance discontinuity, part of the incident sound energy is reflected and part is transmitted across the boundary (Azhari, 2010). Reflection can be categorized as either specular or diffuse. If US waves encounter a large plane and smooth reflective structures, such as bone, *specular reflection* occurs, where the wave is reflected back in a singler direction. In this type of interaction energy is conserved, because the sum of the reflected and transmitted energy is equal to the original incident wave.

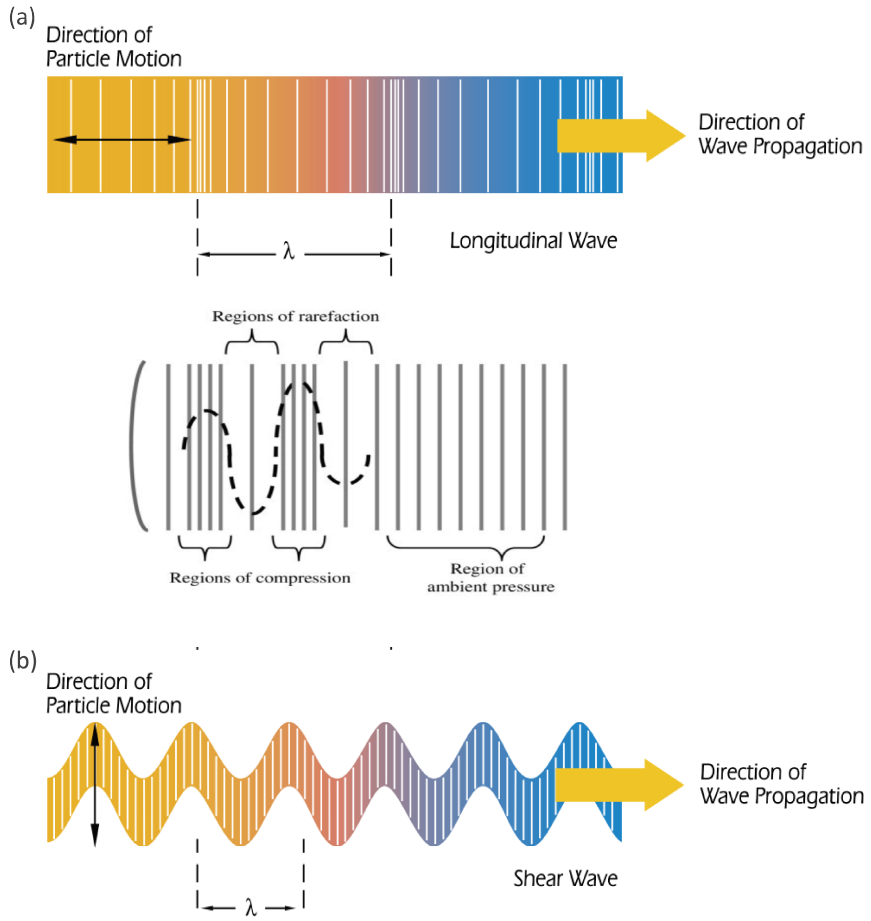

Figure 10: **US induced particle motion and wave propagation for longitudinal and shear waves.** Representation of Longitudinal waves (a) and Shear waves (b). Adapted from: (Hangiandreou, 2003; Panametrics-NDT™, 2006)

In contrast, when US waves travel through a soft tissue, the interface between two tissues with different acoustic impedance is more likely to be uneven and rough and the reflected wave, the echo, will be therefore diffusely reflected through a wide range of angles and refracted waves. This deflection is called *diffuse reflection*. Snell's Law describes the relationship between the angles and the velocities of the incident, reflected and refracted waves (Figure 11). The angle of refraction is dependent on two factors: the angle at which the sound wave strikes the boundary between the two tissues, and the difference in the two tissues' propagation velocities. According to this law, if the propagation velocity is greater in the first medium, refraction occurs perpendicularly to the incident wave. If the velocity is

greater in the second medium, refraction occurs away from the originating beam.

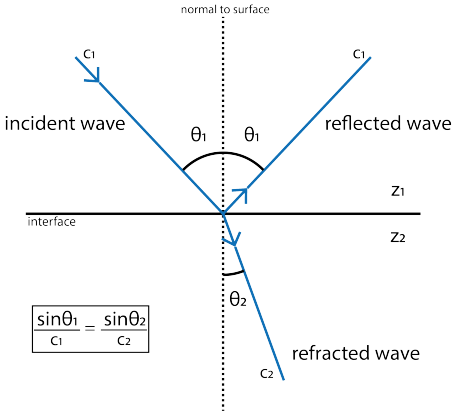

Figure 11: **US Refraction and Snell's Law.** Snell's law equates the ratio of wave velocities c_1 and c_2 to the ratio of the sine's of incident (and reflected) θ_1 and refracted θ_2 angles.

Specular and diffuse reflection occurs when the sound wave hits an object that is much larger than the wave's wavelength. When US encounters a structure whose dimension is smaller than the wavelength, *scattering* occurs, resulting in waves that are reflected in a very wide range of angles (Cobbold, 2007). Fibres, cells and organelles are examples of scatters that can be found in biological tissues.

Therefore, the global effect of tissue on US waves is *attenuation*. As the wave passes through a medium, its intensity decreases exponentially as a consequence of reflection, scattering and absorption. In absorption, the energy of the wave is converted into thermal energy, causing localized heating. There are two main reasons for this phenomenon: the friction between particles as the wave propagates and their motion to return to the original position after being displaced by the pressure wave (relaxation). Attenuation depends on the distance travelled, tissue and the ultrasound wave's frequency.

1.2.1.3 *Acoustic Intensity, Mechanical an Thermal index*

The acoustic intensity carried by an US wave is defined as the ultrasonic power transmitted in the direction of the wave propagation per unit area. Instantaneous intensity I (W/cm^2) is defined as follows, were P (Pa) is the instantaneous acoustic pressure and v the particle displacement velocity (m/s):

$$I = Pv = P^2/Z, \text{ where } P = Zv$$

Acoustic intensity varies with time and also depends on the point in space where it is measured. Therefore, it can be defined in different manners: I_{PA} (pulse average), I_{TA}(temporal average), I_{SATA} (spatial-average temporal –average), I_{SPPA} (spatial-peak pulse-average- average intensity of one individual pulse) or I_{SPTA} (spatial-peak temporal-average-average intensity over the experimental time) (FDA, 2008).

When talking about the possible negative effects of US on tissue, acoustic intensity is an important parameter. In addition to acoustic intensity, two more metrics are typically defined to measure US safety: the Mechanical Index (MI) and the Thermal Index (TI), given that US interacts with tissues both thermally and mechanically.
Thermal energy absorption is related to the wave's acoustic intensity and frequency. The TI measures the heating that occurs within the tissue. It is defined by the following equation (Blackmore et al., 2019):

$$TI = W_p/W_{p1deg}$$

Where W_p is the acoustic power and $W_{p_{1deg}}$ is the power required to raise tissue temperature by $1^{\circ}C$.
The MI has been introduced to evaluate the mechanical effects of US on tissue and the risk associated with cavitation phenomena (Blackmore et al., 2019). It is defined as follows:

$$MI = P_{neg}/\sqrt{F}$$

Where P_{neg} is the peak negative pressure of the wave and F is its fundamental frequency.
The Food and Drug Administration's (FDA) guidelines impose the following limits in terms of intensity, MI and TI for diagnostic US imaging devices: I_{spta} must not exceed 720 mW/cm^2, I_{sppa} must be lower than 190 W/cm^2, TI and MI must not exceed 6 and 1.9 respectively (FDA, 2008).

1.2.1.4 *Ultrasound wave delivery*

US waves are produced by devices called ultrasonic transducers. In general terms, a transducer is a device that converts one

form of energy to another; an ultrasonic transducer converts electrical energy into mechanical energy in the form of a sound wave and vice versa. The piezoelectric effect is used for this purpose: when electrical energy is applied to a given piezoelectric element it repeatedly expands and contracts, causing mechanical vibrations that generate the sound wave. US pulses are formed by applying oscillating electrical waveforms to the piezoelectric element, causing it to vibrate at a given resonant frequency that depends on the geometry of the crystal.

US can be delivered to tissue in the form of a continuous wave or in a pulsed manner. The following parameters describe a US wave: Pulse duration (PD, in s), Pulse repetition frequency (PRF, in Hz), Duty cycle (DC, %), Fundamental frequency (FF, in Hz) and Pressure (P, in Hz) (Figure 12).

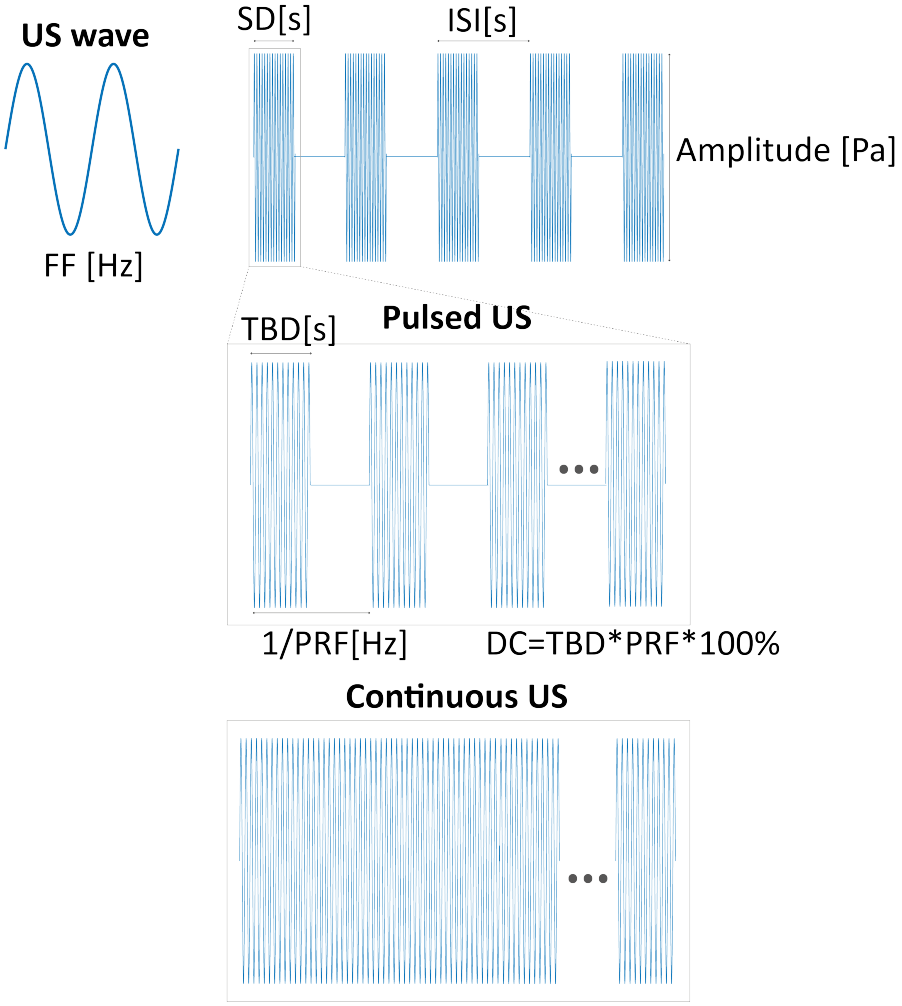

Figure 12: **Ultrasound stimulation parameters.**

For transducers composed of a single piezoelectric element, ultrasound waves can be emitted in a focused or non-focused manner. Focusing is accomplished by either adding an acoustic lens or curving the active element itself.
The sound field of a transducer (focused or not) is typically divided into two zones: the near field and the far field. The near field is the region directly in front of the transducer where the echo amplitude goes through a series of maxima and minima and ends at the last maximum, at distance N from the transducer. The location of the last maximum is known as the near field distance (N). The far field is the area beyond N where the sound field pressure gradually drops to zero.
Thus, the lateral resolution of an ultrasound beam varies with the distance from the transducer. For unfocused transducers, the point with the narrowest beam width occurs at the near field distance N. For focused transducers, the distance of the focal spot size is defined by the mechanical focus and spot size depends on the geometry of the transducer and the focal depth (the focal spot has typically the shape of an ellipsoid) (Figure 13).

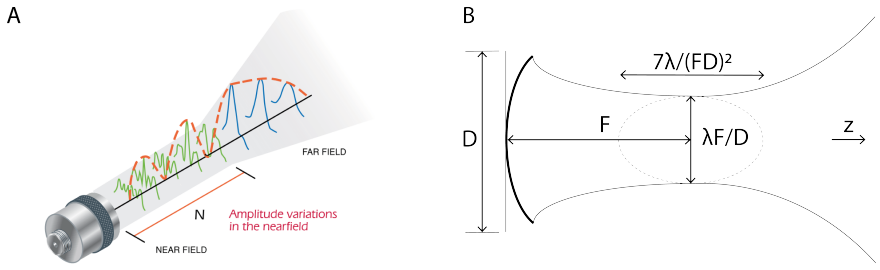

Figure 13: **Ultrasound beam profile of a single element transducer.** (A) Ultrasound beam profile for an unfocused transducer. (B) Beam profile for a focused ultrasound transducer. Adapted from: (Panametrics-NDT™, 2006)

1.2.2 *Interaction of US with biological structures*

When US waves propagate in a biological tissue, we can distinguish two different mechanisms: the physical mechanism that the US wave applies to the tissue and the bio-physical mechanism that involves the response of the cells to this energy. US physical mechanisms are diverse but are typically grouped into thermal and non-thermal effects (Figure 14).

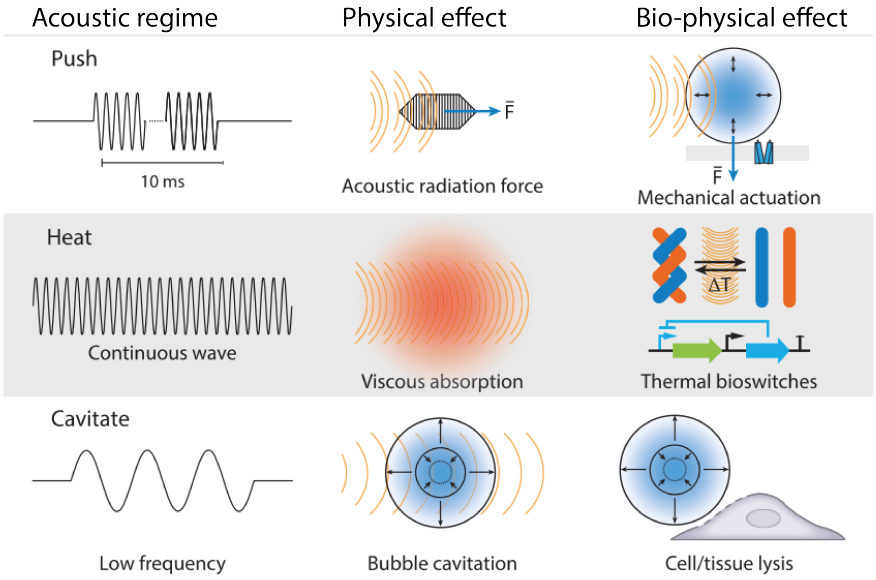

Figure 14: **Interaction of US with tissue: physical mechanisms.** (Top) Extended ultrasound pulses induce an acoustic radiation force causing displacement of the tissue. (Middle) Continuous ultrasound waves lead to local heating and can be used to turn on thermal bioswitches. (Bottom) Low-frequency ultrasound can be used to cavitate microbubbles that can induce cell disruption. Source: (Maresca et al., 2018)

When US waves propagate in a tissue, they are attenuated through either absorption or scattering. In absorption, a part of the energy carried by the wave is converted into heat. A temperature rise can therefore occur if the rate at which heat is produced is greater than the rate at which it is dissipated. These thermal mechanisms can be effectively estimated through mathematical models (Curley, 1993; O'Brien and Ellis, 1999). US-induced tissue heating increases with acoustic frequency and intensity and also depends on the type of tissue that is exposed to US energy and the exposure time.

US also induces non-thermal mechanical effects on tissue. A US beam is able to exert mechanical forces on a tissue: oscillatory and steady forces. The periodic forces generate vibrations and consequent nano-metric displacement of the tissue at the frequency of the US wave (Kubanek, 2018). The steady acoustic radiation force arises from the transfer of momentum from the wave to the tissue, which results in a net force on the tissue. This constant force leads to macro-metric displacements. It is a non-linear effect which is proportional to the intensity of the acoustic

wave (Rudenko, Sarvazyan, and Emelianov, 1996). Acoustic Radiation Force (ARF), force per volume of tissue ($kg/(s^2cm^2)$, for a time-harmonic plane wave is given by the following equation (Nyborg, 1965):

$$F_{ARF} = 2\alpha I/c$$

Where α is attenuation, I the acoustic field intensity and c the speed of sound.

When tissue contains pre-existing gas bubbles, cavitation can occur, leading to the oscillation of the bubbles and eventually, at sufficiently high pressure levels, their collapse. Cavitation may be inertial or non-inertial. Non-inertial cavitation occurs when a bubble that is exposed to an acoustic field oscillates around its equilibrium radius. These non-inertial oscillations can result in heat generation and shear stress due to flows at the periphery of the oscillating bubbles (Dalecki, 2004). They can also cause microstreaming, which can alter ion transport across cell membranes (Haar, 2011). Inertial cavitation occurs when microbubbles arise and collapse. High pressure and temperature can generate from the bubble's collapse. The motion of the bubble's wall during collapse produces a spherically diverging shock wave in the surrounding liquid. When this happens close to a solid surface, it can generate high-speed microjets that can result in cell damage. The likelyhood of inertial or non-inertial cavitation depends on the acoustic pressure amplitude and the MI: the higher the MI and the pressure amplitude, the more likely the occurrence of inertial cavitation. Opposite to radiation force and heating, which are expected to increase with higher acoustic frequencies, the probability of cavitation decreases with higher carrier frequencies.
These different physical mechanisms are the basis of various therapeutic applications that rely on ultrasound.

1.2.3 *A brief history of medical ultrasound*

The first experiments that indicated that living systems were able to use non-audible sound were performed by Lazzaro Spallanzani in 1794. He demonstrated that bats were able to navigate in space using sound waves over the audible limits, US waves, rather than sight. Bats can indeed locate the position of objects by sending sound waves and processing the reflected echo to

detect their position in space. The same principles are used today for medical US imaging. Almost one century later, in 1877, the Curie brothers discovered the piezoelectric effect and laid the foundation for the development of probes able to emit and receive US waves (Curie and Curie, 1880). After the sinking of the Titanic in 1912, ultrasound was proposed as a mean to detect icebergs at sea and for the underwater navigation of submarines in World War I. For this purpose, in 1915 the first ultrasound transducer was invented by the French physicist Paul Langevin; it was called hydrophone. Later, in the 1940s it was realized that the nature of US waves could also give them great potential in the medical field. Dussik is credited with having been the first, in 1942, to propose US waves as a diagnostic tool using the echo-reflection methods. He tried to detect brain tumors by transmitting ultrasound waves through the human skull (Dussik, 1942). Systematic investigations into using US as a diagnostic tool finally took off in the late 1940s, thanks to the availability of the necessary equipment and electronics. This started the development of US as a diagnostic tool, eventually leading to its present role as a mainstay technology used in clinical routine. In the 1940s, the use of US in treatment also started to be investigated, using its heating and disruptive effect on tissues when applied at high intensity. Langevin was the first to observe that ultrasonic energy could have a detrimental effect on biological material when used at high intensity. Fry and Meyers used high-intensity ultrasound to destroy parts of the basal ganglia in patients suffering from Parkinson's disease. In the 1940s, US was extensively used to treat a number of conditions such as arthritic pain, asthma or eczema, as a cure-all remedy despite the lack of strong scientific evidence (Woo, 2002). In the 1950s, the ability of US to modify the activity of excitable tissue also started to be investigated. In 1929, Harvey was the first to discover that pulsed US applied to a turtle's heart could pace the heart's rhythm, presumably by initiating bioelectric events in the myocardium. In the 1950s, several studies showed that US energy could change the normal electro-physiology of excitable tissue. It was shown that US had distinct effects, often stimulatory and sometimes suppressive, on cells of nervous structures and muscles (Fry, Ades, and Fry, 1958; Mazoue, Chauchard, and Busnel, 1953; Welkozitz and Fry, 1956). However after these promising early works it was only later, with the work of Tyler in 2008 and Tufail in 2010 (Tufail et al., 2010; Tyler et al., 2008) that ultrasonic neuromodulation became a rapidly growing field.

A comprehensive review of US neuromodulation is presented in the following section.

1.2.4 *US neuromodulation*

As previously mentioned, the idea of using US waves to modulate the activity of neurons dates back to the 1950s, when William Fry and colleagues published their work showing that US waves were able to suppress temporarily visual evoked potentials recorded in the visual cortex of cats when US stimulation was applied for over 20 seconds to the LGN. (Figure 15) (Fry, Ades, and Fry, 1958). However it is only recently that this field has attracted increasing attention, because technological advance has made it possible to efficiently focus US waves through the skull without major beam aberrations. Compared with other neuromodulation techniques, such as transcranial magnetic or electrical stimulation, deep brain electrical stimulation or optogenetics, US waves, because of their physical properties, offer unique advantages such as non-invasiveness, deep brain penetration and precise focus. In the following sections an overview on the state of the art, the underlying mechanisms and the limits of this approach are presented.

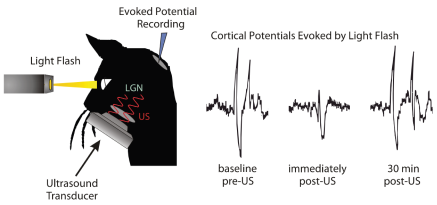

Figure 15: **IIllustration of the experiments conducted by Fry and co-workers on US neuromodulation.** (Left) Experimental setup. (Right) Visual evoked potential traces obtained before and after US stimulation of the LGN in living cats. Source: (Fry, Ades, and Fry, 1958; Tyler, 2011)

1.2.4.1 *State of the art*

In 2008, the work of William Tyler and colleagues (Tyler et al., 2008) showed that US is capable of opening voltage-gated ion channels and leading to evoked action potentials in brain slices. Tufail and co-workers (Tufail et al., 2010) then reported these excitatory responses also *in vivo*: US waves targeting the motor cortex and the hippocampus in mice resulted in increases of

cortical spiking activity as well as after discharge activity with gamma (40-100 Hz) and sharp-wave ripple (160-200 Hz) components. US stimulation was also able to evoke tail twitches and electromyography spikes. Subsequently, several studies demonstrated the ability of US to modulate neuronal activity in both the central and peripheral nervous system. US neuromodulation has been shown to be effective in a wide set of preparations: from *ex vivo* brain and retinal slices to *in vivo* preparations from mice to humans (Deffieux et al., 2013; Lee et al., 2016; Legon et al., 2018, 2014; Mehić et al., 2014; Menz et al., 2013; Tufail et al., 2010; Tyler et al., 2008). US stimulation has been shown to be able to excite or inhibit neuronal activity depending on the stimulation parameter. Moreover, when applied for longer time periods (>10 s) it can also induce long-term changes in neural activity (Dallapiazza et al., 2018; Velling and Shklyaruk, 1988; Yang et al., 2012). In Table 1, an overview of significant studies in the literature on US neuromodulation is given, outlining the main findings and the US stimulation parameters used.

In vivo, US stimulation is typically performed at relatively low sub-megahertz frequencies, from 0.2 to 5 MHz, because of the possibility of crossing the skull without major attenuation or aberrations. Low US intensity values are typically used, from 0.01 to 15 W/cm^2, to avoid potential side effects such as cavitation and heating. On the other hand, using higher US frequencies would lead to increased anatomical specificity. 5 MHz US has been shown to be effective in inducing electromyographic responses *in vivo* in mice (Li et al., 2016). However, Ye and colleagues showed that success rate decreased with higher US frequencies for a given intensity (Ye, Brown, and Pauly, 2016), suggesting that higher intensities are necessary for higher frequency US stimulation. High frequency US stimulation has been applied mostly *ex vivo*, up to 43 MHz, using relatively high intensities when compared to *in vivo* studies. 43 MHz US has be shown to be effective in mediating retinal ganglion cells responses in isolated salamander retinas, where the required intensity attained 180 W/cm^2 (Menz et al., 2013).
Moreover, between studies, different US stimulation parameters have been investigated, such as pulse repetition frequency, burst duty cycle or burst duration. However, no clear evidence of a more effective subset of parameters has been obtained (Table 1). Similarly, no clear evidences have defined whether pulsed or continuous US delivery is more effective.

On the other hand, to further optimize and develop this technique it seems crucial to identify the optimal stimulation protocol for a given application and obtain an insight into the related underlying bio-physical mechanisms.

Table 1: **Ultrasonic neuromodulation studies overview.** Studies are separated into *in vitro* and *in vivo* by a horizontal line. For US parameters: * states that a given parameter has been calculated from the one given in the cited reference. The reported US intensity values are the maximum values that have been used in a given reference. NR: not reported. Adapted from: (Pasquinelli et al., 2019).

Reference	Target	Measured effects	US frequency (MHz)	Sonication duration	Inter stimulus interval	Nb of sonications per trial	Pulse repetition frequency	Tone burst duration or Duty Cycle	Acoustic intensity(Ipa, Isppa or Ispta) and MI	Adverse effects
(Tyler et al., 2008)	Hippocampal slices and isolated mouse brain	US-induced APs during whole-cell current clamp recordings in CA1 pyramidal neurons. Triggering of voltage-gated Na+ and Ca2+ channels, vesicle exocytosis and synaptic transmission. Addition of TTC and Cd2+ blocked Na+ and Ca2+ transients respectively.	0.44	5.6 ms-2.5 s (for continuous and 100 Hz PRF respectively)*	5 s	NR	Continuous-100 Hz	22.7 µs	Ipa:2.9 W/cm^2	NR
(Menz et al., 2013)	Isolated salamander retina	US evoked strong responses of RGCs similar to visual response but with shorter latencies. US activated other cells beyond RGCs. PRF 15 Hz to 1 MHz had no effect on responses; only temporal-averaged power was important.	43	1 s	2-66 ms	NR	Continuous, 10 Hz-1 MHz	50 ms-0.5 µs	Ispta/Ippa: up to 180 W/cm^2	NR
(Kubanek et al., 2016)	Xenopus ovocytes	US modulates reversibly the currents flowing through potassium and sodium mechano-sensitive ion channels by up to 23% depending on the channel and stimulus intensity.	10	1 s	5 s	7-5	Continuous - pulsed 1 kHz	NR	Isppa/Ispta:2 W/cm^2 (for continuous stimulation); Ispta: 4.9 W/cm^2 (for pulsed stimulation)	NR

(Menz et al., 2017)	Isolated salamander retina	US stimulation results in micron-scale displacements. Efficacy increased with frequency, consistent with an ARF-mediated mechanism.	43- 15- 2.25- 0.5 ,	1 ms -100 ms	5, 15 s	NR	Continuous	NR	Isppa/Ispta: up to 100 W/cm^2 (43 MHz-15 MHz-2.25 MHz); Isppa: up to 10 W/cm^2 (0.5 MHz)	NR
(Prieto et al., 2018)	Cell culture	Activation of Piezo1 but not NaV1.2 with US stimulation through membrane stress as a result of acoustic streaming.	43	200 ms	NR	NR	Continuous	NR	Isppa, Ispta: 90 W/cm^2	NR
(Tufail et al., 2010)	Mouse motor cortex	Neuron's spike frequency and c-fos cell density increase and the activity of endogenous brain-derived neurotrophic factor were stimulated. Low frequency and low intensities resulted in more robust EMG response. The EMG failure probability increased with shorter inter-stimulus intervarls, but decreased with multiple stimuli.	0.5	67 * (53) ms	10 s	180 *	1.5 kHz	0.45 ms	Ispta: 0.142 W/cm^2; Isppa:0.211 W/cm^2 *; MI=0.13 (after cranial tx)	NR
(Yoo et al., 2011)	Rabbit SM and Visual area	BOLD activation was observed at a much lower acoustic intensity (Isppa: 3.3 W/cm^2, Ispta:1.6 W/cm^2) compared to the intensity that resulted in forepaw movements (Isppa: 12.6 W/cm^2, Ispta: 6.3 W/cm^2)	0.69	0.5, 1, 1.5, 2, 9 s	NR	1	10, 20, 100, 1000 Hz	0.05, 0.5, 10, 50 ms	Ispta: 1.6 W/cm^2 (for Isppa: 3.3 W/cm^2) ; Isppa=3.3, 6.4, 9.5, 12.6 W/cm^2; MI<0.5 (for Isppa: 3.3 W/cm^2)in water	NR

(Yoo et al., 2011)	Rat Thalamus	The sonication reduced the time to emergence of voluntary movement from intraperitoneal ketamine-xylazine anesthesia. A preliminary test showed that a Isppa 3.3 W/cm^2 failed to decrease the duration of the anesthetic state.	0.65	20 min	NR	1	100 Hz	0.5 ms	Ispta: 0.3 W/cm^2, Isppa: 6 W/cm^2, MI: 0.61, after cranial tx	NR
(Kim et al., 2012)	Rat abducens nerve	US frequency of 650 kHz and Isppa in the range 0.5-20 W/ cm2 did not elicit eye movement in any animals. Movements observed when fc=0.35 MHz and Isppa=8.6 W/cm^2	0.65, 0.35	200 ms	1s	10	1.5 kHz	0.36 ms	Ispta: 4.6 W/cm^2 Isppa:8.6 W/cm^2 MI=0.9 after cranial tx (estimated)	NR
(Yang et al., 2012)	Rat Thalamus	Extracellular GABA level started to decrease upon sonication and remained reduced compared to control group up to 100 min after the end of sonication. The same effect was not observed for extracellular glutamate level.	0.65	20 min	NR	1	100 Hz	0.5 ms	Ispta:0.175 W/cm^2 , Isppa:3.5 W/cm^2, MI: 0.2, (after cranial tx)	NR
(Younan et al., 2013)	Rat cortex (target to elicit motor response, not corresponding to motor cortex)	A pressure threshold of 0.79 and 0.59 MPa was required to reach 50% of responsiveness, for deep or light anaesthesia stage, respectively, and the sigmoid response was less sharp in the light anaesthesia stage. These pressures corresponded to an average Isppa of 7.5 W/cm^2.	0.32	250 ms	10 s	NR	2 kHz	0.23 ms	Ispta:8.75 W/cm^2 * , Isppa:17.5 W/cm^2, MI: 1.77*, (values to have 50% response, after cranial tx)	NR

(Kim et al., 2014)	Rat somatomotor area	Motor responses were observed at minimum threshold (Isppa: 4.9-5.6 W/cm^2,Ispta:2.5-2.8 W/cm^2) in a limited range of sonication parameters (TBS: 1-5 ms, 50% of duty cycle, and SD:300 ms, at fc: 350 kHz). Pulsed sonication elicited motor responses at lower acoustic intensities than its equivalent continuous sonication (Isppa:7.73 W/cm^2).	0.35, 0.65	150, 200, 300, 400 ms	2 or 3 s	NR	0.06-2.8 kHz and continuous	0.25, 0.5, 1, 2, 3, 5 ms	Ispta: 11.2 W/cm^2, Isppa: 22.4 W/cm^2, MI: 1.38(after cranial tx)	One animal which underwent a sonication of Ispta:11.2 W/cm^2 for a short period of time (9 s using 1ms TBD, 50% duty cycle and 300 ms SD) showed signs of local bleeding.
(Kim et al., 2015)	Rat visual cortex	Isppa: 3 W/cm^2 with TB: 0.5 ms and PRF:100 Hz (5% duty cycle) successfully suppressed the VEP. Higher duty cycle (8.3%) increased the VEP. The same effect was observed at Isppa: 5W/ cm2.	0.35	150 s		1	20, 100, 166 Hz	0.5 ms	Ispta: 0.25 W/cm^2 , Isppa:5 W/cm^2, MI: 0.75 (not clear if in water or after cranial tx)	NR
(Li et al., 2016)	Mouse motor cortex	The peak EEG amplitude increased with increasing Ispta.	1 and 5	300 ms	3 s	20 *	1 KHz	0.5 ms	Ispta: 0.23 W/cm^2 , Isppa:0.46 W/cm^2 * (after cranial tx)	NR
(Ye, Brown, and Pauly, 2016)	Mouse motor cortex	Success rate decreases with frequency for given intensity. Focal spot size did not have consistent effect on success rates; most of the variance can be explained by frequency. Success strongly correlated with cavitation index and particle displacement but not ARF.	0.3-2.9	80 ms	2 s	NR	Continuous	NR	Isppa - Ispta: 3.5 (for 0.3-0.6 MHz), 9.4 (for 0.6-1.4 MHz), 127 W/cm^2 (for 1.4-2.9 MHz)	NR

(Lee et al., 2018)	Rat motor cortex (anesthetized and awake)	Different thresholds to evoke observed motor responses: Isppa: $3.4 \pm 1.8\ W/cm^2$ for the awake condition (grand mean response rate 76.2%); Isppa: $10.2 \pm 2.4\ W/cm^2$ (grand mean response rate 68.6%) or $12.4 \pm 2.8\ W/cm^2$ (grand mean response rate 38.6%) for 2 different anaesthetics.	0.6	300 ms	5-10 s	10	500 Hz	1 ms	Ispta:7.5 W/cm^2 , Isppa:14.9 W/cm^2, MI: 1.38 (not clear if in water or after cranial tx)	NR
(Guo et al., 2018)	Various target including A1 and S1 in guinea pig	US responses were related to indirect cochlear fluid pathway rather than direct activation. Similar responses were recorded in A1 and SC1 independently of the stimulated location. US evoked responses were eliminated by removing cochlear fluid.	0.22	3-360 pulses per trial	0.5-6 s	NR	10 Hz- 16 kHz (0.2-60 % duty cycle)	0.1 ms - 10 ms	Isppa: 0.3 W/cm^2	NR
(Sato, Shapiro, and Tsao, 2018)	Mouse visual cortex	Widespread neural activation through indirect auditory mechanism. Chemical deafening greatly reduced motor outputs.	0.5	80 ms	NR	NR	1.5 KHz	0.2 ms	Ispta: 4.2 W/cm^2	NR
(Lee et al., 2016)	Sheep SM1 and V1	MEP or VEPs were detected over a certain intensity threshold, which varied across animals and was always above diagnostic limits, and in some cases also above the physiotherapy limit. In both cases, higher Isppa result in stronger response amplitude.	0.25	300 ms	5s for motor cortex and 1 s for visual cortex	100	500 Hz	1 ms	Ispta:up to5,9/7.15 W/cm^2 *; Isppa=up to 11.8/14.3 W/cm^2 for SM1 and V1 respectively; MI=0.5-14 (after cranial tx)	Four animals showed micro-hemorrhages in V1 after 600 sonications at Isppa= 6.6-10.5 W/cm^2.
(Deffieux et al., 2013)	Monkey frontal eye field	Ultrasound increased antisaccade latencies in two monkeys.	0.32	100 ms	30 s	40	1 kHz	1 ms	Ispta: 0.0135 W/cm^2, Isppa: 4 W/cm^2, MI: 0.6, after cranial tx	NR

(Yang et al., 2018)	Monkey S1	Excitation effects with BOLD fMRI not only at the target but also off-target somatosensory and associated brain regions as a cause of modulation in downstream brain regions.	0.25	300 ms	3 s	10 *	2 KHz	0.252 ms	Ispta: 0.452 W/cm^2 , Isppa: 9.9 W/cm^2, MI: 1.08 (after cranial tx)	NR
(Folloni et al., 2019)	Monkey amygdala and anterior cingulate cortex (ACC)	After sonication, the functional coupling of the stimulated areas, but not of control areas, was selectively reduced. This effect was measured by fMRI and lasted for more than 1 h after stimulation.	0.25	40 s	NR	1	10 Hz	30 ms	Ispta: 15.3, 5.3 W/cm^2 , Isppa:51, 17 W/cm^2, MI: 2.64, 1.64* (after cranial tx, for amygdala and ACC respectively)	NR
(Lee et al., 2015)	Human S1	Tactile sensation that varied among subjects, mostly at the hand area controlateral to the sonicated hemisphere. 1 subject out of 12 did not report any sensation. Different peak amplitudes of EEG recording of SEP with and without stimulation.	0.25	300 ms	3 s	200	500 Hz *	1 ms	Ispta: 1.25 W/cm^2 *; Isppa=2.5 W/cm^2; MI=0.62. Simulated values (after cranial tx)	NR
(Legon et al., 2014)	Human S1	Amplitudes of sensory evoked potentials (recorded by EEG) elicited by median nerve stimulation were significantly attenuated. The spectral content of sensory-evoked brain oscillations were significantly modulated by US.	0.5	500 ms	NR	NR	1 kHz	0.36 ms	Ispta: 8.6 W/cm^2 * , Isppa: 23.9 W/cm^2, MI: 1.13, in water	NR

(Lee et al., 2016)	Human S1 and S2	Response rates of elicited sensations during US stimulation were different among subjects (S1: 68 ± 28%, S2: 59 ± 22%, average ± SD).	0.21	500 ms	7 s	20	500 Hz	1 ms	Ispta <4.4 W/cm^2, Isppa <8.8 W/cm^2 estimated (after cranial tx)	NR
(Lee et al., 2016)	Human V1	11 out of 19 participants reported the perception of phosphenes, and a clear fMRI response. EEG: 10/10 subjects reported phosphene sensation. Changes in VEP EEG peak.	0.27	300 ms	13 s (fMRI), 2.5 s (EEG)	50	500 Hz	1 ms	Ispta: 5.8 W/cm^2 *, Isppa: 11.6 W/cm^2, MI: 1.2 , simulated values (after cranial tx)	NR

1.2.4.2 *Underlying mechanisms*

In US neuromodulation, low-intensity US is delivered to neurons and results in a transient modulation of neuronal activity. It is known that the excitation and inhibition of neurons can be gated by different kind of stimuli: electrical (Hodgkin and Huxley, 1952), chemical (Fillafer and Schneider, 2016; Newman and Zahs, 1998), mechanical (Guharay and Sachs, 1984; Julian and Goldman, 1962; Newman and Zahs, 1998; Spyropoulos, 1957) and thermal (Inoue, Kobatake, and Tasaki, 1973; Shapiro et al., 2012). The existence of a mechanical pathway in the excitability of neurons provides the basis for US neuromodulation. However, to date, the mechanisms that make neurons modulate their activity when US energy is applied are not fully understood, and different hypothesis have been advanced. In subsection 1.2.2 a summary of the physical mechanisms that US exerts on tissue is given. As previously stated, the physical mechanisms that US applies on tissue can be of thermal or mechanical nature, and different mechanical effects can intervene depending on the acoustic regime and preparation. In practice, when US is applied to a complex tissue like the brain, these effects cannot be easily identified and separated. Depending on the US stimulation parameters used and the experimental conditions, one effect can be more important than the other but it is quite unlikely that only one occurs. It is therefore difficult to conclude which physical mechanism is the most likely to be responsible for neuronal modulation. In addition, it might be possible that at different US frequencies different mechanisms are responsible for coupling acoustic energy into neural activity. At high US frequencies, cavitation is unlikely to happen and an ARF-based mechanism provides a better explanation. Conversely, at low frequencies a US cavitation-based mechanism is more likely to occur.

It also remains to be assessed how cells respond to the above-mentioned physical effects. Besides potential tissue heating, the principal interface through which US affects neurons is their cell membrane. Different hypotheses have been proposed. US could trigger neuronal discharge through the following bio-effects:

- **Mechano-sensitive ion channels.** Several ion channels have mechano-sensitive properties: their activity is modulated by mechanical deformation of the cell membrane

they are embedded in (Morris, 2012) and may therefore also be modulated by US-induced mechanical deformation. It has been reported that various ion channels respond to US stimulation, including: the two-pore-domain potassium channels (Kubanek et al., 2016), the NAv 1.5 channels (Kubanek et al., 2016), the voltage-gated sodium and calcium channels (Tyler et al., 2008), the transient receptor potential channels (Ibsen et al., 2015) and the PIEZO1 channels (Prieto et al., 2018). According to the model published by Krasovistki and co-workers, the cellular membrane is capable of absorbing US mechanical energy and transforming it into periodical expansion and contraction of the inter-membrane space (Krasovitski et al., 2011). According to this model, the bio-effect of US is dependent on the tension that US applies to the membrane. At relatively low membrane tension, US first activates mechano-sensitive proteins embedded in the cell membrane (state S_1, Figure 16), and then, with increasing intensities, it leads to pore formation and finally membrane rupture.

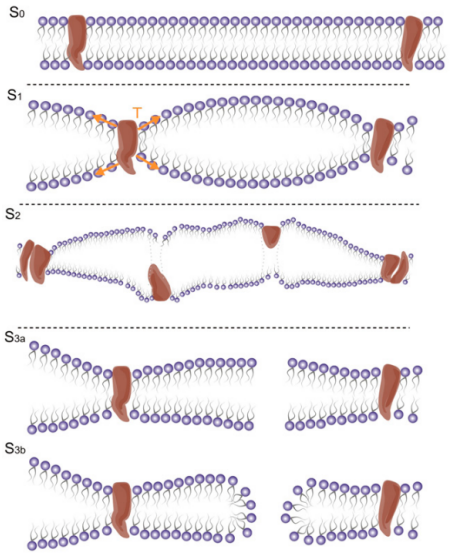

Figure 16: **Effects of US-induced tension on cell membrane according to Krasovitski's model.** S_0, reference stage, S_1 US-induced tension leads to mechano-sensitive ion channel opening, S_2 increasing tension can damage membrane proteins and induce pore formation or membrane disruption (S_3a,b). Source: (Krasovitski et al., 2011)

- **Sonoporation.** US stimulation could also cause the opening in the cell membrane of transient physical pores lead-

ing to ion transport driven by the gradients across the membrane. The probability of pore formation depends on its compressibility and specific heat (Blicher et al., 2009; Wunderlich et al., 2009). The combination of US stimulation and micro-bubbles enhances the modulatory effects on neurons (Li et al., 2018), potentially via pore formation. However, US-induced micro-bubble cavitation may also cause unwanted side-effects and is therefore generally avoided.

- **Changes in membrane capacitance.** The electrical properties of the cell membrane at rest can be approximated to those of a parallel plate capacitor. Neurons have a capacitance that depends on membrane properties (Petrov, 2002; Taylor et al., 2017). US has been shown to be capable of inducing capacitive currents in lipid membranes through their conformational changes resulting in either excitatory or inhibitory currents when compression or dilation are applied respectively (Prieto et al., 2013). It has also been suggested that US may lead to nucleation of bubbles and cavitation inside the lipid bilayer resulting in capacitive currents (Plaksin, Shoham, and Kimmel, 2014).

- **Thermal effects.** As absorption of ultrasonic energy can lead to temperature increases, US stimulation can lead to thermal neuromodulation. Neural activity can indeed be affected by temperature changes in the order of a few degrees (Lee, Callaway, and Foehring, 2005). Moreover, ion channels with heat-sensitive properties (Cesare et al., 1999) exist and could also be involved in this kind of response.

Given the complexity of a biological tissue like the brain, it is likely that a combination of different mechanisms might lead to the modulation of neuronal activity through US and that their relative contributions may change depending on the acoustic parameters used. It is evident that, to further develop and optimize US neuromodulation, a mechanistic understanding of the underlying mechanism is of fundamental interest.

1.2.4.3 *Limits*

Despite its non-invasiveness and high penetration capacity, US neuromodulation has several limitations for brain applications:

- **Spatial resolution** is directly proportional to US frequency. To be non-invasive and to reach a specific target in the brain, US has to be delivered through the skull bone that represents a high acoustic impedance mismatch because of its multi-layered structure composed by a compact and hard shell and an inner spongy bone layer with a trabecular structure. As a consequence, strong scattering occurs at US frequencies above 1 MHz (Pinton et al., 2012). To avoid attenuation and US beam aberration, the range of US frequencies that can be used for effective transcranial stimulation is therefore limited and does not permit to attempt high spatial precision. To date, high spatial resolution US stimulation has not been achieved successfully *in vivo* also because higher US carrier frequency require higher energies causing possible side effects like heating (Ye, Brown, and Pauly, 2016) or haemorrhages (Lee et al., 2016). Additionally, low frequency US has been found to be more effective. Two studies found that the probability of observing behavioral responses to US stimulation of the motor cortex in mice was higher at lower US frequencies (King et al., 2013; Ye, Brown, and Pauly, 2016). This phenomenon could be explained by the fact that increasing US frequencies a smaller brain zone is activated, also lowering the probability of stimulating neurons that are involved in the behavioral response (Kubanek, 2018). Because of the above-mentioned reasons US neuromodulation with high spatial resolution still remains unexplored and difficultly implementable.

- **Off target stimulation.** Recently, two independent studies showed that US stimulation can cause indirect activation of the auditory system (Guo et al., 2018; Sato, Shapiro, and Tsao, 2018). Although the frequencies used for US stimulation are not in the audible range, they may produce harmonics at lower frequencies that could be transmitted to the ears. In addition, standing wave phenomena can arise at low-frequency US because of reflections of the waves inside the skull leading to complex pressure fields and to the activation of brain areas outside the target location (Baron et al., 2009; Constans et al., 2017; Younan et al., 2013). These phenomena are more likely to happen especially in small animal models because of the small size of the braincase, leading to possible indirect activation of non-targeted structures.

- **Side effects and safety**. US stimulation may generate unwanted side effects, depending on the acoustic regime that is used and the experimental setup. Potential adverse effects that have been considered in the literature include: Blood-Brain Barrier (BBB) opening, bleeding, cell damage and irreversible effects on physiological neural activity. These side effects can be caused principally by either US-induced cavitation or tissue heating. Concerning BBB opening, no actual cases have been reported by any of the studies that investigated this potential side effect (Kim et al., 2012; Lee et al., 2018; Yoo et al., 2011). On the other hand, local micro-haemorrhages have been reported in rats (0.35 MHz US, $I_{\text{sppa}} = 22.4\ W/cm^2$, $MI = 1.38$) (Kim et al., 2014) and sheep for repeated stimulations (500 trials, 1 s inter stimulus interval) (Lee et al., 2016), following US stimulation. Acoustic intensity and inter-stimulus intervals appear to be important parameters to consider when designing a US sequence, in order to avoid potential bleeding. Concerning cell damage, US stimulation did not provoke any tissue damage in several works both *in vivo* and *ex vivo* (Dallapiazza et al., 2018; Mehić et al., 2014; Tufail et al., 2010; Tyler et al., 2008). While no irreversible effect on neural activity has been reported, long-time effects after US stimulation have been reported. Yoo and co-workers reported an inhibitory effect that lasted several minutes after stimulation on rats for long sonication durations (9 s) (Yoo et al., 2011). Another study found that somatosensory evoked potentials required up to 20 minutes to return to baseline (Dallapiazza et al., 2018). Yang and co-workers observed reduced extracellular GABA level up to 100 minutes after sonication (Yang et al., 2012). Two related works on primates (Folloni et al., 2019; Verhagen et al., 2019) observed changes in functional connectivity after long sonications (40 s), which lasted 1 hour after sonication.

While undesired side-effects appear to be controllable by accurately choosing the acoustic regime, limited spatial resolution and off-target stimulation remain major limits of US neuromodulation.

1.3 SONOGENETICS

The aim of sonogentics is to sensitize neurons to US waves through the expression of US-sensitive proteins on the cell membrane via gene therapy. The main assumption of this approach is that US waves are able to induce local temperature increase or mechanical displacement of the cell membrane, which leads to the activation of mechano-sensitive or thermo-sensitive proteins. The activation of these proteins leads subsequently to the influx of ions and cell discharge. Sonogenetics has the main aim of overcoming the current limits of US neuromodulation listed in the previous section. By the selective expression of US-sensitive actuators, it would be possible to target a specific subpopulation of neurons. Moreover it would be possible to lower the required activation threshold via the over-expression of the US-sensitive proteins. Lowering of the required US energy would prevent undesired side effects and, more importantly, would enable the use of higher US frequencies, hence the attainment of higher spatial resolution.
In the following section an overview about the state of the art of sonogenetics is presented.

1.3.1 *State of the art*

The concept of sonogenetics was introduced for the first time by Ibsen and co-workers in 2015 (Ibsen et al., 2015). In their study a pore-forming subunit of a mechano-transduction channel (TRP-4) was shown to be able to respond to low-intensity US stimulations when combined with micro-bubbles application. The nematode *C. elegans* expresses the TRP-4 channels naturally to sense when its body is stretching. When the worm stretches, the channels open and allow the flow of calcium. The ectopic neuron-specific expression of TRP-4 channels made the neurons sensitive to the mechanical deformation induced by US, resulting in behavioral outputs in *C. elegans*. However, US-induced bubble cavitation was necessary to induce behavioral changes, making this approach hardly applicable to the mammalian brain. Microbubbles have a short lifespan *in vivo* (<5 minutes in blood), are difficult to deliver to extra-vascular tissues and their US-induced cavitation might cause undesired effects, such as BBB opening. Nonetheless, the approach introduced by Ibsen et al. advanced, for the first time, the possibility of selectively and non-invasively stimulating genetically sensitized neurons with US.

While most of the published studies investigated the sonogenetic approach *in vitro* (Prieto et al., 2018; Qiu et al., 2019; Ye et al., 2018), recent studies have reported that three different sonogenetic actuators can be used to control brain activity *in vivo* in mice.

The *TRPV*1 channel has been proposed as a US-actuator for sonogenetics (Yang et al., 2020). This channel is not sensitive to US-induced mechanical stress directly but is sensitive to US-induced heating of tissue. According to the work of Yang and co-workers the induced tissue heating (around 42°*C*) is safe on mice brain based on neuronal integrity, apoptosis and inflammation markers. However, since many neuronal circuit processes are temperature-dependent it remains to be assessed whether the heating might affect neuronal activity. Indeed, modest tissue heating has been found to be sufficient to inhibit neural activity and affect behavior (Owen, Liu, and Kreitzer, 2019). Furthermore, the US-induced heating did not provide a fast response controlled in time.

Two other recent studies by the same group used an engineered auditory-sensing protein, Prestin, to modulate neural activity with US *in vivo* in mouse brain (Huang et al., 2020; Wu et al., 2020). Prestin is not directly an ion channel, it is a transmembrane protein residing in the outer hair cells of the cochlea and is believed to act as an electromechanical transducer and to be involved in high-frequency hearing. Prestin is highly associated with actin filaments and microtubules in cells and its US-induced oscillation leads indirectly to calcium influx and cell discharge. Prestin has been able to induce neural activation only at 0.5 MHz and not at other US frequencies (i. e. 80 kHz, 1, 2, 3.4 MHz).

Following previous *in vitro* studies (Maresca et al., 2018; Ye et al., 2018), Qiu and coworkers demonstrated very recently that a mutated form of the mechano-sensitive Mechano-sensitive channel of Large conductance (MscL) ion channel (G22S mutation) is able to sensitize cortical neurons *in vivo* to low-frequency and low-intensity US. Ultrasonic stimulation was able to evoke muscular responses and targeted c-Fos expression (Qiu et al., 2020). If this work validates the use of the MscL ion channel as a valid sonogenetic actuators, investigation about its temporal resolution and its ability to increase spatial resolution is still missing.

Thus, while these studies reported for the first time an application of sonogenetics *in vivo*, on the other hand they failed to

increase the spatial and temporal resolution of US stimulation. In the following Table 2 a summary of the published studies on sonogenetics approaches is presented.

Table 2: **Overview on Sonogenetic literature.** For US parameters: * states that a given parameters has been calculated from the one given in the reference.

Experimental preparation				Sonogentic preparation			US parameters						
Reference	**Target**	**Measured effects**	**Temporal latency of the response**	**Sonogenetic actuator**	**Mechanism of action upon US stimulation**	**Transfection method**	**US frequency (MHz)**	**Sonication duration**	**Inter stimulus interval**	**Pulse repetition frequency**	**Duty Cycle**	**Acoustic intensity**	**Peak negative pressure (MPa)**
(Ibsen et al., 2015)	*C. elegans*	Neuron-specific mis-expression of TRP-4 in *C. Elegans* sensitizes neurons to ultrasound stimulus in presence of microbubbles, resulting in behavioural outputs.		TRP-4	TRP-4 is a stretch-sensitive pore-forming cation channel that opens upon US induced stretch of cell membrane	Plasmid transfection	2.25	10 ms			Continuous	Ispta/Isppa: 54 W/cm^2*	0.9
(Ye et al., 2018)	Cultured rat hippocampal neurons	Low pressure ultrasound pulses activate neurons expressing MscL. The gain-of-function MscL mutation, I92L, lowered the pressure activation threshold.	Latency is dependent on the peak negative US pressure (26.8 ± 4.1 ms at 0.45 Mpa)	MscL I92L (increased mechano-sensitivity) form *E.coli*	US induced stress on the bilayer's internal profile cause a helix movement and the opening of a pore of 30 Åin diameter, allowing the passage of ions and small molecules	Lentiviral vector	29.92	50-400 ms	0.1-1 s			Ispta,Isppa: 13.5 W/cm^2 *	0.45
(Prieto et al., 2018)	Chinese hamster ovary cells and HEK cells	Piezo1 channels are activated by continuous wave US at 43 MHz and 50 or 90 W/cm^2 through cell membrane stress caused by acoustic streaming.		Piezo1	Acoustic streaming caused by US stimulation cause channel opening and ion influx	Plasmid transfection	43	200 ms			Continuous	I: 90 W/cm^2	
(Qiu et al., 2019)	HEK293T	Ultrasound activates Piezo1 expressed in HEK293T and neurons increasing Ca2+ influx and C-fos levels. Ca2+ influx depends on acoustic pressure.		Piezo1	US induced stress on the bilayer's internal profile cause channel opening an ion influx	Plasmid transfection	0.5	200 ms	10 s	1 kHz	40% DC	Ispta: 6.66 W/cm^2 *	0.5

(Yang et al., 2020)	HEK293T cells and mouse brain (somatosensory cortex)	Ultrasound can selectively activate cells in vitro and neurons in vivo when they are genetically modified to express TRPV1. TRPV1 is activated by spatiotemporal control of ultrasound induced heating and requires long stimulus durations (>4s).	Latency of several seconds dependent on stimulus duration (2.1± 0.3 s for 4 s continuous wave stimulation)	TRPV1	Sensitive to temperature rise, opens if temperature raise>42°C	Lentiviral vector	1.7	7-15 s (for pulsed sonication), 1-4-7 s (for continuous sonication)	80 s	10	40% DC	Ispta: 45 W/cm^2, 112.6 W/cm^2 for pulsed and continuous sonication respectively *.	1.3
(Huang et al., 2020)	HEK293T cells and mouse brain (VTA region)	Low pressure ultrasound induced calcium responses in cultured cells expressing Prestin protein and can non-invasively stimulate target neurons in deep brain regions in mice expressing Prestin.		Engineered mPrestin(N7T, N308S mutations). Prestin is a trasnmembrane protein of the outer hair cell	Prestin oscillation induced by US can create calcium influx and amplify it thanks to a positive feedback loop due to its electromotility	Plasmid transfection (in vitro), AAV vectors (in vivo)	0.5	3 s (in vitro), 5 s (in vivo)		10 Hz	25% DC*	Ispta: 4.16 W/cm^2 *	0.5
(Wu et al., 2020)	Mouse brain	Neurons with Prestin expression stimulated with US were 6-fold more likely to exhibit c-Fos staining than cells without Prestin expression.		Engineered mPrestin(N7T, N308S mutations). Prestin is a trasnmembrane protein of the outer hair cell	Prestin oscillation induced by US can create calcium influx and amplify it thanks to a positive feedback loop due to its electromotility	US induced BBB opening to deliver prestin encoding plasmid loaded into microbubbles	0.5	1 min		1 Hz	1% DC*	Ispta: 0.16 W/cm^2 *	0.5

(Qiu et al., 2020)	HEK293T cells, cultured mouse primary neurons, Mouse brain	The expression of the MscL G22S channel led to Ca^{2+} influx and activation in cultured neurons and HEK cells. *In vivo*, expressing MscL G22S into cortical neurons (M1 region) and the dorsomedial striatum led to EMG responses and to a targeted up-regulation c-Fos following US stimulation compared to control animals.		MscL ion channel (G22S mutation).	The MscL channel is a non selective mechano-sensitive ion channels that opens with US-induced mechanical deformation of cell membrane.	Plasmid transfection (in vitro), AAV vectors (in vivo)	0.5	300 ms	10 s	1 kHz	40% DC*	Isppa: 0.08-8.11 W/cm^2 *	0.05-0.5 MPa

1.3.2 *Selecting the right sonogenetic actuator*

To develop sonogentics as a potential tool to be used to control neural activity, the major challenge is to find the suitable sonogenetic actuator: the ion channel or protein that is activated by the mechanical stress or heating induced by US waves. Selecting an actuator that directly responds to the physical deformation induced by US, such as a mechano-sensitive ion channel, seems to be more appealing if the goal is to obtain fast and precise control of neurons.

Ion channels are proteins embedded in cell membrane that provide a passageway through which ions can cross the plasma membrane. These ion channels have the ability to open or close in response to chemical or mechanical signals and thus permit the rapid movement of ions from the outside to the inside of the cell or vice versa, leading to the generation of an electrical signal. In nature, several ion channels that are able to respond to mechanical stimuli exist and play an important role in transducing physical stress on the cell membrane into an electrochemical response. They enable cells to respond to external stimuli such as touch, sound, gravity and pressure or to internal stimuli like osmotic pressure and membrane deformation, which are responsible for cell growth and health (Hamill and Martinac, 2001; Sukharev and Corey, 2004). However, with some exceptions, the identification and characterization of these mechano-transducing channels remains elusive.
The mechanical activation of ion channels is thought to be mediated by forces that are directly transmitted by the lipid bilayer or by auxiliary proteins (Kung, 2005). The manner in which the cell membrane and the proteins interact in mechano-sensation has been elucidated only in the case of the bacterial Mechano-Sensitive (MS) channels (MscL and Mechano-sensitive channel of Small conductance (MscS)[1]). The characterization of these bacterial channels has been successful because they respond directly to membrane stretch and changes in osmolarity without the need for any other protein (Sukharev et al., 1994). For eukaryotic

1 Mechano-sensitive channels can be described as the tension-dependent equilibrium between two states, closed and open, that differ in conductance (Sukharev et al., 1997). The conductance (G) of a MS channel is a relevant property that determines the sensitivity of the membrane's tension-dependent response. It is defined as the ratio between the ionic current (I) flowing through the channel and the voltage drop (V) across the cell membrane ($G = I/V$, I and V are expressed in Amperes and Volts and G in Siemen).

channels, mechano-sensitivity may require protein complexes or interaction with specialized cytoskeleton and extracellular matrix, rendering these assessments more complicated (Árnadóttir and Chalfie, 2010).

To date, several ion channels are thought to have MS properties, but only few candidates have been fully characterized and meet all the qualifications to be considered transducers of mechanical forces (Árnadóttir and Chalfie, 2010). In Table 3 a summary of the eukaryotic and bacterial proteins that are known to be involved in mechano-transduction is given: the degenerin/epithelial sodium channels (DEG/ENaC) family, the two-pore domain potassium channels (K2P), the transient receptor potential channels (TRP), the Piezo family and the MS bacterial channel family. MscL and MscS are the only known channels that directly respond to membrane tension changes by opening nanoscale protein pores through the interactions between the trans-membrane domain of the proteins and the lipids of the cell membrane (Kung, Martinac, and Sukharev, 2010). Changes in the thickness or composition of the phospholipid bilayer inducing spontaneous membrane curvature directly have an impact on the tension that is required to open MscL (Perozo et al., 2002). The conductance values of bacterial MS channels are several orders of magnitude higher than those of other ion-selective channels because of their larger-diameter pore in the open state.

Table 3: **Mechano-sensitive ion channels overview.**

Channel	Role	Selectivity	Expression	Mechanical gating
DEG/ ENaC channels family (eukaryotic)				
MEC-4 and MEC-10	Senses touch (Árnadóttir and Chalfie, 2010)	Na+ ions	Found in touch receptor neurons (Huang and Chalfie, 1994)	Not possible in a heterologous expression system in vitro (Goodman et al., 2002)
ENaC	Responds to shear stress and fluid flow (Árnadóttir and Chalfie, 2010)	Na+ ions	Renal Epithelia (Duc et al., 1994)	Responds to fluid flow in oocytes (Carattino, Sheng, and Kleyman, 2004)
K2P channels family (eukaryotic)				
TREK-1	Mechanosensation in skin and vascular system, polymodal channel, activated by mechanical force, temperature, and pH (Maingret et al., 1999)	K+ ions	Widely expressed in brain (Fink et al., 1996), small sensory neurons (Alloui et al., 2006) and vasculature (Garry et al., 2007)	Activated in response to applied pressure, osmolarity, and modulators of lipid bilayer curvature in heterologous cells (Patel et al., 1998)
TREK-2	Unclear role (Árnadóttir and Chalfie, 2010)	K+ ions	Pancreas, kidney; lower levels in brain, testis, colon, and small intestine (Bang, Kim, and Kim, 2000; Lesage et al., 2000)	Activated in response to pressure in heterologous cells (Bang, Kim, and Kim, 2000)

TRAAK	Unclear role (Árnadóttir and Chalfie, 2010)	K+ ions	Neurons (Maingret et al., 1999)	Activated in response to pressure in heterologous cells (Maingret et al., 1999)
TRP channels family				
TRPA,TRPC, TRPM, TRPML, TRPN; TRPP; TRPV	Involved in touch, hearing, nociception, proprioception, osmosensation,pressure sensing (Árnadóttir and Chalfie, 2010). Polymodal, activated by numerous stimuli (voltage, temperature and small molecules) (Delmas and Coste, 2013)	Non selective cation channels	Neurons, cilia, hair cells, brain, kidney, vasculature (Árnadóttir and Chalfie, 2010)	TRPA1 can be activated in vitro by osmotic stimuli (Zhang et al., 2008). Heterologously expressed TRPV4 is activated by hypo-osmotic solutions and inhibited by hyper-osmotic solutions (Strotmann et al., 2000)
Piezo channels family				
Piezo1, Piezo2	Involved in membrane indentation and membrane stretch-induced currents (Coste et al., 2010)	Non selective cation channel	Lungs, kidney, DRG neurons	Heterologous expression sufficient to confer robust mechanically activated currents in naive cells (Coste et al., 2010)
Ms channels family (bacterial)				
MscS- MscL	Regulation of osmotic pressure changes (Haswell, Philipps, and Rees, 2011)	Non selective channel	Prokaryotes (Kung, Martinac, and Sukharev, 2010)	Lipid tensions provides the activating force (Sukharev et al., 1999; Sukharev, 2002)

For sonogenetics, a MS channel serves as a nano-valve that opens when the cell membrane is deformed by the ultrasonic wave. To develop an effective sonogenetic strategy, the choice of mechano-sensitive ion channel is crucial. Firstly, the protein should be easily expressed in the neurons. Thus, its gene should be small enough to be packed into AAVs vectors, the leading platform for targeted gene delivery *in vivo*, characterized, however, by a relatively limited cloning capacity (approximately 4.7 Kb). Secondly, its gating mechanism should be known and a fast gating kinetics is preferable, in order to better adjust and optimize US stimulation. Thirdly, the channel should be sensitive only to mechanical deformation, in order to exclude secondary non-mechanical activation pathways.
Different MS ion channels have been proposed and tested *in vitro* as potential sonogenetic actuators: TREK-1 (Kubanek et al., 2016), MscL (Qiu et al., 2020; Ye et al., 2018) and Piezo1 (Prieto et al., 2018; Qiu et al., 2019).
TREK-1, like most mechano-sensitive ion channels, displays an intrinsic sensitivity to other external stimuli (heat, voltage, pH, etc.) besides mechanical stimuli. For sonogenetics, selecting a channel that is exclusively mechano-sensitive has the advantage of excluding other potential non-mechanical effects. Furthermore, the neural over-expression of non-exclusively MS ion

channels could compromise the physiology of neural circuits. On the other hand, only a few ion channels respond exclusively to mechanical stimuli such as the mammalian Piezo channels (Coste et al., 2010) or the bacterial Mechano-sentive channels (Msc family, including MscL) (Perozo et al., 2002; Sukharev et al., 1993). Thus, the Piezo 1 and MscL channels seem more suitable for sonogenetics. However, expressing Piezo channels *in vivo* is challenging because of their large size and complexity (Coste et al., 2010). Because of their size Piezo1 cannot be easily packed into AAVs rendering it difficult to deliver them efficiently *in vivo*. The MscL channel appears therefore as a more promising candidate for being the mechano-transducting element for sonogenetics.

1.3.3 *The Mechano-sensitive channel of Large conductance (MscL)*

The MscL channel appears to be an interesting candidate for sonogentics; it is found in bacteria and has been widely investigated and characterized in terms of biophysics, genetics and structure (Hamill and Martinac, 2001; Perozo, 2006; Sukharev, 2001; Sukharev et al., 1994). The MscL channel is a homopentamer where each subunit contains two trans-membrane α-helices and a cytoplasmatic α-helix (Chang et al., 1998) (Figure 17). This channel is a non-selective and is able to rapidly open when a mechanical stress, over the threshold of channel gating, is applied to the cell membrane (Sukharev, 2001) (Figure 17). When stretch is applied to the cell membrane, a helix movement is caused and a pore of approximately 30 Å opens and allows the passage of ions and small molecules (Perozo et al., 2002; Rosholm et al., 2017; Sukharev, 2001). In bacteria, the MscL channel participates in the regulation of osmotic pressure changes within the cell (Haswell, Philipps, and Rees, 2011).

A large collection of engineered MscL mutants has already been developed, providing a versatile tool for further adapting and developing sonogenetics. For instance, the gain-of-function mutant MscL G22S presents a mutation of a glycine residue, positioned within the constriction that closes the protein's pore, into a hydrophilic residue (serine) and presents a lower pressure threshold at which the channels opens compared to Wild-Type (WT) MscL (Yoshimura et al., 1999). The *E. coli*-derived MscL has been expressed in cultured primary neurons and has been shown to be effective in sensitizing neurons to mechanical stim-

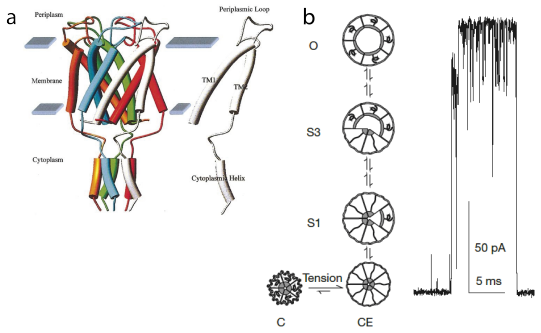

Figure 17: **The MscL channel's structure and gaiting.** (a) Drawing of the MscL pentamer (left) and monomer (right) from *M. Tuberculosis*. (b) MscL gating. The channel has five identical subunits, each contributing to the closed gate assembly in the centre and the elastic outer rim on the periphery. The trans-membrane rim must expand substantially before stress in linkers that connect the rim to the gate pulls the gate assembly apart. The channel reaches the open conformation (O) through a series of short-lived subconducting states (S1, S2, etc.) as the central gate breaks apart. A typical single MscL current (right) recorded at -50 mV shows an opening through a substate followed by flickering to substates once the channel has opened. Source: (Hamill and Martinac, 2001; Sukharev, 2001)

uli. The G22S mutation was expressed in neurons that were able to respond even at lower pressure levels *in vitro* compared to neurons expressing the WT form (Soloperto et al., 2018). Recently, the same mutation has been shown to be able to sensitize neurons to low intensity US stimulation *in vitro* and *in vivo* in mice (Qiu et al., 2020). Another mutation of the MscL channel, the I92L mutation, has been shown to be able to induce cultured neurons to respond at very low US pressure values (0.25 MPa) with a millisecond temporal precision up to 5 Hz (Ye et al., 2018).

The MscL channel represents therefore a suitable choice for sonogentics, firstly because it is to date the most thoroughly analyzed and characterized mechano-sensitive channel and, secondly, because of its small gene, it can be easily packed into AAVs vectors, allowing its targeted delivery *in vivo*. Furthermore, because of it simple sub-molecular structure, a large collection of MscL mutants with different sensitivities has already been designed and could be used to fulfill different experimental needs (Blount et al., 1996; Maurer and Dougherty, 2003; Yoshimura

et al., 1999). The heterologous over-expression of this bacterial channel on mammalian cell membrane could therefore selectively sensitize neurons to ultrasound, enabling the targeting of specific populations of neurons also in deep brain regions and overcoming the spatial resolution limitations of US stimulation only.
Even if its application for *in vivo* sonogenetic stimulation was refuted in a review on this emerging field (Maresca et al., 2018), the recent study of Qiu and co-workers confirmed its potential as sonogenetic actuator for *in vivo* use (Qiu et al., 2020).

1.3.4 *AAV gene therapy for sonogenetics*

Gene therapy uses viruses (such as the lentivirus, adeno-virus or adeno-associated virus) or other non-viral vectors (such as nanoparticles) to deliver genes to cells or tissue. AAVs represent nowadays the leading delivery platform for genetic material. This popularity is based on their non-pathogenic nature and their excellent safety profile rendering them a powerful tool both in research and clinics. AAVs are composed of an icosahedral protein shell surrounding and protecting a single-stranded DNA genome of approximately 4.7 kilobases with two open reading frames (rep and cap) surrounded by two inverted terminal repeats (ITRs, critical components facilitating genome packaging and transcription) (Dong, Nakai, and Xiao, 2010). To replicate, AAVs are dependent on co-infection with other viruses, mainly adenoviruses. AAVs can be easily engineered to obtain recombinant AAVs (rAAVs). rAAVs particles lack viral DNA and serve basically as protein-based nanoparticles loaded with the gene of interest. They are able to cross the cell membrane and deliver their DNA cargo to the nucleus of the host cell. rAAVs are engineered so that they lack the Rep gene that encodes the proteins that are required for viral genome replication and packaging. rAAVs are therefore replication-defective viruses. Thus rAAV form episomal DNA that persists in the nucleus of the transduced cell but does not integrate with the host genome (Choi, McCarty, and Samulski, 2006). The episomal DNA introduced by rAAV will be eventually diluted over time as the cell replicates, resulting in the eventual loss of the transgene expression with a delay that depends on the turnover of the transduced cell. Unlike most cell types, neurons are generally considered as quiescent cells, thus the DNA introduced by AAVs will be

expressed for a long time, making AAV the vector of choice for many nervous targets.

To obtain high efficiency and cell-type specific expression of the transgene of interest, different features must be considered when designing an AAV vector: the viral dose, the viral capsid, the design of the viral genome and the animal model and the route of administration (Schön, Biel, and Michalakis, 2015). The vector genome plays a critical role in the efficiency of transgene expression. The minimal components that are required in the AAV genome are the two ITRs that flank the gene of interest. Additional regulatory sequences such as promoters[2] are inserted in the genome to drive expression. Commonly used promoters that lead to high-level expression of the gene of interest are the CMV (cytomegalovirus) promoter, EF1a (elongation factor 1a) and the CAG promoter (Powell, Rivera-Soto, and Gray, 2015). To drive cell-specific expression, specific promoters have been developed to achieve high level of expression in targeted cell types. The SNCG promoter, based on the regulatory region of the gamma-synuclein gene, has been shown to drive strong expression in retinal ganglion cells across different species: from mice to non-human primates (Chaffiol et al., 2017). The CaMKII promoter is a neuron-specific promoter that has been shown to be effective in transducing efficiently cortical neurons by different AAV serotypes in different species (Watakabe et al., 2015). The viral capsid has a determining role in host response, cell attachment, cell entry, escape from the endosome, nuclear trafficking and release from the genome to the nucleus (Hudry and Vandenberghe, 2019). Combined, these features render the capsid determining for cellular tropism and expression kinetics. Moreover, engineered variations of the capsid can further enhance certain features such as tropism and alter transduction efficiency dramatically. Various natural-occurring AAV serotypes exist and vary in their transduction efficiency and specificity for different cell types (Rabinowitz et al., 2002). For example, AAV2 has been the first serotype successfully used in retinal gene transfer for RPE cells and RGCs (Auricchio et al., 2001). To optimize the AAV's gene transfer functionality for specific applications, different approaches have been developed. For instance, to improve

2 A Promoter is a site in a DNA molecule at which RNA polymerase and transcription factors bind to initiate transcription of messenger RNA. A cell-specific promoter performs its function only in a certain cell type and makes it possible to restrict transgene expression.

AAV capsid properties, random mutageneses of wild-type AAC capsids have been screened to find some with specific features. The 7m8 AAV2 variant has been created with this technology and it is able to efficiently transduce photoreceptors and RPE cells through intra-vitreal injection (Dalkara et al., 2013).

In conclusion, AAVs have become the standard tool for gene delivery into the central nervous system because they benefit from strong neuronal tropism and a good safety profile. They have been widely used to transduce neurons with optogenetic molecules to manipulate neural circuits (Fenno, Yizhar, and Deisseroth, 2011) and they have been proved to be most suitable vector to deliver efficiently and drive a long-lasting expression of the transgene in retinal cells (Boye et al., 2013). AAVs appear therefore to be the best choice also for transducing mechano-sensitive proteins into neurons for sonogenetics.

1.4 MAIN OBJECTIVES OF THE THESIS

The aim of this work was to investigate whether the sonogenetic approach might be applied for vision restoration, i. e. might be used to stimulate the neurons of the visual cortex selectively, with high spatio-temporal resolution.
To pursue this final aim the following research objectives have been defined:

- Identify a suitable mechano-sensitive channel for sonogenetics and its expression in neurons. To develop sonogenetics it is necessary to accurately choose an US sensitive channel. This channel has to be expressed into the neuron's membrane with a sufficient expression rate and its gating mechanism should be activated by mechanical deformation induced by US waves.

- Investigate the ability of the mechano-sensitive channel to be activated by US stimulation. After the selection of the mechano-sensitive channel, it has to be determined whether it can be reliably activated by US waves when expressed in neurons. Moreover, it has to be established whether it expression leads to increased US sensitivity compared to US stimulation alone.

- Determine effective ultrasonic stimulation parameters. As discussed in subsubsection 1.2.4.1 a wide set of acoustic parameters have been used to stimulate neurons with US in different experimental preparations. An analysis of the different stimulation protocols is necessary to determine whether an optimal stimulation exists for sonogenetics. Defining a subset of optimal stimulation parameters would also make it possible to make assumptions on the potential underlying bio-physical mechanism of ultrasonic neurostimulation.

- Test the spatial and temporal resolution of the sonogenetic approach. To use US stimulation as a tool in vision restoration and achieve high-quality visual perception, higher spatial resolution than that currently offered by US neuromodulation is necessary. One of the main interests in developing sonogenetics is indeed the increase in spatial resolution given by the cell targeting and the increased sensitivity to US of high frequencies. It is therefore important to verify whether sonogenetics can provide higher

spatial resolution. Moreover, it must be verified that high temporal resolution can also be reached, as this is another important factor in vision restoration. The human visual system has indeed a high temporal dynamics: the cortical neurons in the visual areas are able to process information with a millisecond resolution (Bair and Koch, 1996) and high refresh rates are essential for the perception of moving stimuli (Kime et al., 2016). Moreover to enhance the quality of vision restoration provided by visual prostheses not only spatial resolution but also temporal resolution have to be improved to be used in dynamic environments (Kime et al., 2018).

- Validation of the sonogenetic approach *in vivo* in the depth of the visual cortex. Ultimately it has to be determined whether this approach can also be applied efficiently *in vivo* for the stimulation of neurons of the visual cortex without inducing any side-effect.

To attempt these goals, first the sonogenetic approach was tested and characterized in the isolated retina, a reliable and easily acessible neuronal network. Next, we extended the sonogenetic strategy to an *in vivo* brain structure using the rat visual cortex. In the next chapter the main experimental results of this work are presented, followed by a general discussion of these findings and perspectives.

Part II

Precise sonogenetic stimulation for vision restoration

2

PRECISE SONOGENETIC STIMULATION FOR VISION RESTORATION

2.1 SUMMARY

The main aim of this work was to develop a proof of concept of sonogenetics as a brain-machine interface to stimulate the primary visual cortex for vision restoration. We identified the MscL channel as a potential sonogenetic actuator and decided to investigate its effects in sensitizing neurons first in a natural neuronal circuit that is easily accessible, the retina, and then *in vivo* in the primary visual cortex of rats.

The MscL channel in its wild-type (WT) and mutated form (G22S) has been expressed efficiently in RGCs of rat retina (Figure 1 A-D). The expression of MscL on RGCs induced sustained responses to high-frequency US (15 MHz) with short latencies (Figure 1 F-left-G) and rapid return to the control levels after the US OFFset. The MscL channel increased the retina's sensitivity to lower US pressures compared to the non-transfected retina (Figure 1 I). Blocking synaptic transmission suppressed all US-elicited responses in the non-transfected retina but maintained the short latency responses in the MscL-tranfected retina (Figure 1 L). MscL-transfection of blind P23H[1] led to US-evoked responses but not for non-transfected retina (Figure 1 L). These results demonstrate that the short-latency responses observed in the MscL-transfected retina were induced by the MscL channel expressed in RGCs.

The G22S mutation of the MscL channel further enhanced the US sensitivity of RGCs to lower US pressures compared to the MscL WT form (Figure 1 K). Neurons were able to respond with high temporal resolution to stimuli as short as 10 ms (Figure 2 A-C) and were able to follow the rhythm to stimulus repetition rates up to 10 Hz (Figure 2B-E). When comparing with stimuli of different US frequencies 15 MHz stimulation was able to elicit responses from a much more confined area compared to 0.5 and 2.25 MHz (Figure 2 F) with a weighted mean distance between

1 The P23H is a rat model for autsomal dominant retinitis pigmentosa.

cells of 0.59 ± 0.03 mm, consistent with the size of measured US pressure fields. When the US stimulus was moved above the retina a shift in the responding cells was triggered in accordance with the displacement of the US transducer (Figure 2 I-J). These results on isolated retina demonstrated that the MscL-based sonogenetic approach is able to lead to direct depolarization of transfected neurons with high spatiotemporal resolution stimulation an essential feature for vision restoration.

We then explored the ability of this approach to stimulate directly neurons of the visual cortex in rats. MscL G22S was successfully expressed in cortical neurons of V1 as indicated by the red fluorescence of the reporter gene tdTomato on the brain or on brain sections (Figure 3 A-C). US-evoked local field potentials were recorded using an µECoG electrode array placed directly on the primary visual cortex. 15 MHz US stimulation was not able to evoke any response in non-transfected animals whereas it produced large negative potentials when the sonogenetic actuator was expressed (Figure 3 E). The size of the US responding cortical area varied with the US pressure and was as small as 0.35 ± 0.19 mm^2 for the smallest pressure value (Figure 3 L). Again, as observed in the retina, the activated area moved when the stimulus was shifted (Figure 3 M). By recording neurons with intra-cortical multi-electrode arrays we were able to record also the US evoked response of neurons in different layers of V1. In the cortical depth, neurons responded to US stimuli as short as 10 ms with rapid return to the control level at the stimulation OFFset. Neurons were even able to follow a stimulation rate up to 13 Hz (Figure 3 O).

These *in vivo* results confirmed that MscL based sonogenetics is able to locally activate neurons of the visual cortex with a good spatial and temporal resolution and with US pressure values that were not able to elicit a response in control animals. Moreover, the acoustic energy that has been used did not induce any undesired tissue heating (Figure E4). With this study we provide to our knowledge the first *in vivo* evidence that the MscL channel is adapted for high spatiotemporal sonogenetic activation. This approach appears to be promising tool not only for vision restoration but also to treat all neurological disorders requiring precise stimulation of cortical or sub-cortical brain regions.

2.2 RESEARCH STUDY

Sonogenetic stimulation of the brain at very high spatiotemporal resolution and its use for vision restoration

S. Cadoni [1], C. Demené [2], M. Provansal [1], D. Nguyen [1], G. Labernede [1], G. Gauvain [1], F. Arcizet [1], O. Marre [1], D. Dalkara [1], J. A. Sahel [1,3,4,5], M. Tanter *[2], and S. Picaud *[1]

[1] Sorbonne Université, INSERM, CNRS, Institut de la Vision, 17 rue Moreau, F-75012 Paris, France;
[2] Physics for Medicine Paris, INSERM, CNRS, École Supérieure de Physique et de Chimie Industrielles (ESPCI Paris), Paris Sciences et Lettes (PSL) Research University, 75012 Paris, France;
[3] Department of Ophthalmology, The University of Pittsburgh School of Medicine, Pittsburgh, PA 15213, United States;
[4] Department of Ophthalmology and Vitreo-Retinal Diseases, Fondation Ophtalmologique Rothschild, F-75019 Paris, France;
[5] Centre Hospitalier National d'Ophtalmologie des XV-XX, F-75012 Paris.

* These authors contributed equally to this work.

Abstract

The non-invasive, remote and precisely controlled activation of the brain is the fundamental challenge of Brain-machine interfaces, especially within the development of rehabilitation strategies for diverse neurological disorders. Ultrasound waves can be used to modulate neuronal activity of deep brain regions (Deffieux et al., 2013; Lee et al., 2016; Legon et al., 2018, 2014; Mehić et al., 2014; Tufail et al., 2010, 2011), but they require high acoustic energy deposition and lack spatial resolution and cell selectivity. Following the expression of ultrasound-sensitive proteins by gene therapy, sonogenetic strategies have been shown to provide higher sensitivity to ultrasound in addition to cell selectivity, but, to date, such strategies have been subject to severe limitations in terms of spatiotemporal resolution *in vivo* (Huang et al., 2020; Qiu et al., 2020; Yang et al., 2020) preventing a real potential for rehabilitation therapies. We show here that by combining high-frequency ultrasonic stimulation with the expression of the mechanosensitive ion channel of large conductance (MscL), we can selectively activate neurons with high spatiotemporal resolution following millisecond stimulations in both the *ex vivo* retina and *in vivo* primary visual cortex. This high spatiotemporal resolution was generated at energy levels associated with negligible tissue heating and far below those leading to complications in ultrasound neuromodulation (Kim et al., 2014; Lee et al., 2016). Our findings demonstrate that this sonogenetic therapy is compatible with millisecond pattern presentation for visual restoration at the cortical level. It represents an important step towards very high throughput, precise and distant transfer of information to cortical and subcortical brain regions with a wide range of applications in neurological disorders.

It was anticipated that brain-machine interfaces (BMIs) based on multi-electrode arrays would provide solutions for many neurological disorders and rehabilitation strategies as for blindness (Obidin, Tasnim, and Dagdeviren, 2020). However, their clinical applications remain limited to conditions such as hearing disabilities and Parkinson's disease. Cortical multi-electrode arrays raised great hopes for the restoration of form vision in patients with a lost eye-to-brain connection (Beauchamp et al., 2020), but their resolution remains too low for complex tasks, such as navigation and face recognition. Furthermore, their long-term use is also hindered by a reported loss of efficacy over time (Dobelle, 2000) . Optogenetic therapy has provided an alternative for the non-invasive stimulation of neurons with a higher resolution, as demonstrated on the retina (Ferrari et al., 2020; McGregor et al., 2020). However, despite encouraging preliminary results in studies aiming to elicit visual perception at the cortical level (Chernov et al., 2018; Jazayeri, Lindbloom-Brown, and Horwitz, 2012; Ju et al., 2018), optical stimulation approaches are hindered by the dura mater and by tissue diffraction and absorption of light (Jazayeri, Lindbloom-Brown, and Horwitz, 2012; Ju et al., 2018; McAlinden et al., 2019). Ultrasound (US) waves overcome these limitations, allowing in depth focusing and the non-invasive neuromodulation of cortical and subcortical brains areas (Deffieux et al., 2013; Lee et al., 2016; Legon et al., 2018, 2014; Mehić et al., 2014; Tufail et al., 2010, 2011). Unfortunately, the trade-off between spatial resolution and acoustic intensity greatly limits the applicability of US neuromodulation for BMI, as high spatial resolution is obtained only with high frequency US, at the expense of the required energy (Ye, Brown, and Pauly, 2016), with a risk of thermal heating and US-mediated tissue damage (Kim et al., 2014; Lee et al., 2016). Sonogenetic therapy proposed in this paper aims 1) to boost neuronal sensitivity to US through the expression of US-sensitive channels on cell membrane (Huang et al., 2020; Ibsen et al., 2015; Qiu et al., 2020; Yang et al., 2020; Ye et al., 2018), 2) to induce responses with a high temporal precision and 3) to offer cell specificity, which is absent from current non-specific US neuromodulation strategies. This unique combination of high spatial and temporal resolution in conjunction with render sonogenetic therapy perfectly compatible with applications for vision restoration, which require video-rate patterns of stimulation.

We investigated sonogenetic therapy in a natural mammalian neuronal circuit, by expressing the mechanosensitive ion channel of large conductance (MscL) (Hamill and Martinac, 2001; Perozo, 2006; Soloperto et al., 2018a; Sukharev, 2001; Sukharev et al., 1994) in rat retinal ganglion cells (RGCs), with *in vivo* intra-vitreal adeno-associated vector (AAV) delivery. Vectors were produced with the MscL gene from *Escherichia coli* in its wild-type (WT) form and with a mutation, G22S (Yoshimura et al., 1999), which increased the sensitivity of cultured neurons to mechanical and ultrasonic stimulation (Soloperto et al., 2018b; Ye et al., 2018). A AAV2.7m8 (Dalkara et al., 2013) serotype vector was used to encode the MscL channels fused to the red fluorescent protein tdTomato, under control of the SNCG promoter specific to RGCs (Chaffiol et al., 2017). Following injections, tdTomato expression was detected *in vivo*, on the eye fundus (Figure 1A). Examination of the flat-mounted retina showed that tdTomato expression was restricted to the ganglion cell layer and the optic fiber bundles (Figure E1B). We further demonstrated that expression was limited to RGCs, by labeling these cells with a specific antibody, RPBMS (Figure 1B). Expression of the MscL gene seemed to be concentrated at the cell membrane on the soma and axon (Figure 1C). The staining indicated that, in the transfected area,33.73% and 45.83% of RPBMS-positive cells expressed tdTomato, for the MscL-WT and MscL-G22S proteins, respectively (Figure 1D).

We next evaluated RGCs sensitivity to US, by performing *ex vivo* recordings of the retina on a multi-electrode array (Figure 1E). In retinas expressing the

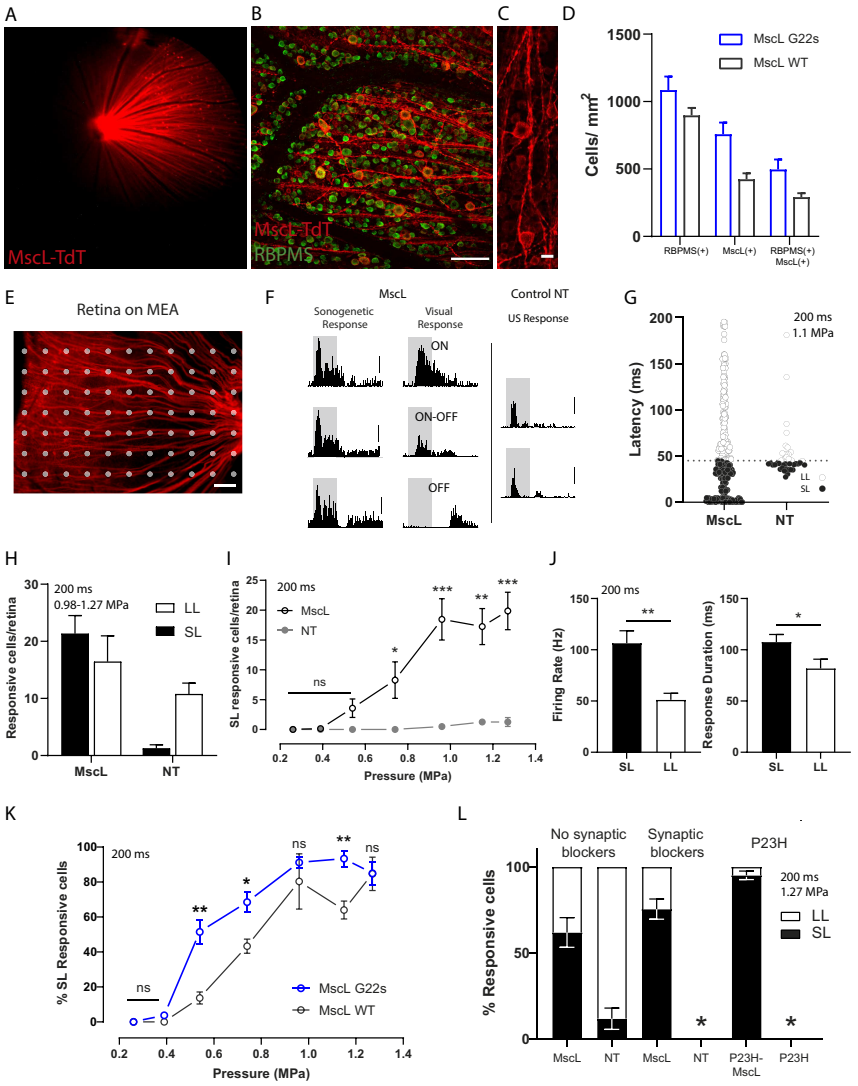

Figure 1 – Sonogenetic therapy in retinal ganglion cells. (A) Retinal fundus image showing MscL-tdTomato expression in rat retina. (B) Representative confocal stack projection across the RGC layer of a flat-mounted retina expressing MscL-tdTomato (red) and labeled with anti-RBPMS antibody (green). (C) Magnification of a few RGCs expressing MscL-tdTomato, showing its expression at the soma and axonal levels of the membrane. (D) Density of RBPMS-positive, MscL-positive and double-labeled cells for five MscL G22S and five MscL WT retinas. (E) Retina expressing MscL-tdTomato on a MEA chip. White dots represent electrodes. (F) Representative peri-stimulus time histograms (PSTH) for RGCs, for different stimuli. (Left) PSTH of three RGCs expressing MscL, showing a short latency and a sustained response after the start of a 15 MHz US stimulus (1.27 MPa). (Middle) Corresponding PSTH of the same RGCs in response to a visual stimulus, showing typical ON, ON-OFF and OFF responses. (Right) PSTH of two RGCs from a non-transfeted (NT) retina in response to a 15 MHz US stimulus (1.27 MPa), showing a response to the start and end of the stimulus. The scale bars represent 10 spikes per bin. Gray boxes represent 200 ms stimuli. (G) RGC latencies in response to a 200 ms 15 MHz US stimulus for MscL (n=288 cells, 9 retinas) and NT (n=41 cells, 4 retinas) retinas (US pressure: 1.1 MPa). Grey line represents the 45 ms threshold that divides cells into SL (black dots) and LL (white dots) cells. (H) Mean of responding cells per retina to 200 ms 15 MHz US stimulus (0.98-1.27 MPa) for MscL (n=9) and NT (n=4) retinas and for LL and SL cells. (I) Meand number of SL responding RGCs per retina when stimulated with 200 ms US stimuli (1.27 MPa) of increasing US pressure for MscL (n=9) and NT (n=4) retinas.*, p=.0356, **, p=.0010, ***, p=.0008, unpaired t test. (J) Mean maximum firing rate and mean response duration of SL and LL RGCs from MscL retinas to a 200 ms 15 MHz stimulus of increasing pressure (0.2-1.27 MPa) (n=9, **, p=.0017, *, p=.0418, unpaired t test). (K) Percentage of short-latency RGC cells (normalized to the maximum number of responsive cells in the experiment) responding to 200 ms long US stimuli of increasing pressure for MscL WT (n=3) and MscL G22S (n=6) retinas. *, p=.0173, **, p=.0065, **, p=.0083, unpaired t test. (L) Percentage of RGCs responding to US stimulation, for retinas in normal conditions (n=9 retinas for MscL and 4 for NT), and following the application of a cocktail of synaptic blockers (CNQX-CPP-LAP4) (n=3 retinas each for MscL and NT), and for P23H retinas with (n=3 retinas) and without (n=3 retinas) MscL expression. The ratio of SL to LL is shown for each condition. For all panels, error bars represent the SEM. The scale bars represent 100 µm in (B), 20 µm in (C), 200 µm in (E).

MscL channel, RGCs displayed strong and sustained ON responses to 15 MHz US stimulation (Figure 1F- left). Those responses were different from the one recorded in non-transfected (NT) retinas, where RGCs presented an increase in spiking activity after the start of the stimulus (Figure 1F-right, NT) with relatively long latencies (LL), 50.4 ± 4.2 ms (Figure 1G). By contrast,

many RGCs of transfected retinas presented responses with a very short latency (SL), 12.2 ± 2.5 ms, (Figure 1F- left), while others continued to respond with longer latencies (Figure 1G). RGCs were therefore classified into SL and LL in terms of their response, with SL corresponding to a latency of less than 45 ms. The generation of SL ON US responses was not related to a specific RGC type (Figure E2A), as they were measured both in cells with ON responses to light, and those with OFF responses to light (Figure 1F-left). MscL expression decreased latency and increased the average number of cells per retina responding to US (Figure 1H). SL responding cells expressing MscL were sensitive at very low US pressures compared to non-transfected cells and their number increased at increasing US pressures (Figure 1I). SL US responses also had higher firing rates and were more sustained than LL US responses (Figure 1J). Moreover, we observed that the G22S mutation further enhanced the US sensitivity of SL RGCs to lower US pressures (Figure 1K). We further investigated the origin of the sonogenetic responses, by adding a mixture of synaptic blockers (CNQX-LAP4-CPP) to the bath perfusing the retina. These synaptic blockers were found to abolish US responses in non-transfected retinas but not in MscL-transfected retinas, in which they did not suppress the SL US responses and only decreased the number of LL US responses (Figure 1L). This observation suggests that the MscL-mediated SL US responses are initiated by RGCs, whereas LL US responses in the transfected and non-transfected retina originate upstream from RGCs. These conclusions were supported by data recorded from retinas of blind P23H rats. No US responses were recorded for the non-transfected P23H retina (Figure 1L), demonstrating that the LL US responses required synaptic transmission, as previously reported (Menz et al., 2013), and suggesting a possible origin in photoreceptors. MscL-transfected P23H retinas displayed many SL US responses and few LL US responses, demonstrating further that MscL expression generates the SL latency responses in RGCs. We subsequently restricted our analyses to SL US responses. We investigated the temporal kinetics of US responses under various durations of US stimulation (Figure 2A) and at various repetition rates (Figure 2B). Neurons responded to even very short stimulation durations (10 ms), with responses showing a fast return to the control level of activity (Figure 2A). For longer stimuli (100 ms or longer), responses start displaying habituation, with a reduction of the maximum firing rate (Figure 2 2C). US response durations were correlated with stimulus duration (Figure 2D). Using a different repetition rate of a 15 MHz US stimulus, RGCs were able to follow the rhythm up to 10 Hz (Figure 2B-E). The Fano factor in the previous experiments indicated that the response had a low variability in spike count and possibly high information content (Figure 2C-E).

We then investigated whether different US frequencies (0.5, 2.25 and 15 MHz) affected the spatial resolution of the response, in accordance with the measured US pressure fields, which became smaller at higher US frequencies (Figure E3, Figure E4A-C). The features of the responses evoked by the different US frequencies were found to be similar (Figure E2C-D). Figure 2F illustrates the distribution of responding cells on the chip under different US stimulation frequencies with the expected FWHM (full width at half maximum) distribution of the US pressure field (green rings). Cells responding to US were widespread over the recorded area for the 0.5 and 2.25 MHz, but appeared to be more confined for 15 MHz (Figure 2F). For each stimulated retina, we then calculated the spatial dispersion of activated cells, this value decreased significantly from 1.48 ± 0.12 mm ($n = 12$ retinas) and 1.30 ± 0.18 mm ($n = 5$ retinas) at 0.5 MHz and 2.5 MHz, respectively, to 0.59 ± 0.03 mm ($n = 9$ retina) at 15 MHz (Figure 2G). These distances were consistent with the size of the measured ultrasound pressure fields (Figure E4) and the mean distance between two randomly selected electrodes on the MEA chip (1.73 mm). The density of activated cells increased significantly with increasing US frequency and activated cells were more widely

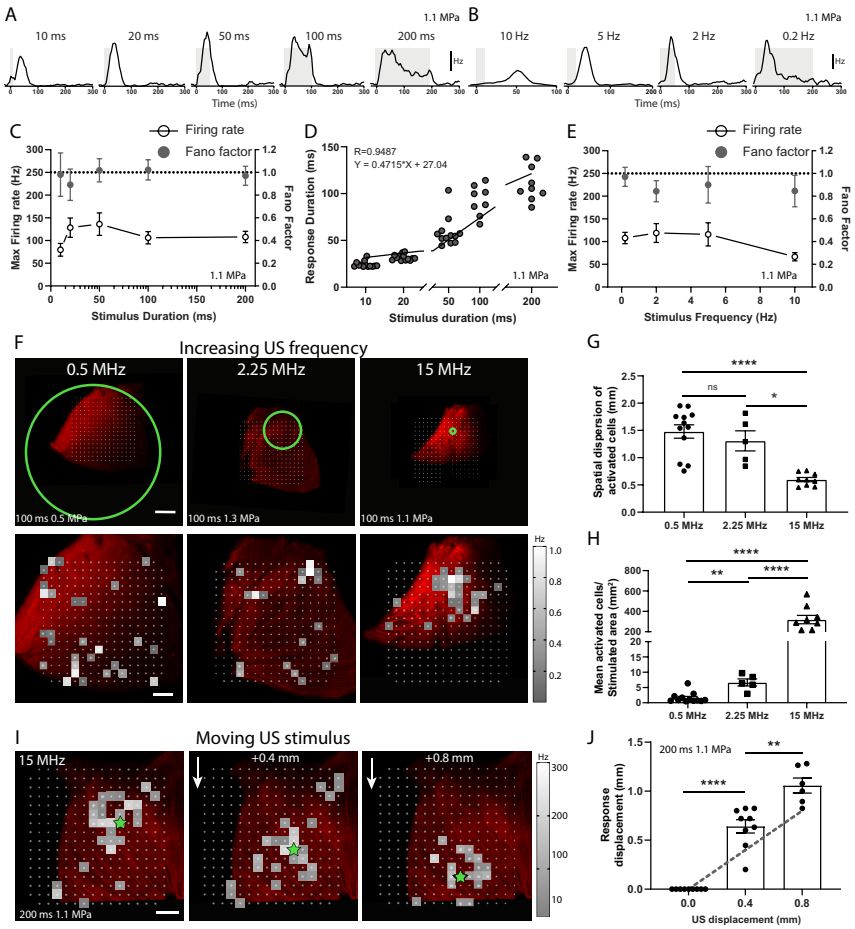

Figure 2 – Spatiotemporal properties of sonogenetic retinal responses. (A-B) Spike density functions of two representative RGCs from a MscL-expressing retina for various 15 MHz stimulus durations (0.5 Hz stimulus repetition rate) (A) and stimulus repetition frequencies (stimulus durations: 10, 20, 50, 200 ms) (B), the scale bars correspond to 100 Hz and 50 Hz, respectively (US pressure: 1.1 MPa).(C) Mean maximum firing rate for different 15 MHz stimulus durations and mean Fano factor values for all cells (n=9 retinas, except for stimulus durations of 10 and 20 ms n=8, 1.1 MPa).(D) Correlation between response duration and stimulus duration, confirmed by the linear regression line (n=9 retinas, 1.1 MPa). (E) Mean maximum firing rate for different stimulus repetition frequencies and mean Fano factor values for all cells (n=9 retinas, except for stimulus frequencies of 5 and 10 Hz n=8, 1.1 MPa). (F) (Top) Retinas on a MEA chip and corresponding size of the incident US pressure beam (green circles represent the FWHM and are centered on the estimated center of response), for 0.5, 2.25 and 15 MHz. The scale bar represents 1 mm. (Bottom) Activation maps following US stimulation at 0.5, 2.25 and 15 MHz. Each square box represents an electrode with at least one US-activate cell. Color map representing the normalized firing rates of the cells. US pressures: 0.5, 1.3, 1.1 MPa for 0.5, 2.25 and 15 MHz respectively (100 ms stimulus). The scale bar represents 0.5 mm. (G) Spatial dispersion of activated cells calculated as the mean Euclidean distance between activated cells weighted according to maximum firing rate and (H) ratio of the number of activated cells to the area stimulated on the MEA chip for the three US frequencies. ****, p<.0001, **, p=.0008,*, p=.0169, unpaired t test. n=12 retinas for 0.5 MHz (0.29-0.68 MPa), n=5 retinas for 2.25 MHz (1.11-1.62 MPa), n=9 retinas for 15 MHz (1.12-1.27 MPa). (I) Heatmaps showing the activated cells of a MscL-transfected retina following a relative displacement (0, +0.4 and +0.8 mm) of the 15 MHz US transducer (200 ms, 1.1 MPa). Each colored box represents an activated cell; the color map shows the maximum firing rate. Green stars represent the estimated center of the response. The scale bar represents 0.5 mm. (J) Relative displacement of the center of the response following displacement of the 15 MHz US transducer. ****, p<.0001, **, p=.0018, unpaired t test. n=9, 9, and 6 positions for 4, 4 and 2 retinas for displacements of 0, 0.4 and 0.8 mm, respectively. US stimulus: 200 ms, 1.1 MPa. The grey dotted line represents the theoretical displacement. For all panels, error bars represent the SEM.

dispersed at lower frequencies on the larger stimulated area (Figure 2H). US stimulation at higher frequencies is more effective as lower acoustic power values are required to activate an equivalent number of cells. Indeed, even if the acoustic intensities at 2.25 and 15 MHz were quite similar (respectively Isptp=40.3 W/cm² and Isptp=56.3 W/cm²), the delivered acoustic power was almost two orders of magnitude lower at 15 MHz (0.03 W) than at 2.25 MHz (0.82 W). Interestingly, at 15 MHz, the stimulated area was small enough for the focal spot of the US probe to be moved above the isolated retina, triggering a shift in the responding cells (Figure 2I). This shift followed the probe's focal spot over the retina, in the same direction and with a consistent

displacement amplitude. The center of the response was found to move in accordance with the displacement of the US transducer (Figure 2J). These results demonstrate that our sonogenetic therapy approach can provide a spatial resolution compatible with the patterned stimulations required for vision restoration.

We then investigated whether the approach could also be applied to the brain *in vivo*, paving the way towards a sonogenetic-based BMI using high frequency ultrasonic arrays implanted in the skull bone. As the G22S mutation enhanced the US sensitivity of RGCs *ex vivo*, we expressed this channel in the cortical neurons of the primary visual cortex (V1) in rats. We injected a AAV9.7m8 vector encoding the MscL-G22S channel fused to tdTomato under the control of the neuron-specific CamKII promoter into V1. TdTomato fluorescence was detected in the brain (Figure 3A) and in cortical slices (Figure 3B). V1 neurons expressed tdTomato, particularly in layer 4 (Figure 3B). Staining with an anti-NeuN antibody showed that 33.4% of cortical neurons in the transfected area expressed tdTomato (Figure 3C). In order to investigate the ability of a 15 MHz US stimulus to activate cortical neurons, we placed a micro-EcoG (µEcoG) electrode array on the cortical surface of V1 (Figure 3D). In non-transfected animals, no US-evoked signal was recorded (Figure 3E-right, n=3 rats), whereas, in V1 expressing MscL-G22S, US stimulation of the cortical surface elicited large negative µEcoG potentials (Figure 3E-middle, n=4 rats).). These US-evoked negative deflections were different from the recorded visual-evoked potentials, which presented typical P0, N1 and P1 positive and negative deflections (Figure 3E-left). The duration of the US responses was clearly related to the duration of the US stimulation (Figure 3F). The amplitude of US-evoked potentials increased with both increasing US pressure (Figure 3G) and increasing US stimulus duration (Figure 3H). V1 cortical responses were again able to follow a repetition rate of up to 8 Hz (Figure 3I) with similar peak amplitude for different stimulation frequencies. We then investigated the spatial distribution of US-evoked neural activity. The peak depolarization of each channel was measured and linearly interpolated to build pseudocolor activation maps (Figure 3J). The size of the US-responding cortical area was dependent on the US pressure (Figure 3J-K), and ranged from 0.35 ± 0.19 mm² (n=3 rats) to 1.57 ± 0.27 mm² (n=4 rats) for US pressures of 0.26 and 1.27 MPa, respectively (Figure 3L). We investigated the possibility of achieving patterned US stimulations, by moving the US transducer in 0.4 mm steps over the recorded area. When the ultrasound probe was moved laterally, the source of the generated neuronal activity moved in a similar direction (Figure 3K). The spatial location of the evoked potentials moved in average by 0.27 ± 0.09 mm (n=4 rats) from the previous location (Figure 3M) although we moved the US transducer with 0.4 mm steps. These measurements were probably conditioned by the 300 µm discrete spatial pitch distribution of the electrodes and the lateral spread of activity in the circuit. These results suggest that our approach of sonogenetic therapy could rely on a spatial resolution of at least 400 µm for stimulations at 15 MHz, the focal spot of our 15 MHz transducer being 276 µm wide (Figure E4C). This opens up the possibility of targeting very small areas (up 0.35 mm² for 0.26 MPa), depending on the pressure level. These very localized US-evoked responses and their dependence on the position of the US probe confirmed that they were due to the activation of MscL-G22S-expressing neurons and not to an indirect response related to auditory activation as previously reported by others (Guo et al., 2018; Sato, Shapiro, and Tsao, 2018).

The possibility of the US stimulation to activate neurons at different depths was then explored. V1 neurons were recorded with a 16-site penetrating multi-electrode array. In V1 expressing MscL-G22S, US stimulation at 15 MHz generated sustained SL responses (Figure 3N) at various cortical depths, ranging from 100 µm to 1 mm (Figure 3P-bottom) (n=3 rats) that differed considerably from natural visual responses (Figure 3N). Deep neurons re-

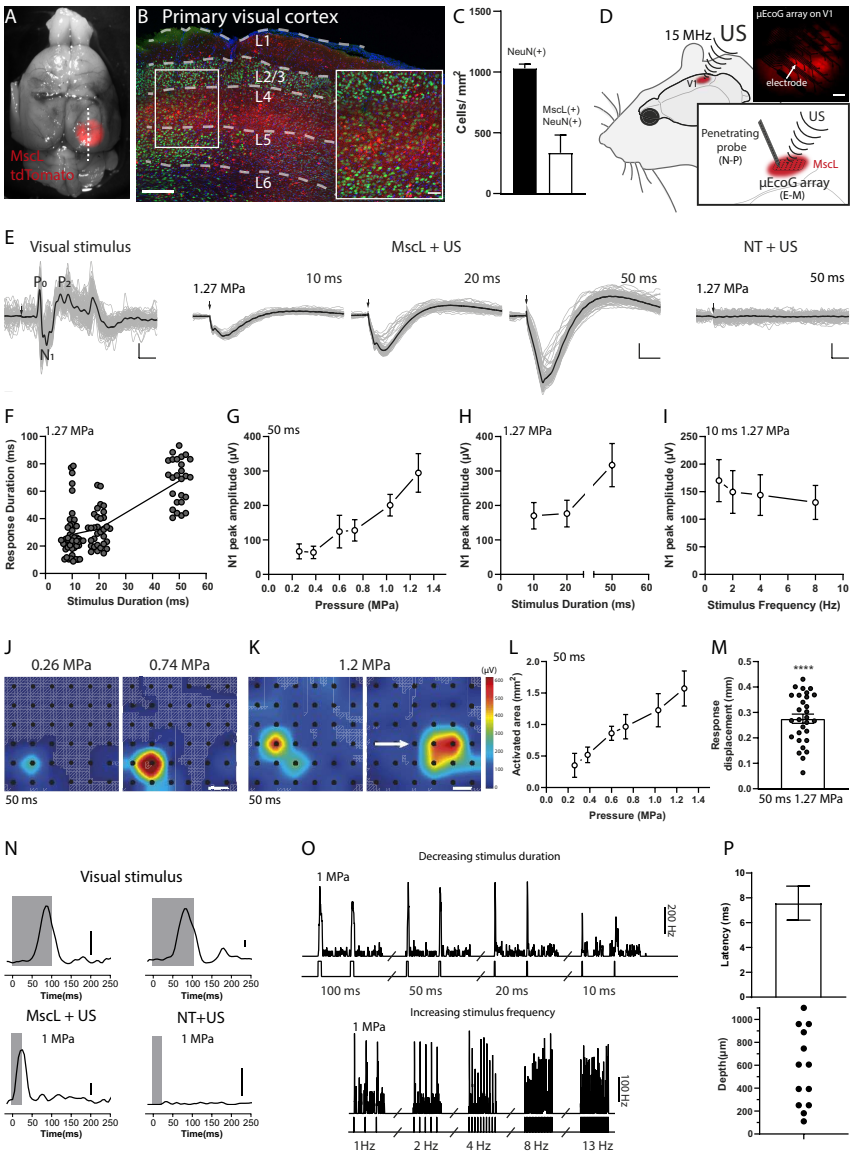

Figure 3 – *In vivo* sonogenetic activation of V1 neurons. (A) Image of a rat brain expressing MscL-tdTomato (red) in V1. The dotted line represents the illustrative location of a sagittal slice. (B) Representative confocal stack projection of a sagittal brain slice expressing MscL G22S-tdTomato (red) and labeled with anti-NeuN antibody (green) and DAPI (blue). The layers of V1 are delineated by white dashed lines. (Lower right) Magnification of layer 4 of V1. (C) Density of NeuN-positive, MscL-positive and double-labeled cells for 3 brain slices. (D) (Top) Schematic diagram of the setup used for *in vivo* electrophysiological recordings and US stimulation; (Top right) μEcoG electrode array placed on V1 of a MscL-transfected rat. TdTomato was detected under the electrode matrix. (E) (Left) Representative visual-evoked cortical potentials in response to a 100 ms flash, in which typical P0, N1 and P1 deflections are visible. (Middle) Representative sonogenetic evoked potentials for 15 MHz US stimuli of various durations (1.27 MPa). (Right) Representative responses of a non-transfected (NT) rat to a 100 ms 15 MHz US stimulus (1.27 MPa). Black traces represent the mean evoked potential over 100 trials. Each gray trace represents one trial. The black arrow indicates the start of the stimulus. The scale bars represent 50 μV/50 ms. (F) Duration of sonogenetic μEcog responses for stimuli of 10, 20 and 50 ms (n=49, 32 and 26 trials on 4 animals, US pressure: 1.27 MPa). (G) N1 peak amplitude for increasing US pressure, (I) increasing duration (1.27 MPa) and (J) frequency (Stimulus duration: 10 ms, 1.27 MPa) (n=4 animals). (J) Pseudo-color activation maps for stimuli of increasing US pressure and (K) for a horizontal displacement of 0.8 mm of the US transducer (the arrow indicates the direction of the displacement). Each black dot represents an electrode of the electrode array. The color bar represents N1 peak amplitude in μV. (L) Area activated for various US pressure values (n=4 animals, 50 ms stimulus duration). (M) Displacement of the activation center relative to the previous position following movement of the US transducer by 0.4 mm. $p<.0001$, one-sample t test, n=29 positions on 4 animals (50 ms, 1.27 MPa). (N) Representative spike density function (SDF) of responses to visual and US stimuli for MscL and non-transfected rats; the scale bars represent 50 Hz. (O) SDF of responses to stimuli of different durations (top) and frequencies (bottom). The top line shows the firing rate of the responses to stimuli with a duration of 10 to 100 ms (1 Hz stimulus frequency) and the bottom line shows the firing rate for a frequency of 1 Hz to 13 Hz (10 ms stimulus duration). The rows at the bottom indicate the pattern of the stimuli. US pressure: 1 MPa. (P) (Top) Mean latency of response to the start of the US stimulus (n=13 cells, 3 animals, US pressure: 1-1.27 MPa). (Bottom) Depth of US-responding cells (n=13) in MscL-expressing rats (n=3) (US pressure: 1-1.27 MPa). For all panels, error bars represent the SEM. The scale bars represent 200 and 50 μm (lower right) in (C), 600 μm in (D).

sponded reliably to stimuli of decreasing duration, from 100 ms to 10 ms (Figure 3O-top), and increasing frequencies of up to 13 Hz (Figure 3O-bottom). The latency of these responses was short (7.57 ± 1.37 ms, Figure 3P-top), consistent with a direct US activation of recorded cortical neurons. No response to US stimulation was observed in the V1 of control non-transfected animals (Figure 3N) (n=3 rats), demonstrating the specificity of US responses to MscL-G22S channel expression.

The development of remotely controlled cortical and subcortical deep neuronal stimulation techniques is of considerable interest for the treatment of diverse neurological diseases and sensory handicaps. Optogenetics has been developed for this purpose in non-human primates, but its potential for transfer into clinical practice is limited by the low level of light penetration into the brain tissue (Jazayeri, Lindbloom-Brown, and Horwitz, 2012; Ju et al., 2018). US stimulation can overcome this limitation (Folloni et al., 2019; Lee et al., 2016; Legon et al., 2014; Tufail et al., 2011). Most of previous studies focused on the combination of intravascular microbubbles and low-frequency US, which has the advantage of being able to cross the skull bone and reach even deep brain regions. Recent demonstration of MscL-based sonogenetic activation in mice brain without the requirement of contrast agent's injection was also performed with long bursts of low frequency US (Qiu et al., 2020). Such low frequency US waves lead to limited centimetric spatial resolutions (typically around 5x5x45 mm^3) and out of control spatial beam pattern distribution due to the formation of standing waves (Baron et al., 2009). In rodent brain, this phenomenon generates reverberations throughout the whole braincase (Younan et al., 2013), with the probable activation of non-target structures, such as the auditory pathway (Guo et al., 2018; Sato, Shapiro, and Tsao, 2018). An alternative approach to restrict US propagation involves the use of higher US frequencies, but this requires higher energy levels that may exceed safety limits and would be more likely to generate complications (Ye, Brown, and Pauly, 2016). Our sonogenetic approach greatly decreased the US pressure required for the activation of RGCs and V1 cortical neurons by high-frequency US using stimulation sequences remaining below the FDA limits for US imaging (e.g. for a 10 ms US stimulus of 0.6 MPa, the Isptp is 12 W/cm^2 and the Ispta value is of 0.12 W/cm^2). For cortical neurons, in the absence of MscL expression, stimulation at 15 MHz evoked no response. In the retina, the natural US responses observed in the absence of MscL expression were not elicited intrinsically in RGCs, but could result from the mechanosensitivity of photoreceptors, as previously suggested (Menz et al., 2013). If MscL has been previously reported to sensitize neurons to US (Qiu et al., 2020; Ye et al., 2018), its use for high spatiotemporal resolution stimulation still remained to be proven *in vivo*. Our results show that MscL G22S channel expression resulted in neuronal responses with millisecond response kinetics and a spatial resolution of at least 400 µm. Simulations of US-induced heating in brain tissue revealed that typical US parameters inducing clear responses, (i. e. 20 ms 1.27 MPa) (Figure 3E-H), were estimated to increase the local temperature by 0.12°C and even their high repetition rates (up to 13 Hz) lead to moderate temperature increase (<0.3°C) (Figure E4 J-K). These low temperature fluctuations tend to prove that our US-elicited responses were not temperature-driven and very likely mediated by the mechanical activation of the MscL channel by US. Following previous demonstrations that the MscL channel is a suitable sonogenetic actuator (Qiu et al., 2020; Soloperto et al., 2018a; Ye et al., 2018), we provide *in vivo* evidence that the MscL channel has appropriate kinetics for the activation of neurons at a high spatiotemporal resolution *in situ* and *in vivo*. Previous *in vivo* studies reported the restoration of form vision at the cortical level with 0.8 to 1 mm electrodes spaced more than 1 mm apart (Beauchamp et al., 2020; Brindley and Lewin, 1968; Dobelle, 2000). The resolution of the proposed sonogenetic therapy appears therefore compatible

with form vision restoration. Further studies are required to generate an interface for coding visual information into US patterns transmitted by an ultrasonic matrix array onto the visual cortex at a video rate. However, our approach provides great hopes for the development of high-resolution visual restoration at the cortical level, through its unique combination of a fast response time, high spatial resolution and high cell selectivity and sensitivity, features that are essential for video-rate brain-wide pattern stimulation. More generally, it paves the way for a new type of brain-machine interface capable of compensating for disabilities and suitable for use to treat neurological disorders.

METHODS

Animals

All experiments were conducted in accordance with the National Institutes of Health Guide for the Care and Use of Laboratory Animals. The experimental protocol was approved by the Local Animal Ethics Committee (registration number 9529) and conducted in agreement with Directive 2010/63/EU of the European Parliament. All rats included in this study were Long Evans rats from Janvier Laboratories or P23H (line 1) transgenic rats.

Plasmid cloning AAV production

Plasmids containing the *Escherichia coli* MscL sequence in the WT form and with the G22S mutation were obtained from Francesco Difato (Addgene plasmids 107454 and 107455) (Soloperto et al., 2018a). For the targeting of retinal ganglion cells, the SNCG promoter (Chaffiol et al., 2017) was inserted into a AAV backbone plasmid containing the MscL sequence fused to the tdTomato gene and the Kir2.1 ER export signal, to drive expression at the plasma membrane. An AAV2.7m8 vector was used for intra-vitreal delivery. In order to target neurons in the cortical layers of V1, the SNCG promoter was replaced by the CamKII promoter and an AAV9.7m8 was chosen. All the recombinant AAVs used in this study were produced by the plasmid cotransfection method, and the resulting lysates were purified as previously described, to yield a high titer of recombinant AAV virus (Choi et al., 2007).

US stimulus

Three transducers with different central frequencies were used, to obtain focal spots of different sizes: 0.5 MHz (V301-SU, Olympus), 2.25 MHz (V306-SU, Olympus) and 15 MHz (V319-SU, Olympus). A TiePie Handyscope (HS3, TiePie Engineering) was used to produce the stimulus waveform, which was then passed through an 80 dB RF power amplifier (VBA 230-80, Vectawave) connected to the transducer. Transducer pressure outputs (pressure at focus, 3D pressure maps) were measured in a degassed water tank with a Royer-Dieulesaint heterodyne interferometer (Royer and Dieulesaint, 1986). The US stimuli used for *ex vivo* and *in vivo* stimulation had the following characteristics: 1 kHz pulse repetition frequency with a 50% duty cycle, sonication duration between 10 and 200 ms and inter-stimulus interval between 0.01 and 2 s. Peak acoustic pressures were 0.11-0.88 MPa, 0.3-1.6 MPa, 0.2-1.27 MPa, for the 0.5, 2.25 and 15 MHz transducers, respectively. The corresponding estimated Isppa values were 0.39-25.14 W/cm², 2.92-83.12 W/cm² and 1.30-52.37 W/cm².

Ex vivo

Intra-vitreal gene delivery and retinal imaging

Rats were anesthetized with isoflurane (5% for induction, 3% for maintenance) and 2 µl of AAV suspension, containing between 8 and $14x10^{10}$ viral particles, was injected into the center of the vitreous cavity while directly observing the tip of the needle. One month after injection, fluorescence imaging was performed on the injected eyes, with a Micron IV retinal imaging microscope (Phoenix Research Laboratories) used to observe MscL expression via the fluorescent tdTomato tag. Electrophysiological recordings were performed at least one month after injection.

MEA recordings

Retinas were isolated under dim red light, in Ames' medium (A1420, Sigma-Aldrich) bubbled with 95% O2 and 5% CO2 at room temperature. Pieces of the retina were flattened on a filter membrane (Whatman, GE Healthcare Life Sciences) and placed on a poly-L-lysine (0.1%, Sigma) coated multi-electrode array (electrode diameter 30 µm, spacing 200 µm, MEA256 200/30 iR-ITO, MultiChannel Systems) with retinal ganglion cells facing the electrodes. The retina was continuously perfused with bubbled Ames medium at 34°C, at a rate of 2 ml/min, during experiments. TdTomato fluorescence was checked before recordings, by using a stereo microscope (SMZ25, Nikon) to observe transgene expression in the recorded area. For some experiments the AMPA/kainate glutamate receptor antagonist 6-cyano-7-nitroquinoxaline-2,3-dione (CNQX, 25 μM, Sigma-Aldrich), the NMDA glutamate receptor antagonist [3H]3-(2-carboxypiperazin-4-yl) propyl-1-phosphonic acid (CPP, 10 μM, Sigma- Aldrich) and a selective group III metabotropic glutamate receptor agonist, L-(+)-2-amino-4-phosphonobutyric acid (L-AP4, 50 μM, Tocris Bioscience), were freshly diluted and added to the bath for application by perfusion for 10 minutes before recording. Full-field light stimuli were delivered with a digital micro-mirror display (DMD, Vialux, resolution 1024x768) coupled to a white light LED light source (MNWHL4, Thorlabs) focused on the photoreceptor plane. An irradiance of 1 µW/cm² was used. The US transducers were coupled with a custom-made coupling cone filled with degassed water, mounted on a motorized stage (PT3/M-Z8, Thorlabs) and placed orthogonally in the recording chamber above the retina. For positioning of the US transducer over the retina, the reflected signal of the MEA chip and the retina was detected with an US-key device (Lecoeur Electronique). The distance between the retina and the transducer was equal to the focal length of the transducer; this was verified with the flight time of the reflected signal. RGC recordings were digitized with a 252-channel preamplifier (MultiChannel Systems). Spikes from individual neurons were sorted with SpykingCircus software (Yger et al., 2018). RGC responses were then analyzed with custom scripts written in Matlab (MathWorks). They were classified as ON, ON-OFF or OFF, with the response dominance index (Akerman, Smyth, and Thompson, 2002). The latency of each cell relative to the start or end of the stimulus was calculated as the time between the start of the stimulus and the maximum of the derivative of spike density function. For cells responding to US stimulation, two classes were identified on the basis of latency — short and long latency — by fixing a threshold equal to the minimum of the latency distribution of the responses of non-transfected cells to US (45 ms). We determined the peak value A of spike density function for the calculation of response duration, which was defined as the time interval between the two time points for which the SDF was equal to A/e (e: Euleur's number). The percentage of cells responding to US stimulation of increasing US pressure was calculated as the ratio of the number of activated cells to the maximum number of responding cells for all the US pressures considered. The Fano factor, quantifying spike-count variability, was calculated as the ratio of the variance of the spike-count to the mean. Values close to 1 indicate that information can be transmitted. The Euclidean distance between two activated cells was weighted according to the maximum firing rate of the cells. The ratio of the number of activated cells to the size of the area stimulated on the MEA chip was calculated considering the size of the US focal spot for 2.25 and 15 MHz and the size of the MEA for 0.5 MHz, because the focal spot was larger than the MEA for this frequency. The center of the response was estimated by weighting the maximum of firing rate of each cell according to its distance from other responding cells, and the displacement of the response was calculated as the Euclidean distance between two center of response positions.

In vivo

Intracranial injections

Rats were anesthetized with a ketamine/medetomidine mixture (40 mg/kg /0.14 mg/kg). The surgical site was shaved and a midline incision was made to expose the skull bone. The animal was placed in a stereotactic frame and two holes were drilled at the injection sites. AAV suspensions were injected into the right hemisphere at two different locations (coordinates from the bregma: 2.6 mm ML, 6.8 mm AP and 3.1 mm ML, 7.2 mm AP). For each location, 200 nl of viral vector (containing 0.2-8 x 10^15 viral particles) was injected at three different depths (1100, 1350 and 1500 µm DV) with a microsyringe pump controller (Micro4 ,World Precision Instruments) operating at a rate of 50 nl/min and a 10 µl Hamilton syringe. Electrophysiological recordings were performed at least one month after injections.

In vivo extracellular recordings

Rats were anesthetized with a mixture of ketamine and medetomidine (40 mg/kg /0.14 mg/kg). Pupils were dilated with tropicamide (Mydriaticum, Dispersa). A small craniotomy (5x5 mm square) was drilled above V1 in the right hemisphere. Before recording, tdTomato fluorescence was checked with a Micron IV retinal imaging microscope (Phoenix Research Laboratories). A 32-site µEcog electrode array (30 µm electrode diameter, 300 µm electrode spacing, FlexMEA36, MultiChannel Systems) was positioned over the transfected brain region for rats expressing MscL G22S or in a similar zone for control rats. After µEcog recordings, multi-electrode (MEA) recordings were performed with a 16-site silicon microprobe (electrode diameter 30 µm, spacing 50 µm, A1x16-5mm-50-703, NeuroNexus Technologies). The MEA probe was advanced 1100 µm vertically into the cortex with a three-axis micromanipulator (Sutter Instruments, Novato, CA). The US transducer was coupled to the brain with a custom-made coupling cone filled with degassed water and US gel, and was positioned over the region of interest with a motorized stage. The probe and the US transducer were perpendicular for µEcog recordings and tilted at 45° for intracortical recording. The distance between the target in the cortex and the transducer was equal to the focal length of the transducer, as checked with the reflected signal with a US-key (Lecoeur Electronique). Visual stimuli were generated by a white lightcollimated LED (MNWHL4, Thorlabs) placed 15 cm away from the eye. Light irradiance at the level of the cornea was 4.5 mW/cm². µEcog and extracellular signals were digitized with a 32-channel amplifier and a 16-channel amplifier, respectively (model ME32/16-FAI-PA, MultiChannel Systems). µEcog recordings were further analyzed with custom-developed Matlab scripts. MEA recordings were further analyzed with SpykingCircus software, and single-cell events were analyzed with custom-developed Matlab scripts. For µEcog recordings, response duration was calculated as the time interval between the two time-points at which the cortical evoked potential was equal to A/e (where A is peak depolarization and e is Euleur's number). The peak depolarization of each channel was linearly interpolated to build pseudocolor activation maps. The activated area was defined as the area of the pseudocolor activation map over which peak depolarization exceeded 30 V. The center of the response was estimated by weighting the peak depolarization of each electrode according to its distance from other electrodes. For intracortical recordings, cell latency was estimated as the time between the stimulus onset and the maximum of the derivative of spike density function.

Immunohistochemistry and confocal imaging

Transduced retinas and brains were fixed by incubation in 4% paraformaldehyde (100496, Sigma-Aldrich) for 30 minutes for retinas, and overnight for

brains. Brains were cryoprotected in 30% sucrose (84097, Sigma-Aldrich), and 50 µm thick sagittal slices were cut with a microtome (HM450, Microm). The slices displaying the highest levels of tdTomato fluorescence from each brain were selected for further immunohistochemistry and imaging. Retinas and sagittal brain cryosections were permeabilized by incubation in 0.5% Triton X-100 in PBS for 1 h at room temperature and then incubated in blocking buffer (PBS + 1% BSA + 0.1% Tween 20) for 1 h at room temperature. Samples were incubated overnight at 4°C with a monoclonal anti-RBPMS antibody (1:500, Rabbit, ABN1362, Merck Millipore) for the retina, and with a monoclonal anti-NeuN antibody (1:500; Mouse, MAB377, Merck Millipore) for brain sections, in 0.5x blocking buffer supplemented with 0.5% Triton X-100. The sections were then incubated with secondary antibodies conjugated with Alexa Fluor (1:500; Molecular Probes) and DAPI (1:1000, D9542, Merck Millipore) for 1 h at room temperature. An Olympus FV1000 laser scanning confocal microscope with 20x objective (UPLSAPO 20XO, NA: 0.85) was used to acquire images of flat-mounted retinas and brain sections.

Transduction efficiency

Confocal images were processed with FIJI (ImageJ) for the assessment of transduction efficiency. RBPMS- and NeuN-positive cells were counted automatically with the Analyze particles FIJI plugin. MscL-tdTomato and MscL-tdTomato-RBPMS/NeuN-positive cells were counted manually by two different users, with the CellCounter FIJI plugin. For the retina, quantification was performed by identifying the transfected area in each retina and acquiring confocal stacks in at least four randomly chosen regions of 0.4 mm^2 per retina (Figure E1). For $V1$ neurons, the sagittal brain slice with the largest MscL-expressing zone was selected for each animal. In some slices, tdTomato also diffused outside V1. A ROI in V1 was, therefore, manually defined and quantifications were performed in at least six randomly chosen regions of 0.4 mm^2.

US-induced tissue-heating simulations

When considering cell stimulation at higher frequencies (15 MHz) than usually described in the neuromodulation literature, it is mandatory to estimate thermal effects as they can become important. This estimation was done through a three-fold process: 1) simulation of the acoustic fields generated by the 3 transducers we used in the study with realistic acoustic parameters, 2) determination that non-linear acoustics did not play an important role in the heat transfer and 3) realistic simulations of the heat transfer and temperature rise induced at focus by the ultrasound in a linear regime for the parameters used in this study. For non-linear simulations we used the Matlab toolbox kWave, by defining the geometry of the transducer in 3D, and using the following parameters for the propagation medium (water): sound speed $c = 1500\ m.s^{-1}$, volumetric mass $= 1000\ kg.m^{-3}$, non-linearity coefficient B/A= 5, attenuation coefficient $= 2.2.10^{-3}\ dB.cm^{-1}.MHz^{-y}$, and frequency power law of the attenuation coefficient $y = 2$ (Duck, Francis A., 1990). We simulated quasi monochromatic 3D wave-fields using long bursts of 50 cycles, this gave us both the maximum pressure field in 3D and the waveform at focus. Simulations were calibrated by adjusting the input pressure (excitation of the simulated transducer) in order to reach the pressure at focus measured in the water tank with the real transducers. The full width at half maximum (FWHM) focal spot diameter in the xy plane was 4.36, 1.61 and 0.276 mm, and the major axis in the xz plane was 32.3, 20.6 and 3.75 mm long for the 0.5, 2.25 and 15 MHz transducers, respectively (Figure E4 A-C). Non-linear effects were evaluated by estimating the relative harmonic content of the waveform at focus. In the representative example of Figure E4, the amplitude of the second harmonic is 19.8 dB

below the fundamental (20.9 dB in the simulated case), meaning that if the fundamental energy is E, the second harmonic has energy E/95. Therefore, we can reasonably neglect the non-linear effects in the calculations of the thermal effects as it accounts for $\sim 1\%$ of the involved energy. Conclusions were the same at 0.5 MHz and 15 MHz. Using linear wave propagation approximation considerably lighten the computing cost of the simulations. Linear propagation simulations were conducted using Field II toolbox in Matlab (Jensen and Svendsen, 1992; Jensen and Jensen, 1996) in monochromatic mode with the same medium properties than using kWave (water), to obtain 3D maximum pressure fields. These maximum pressure fields where used to build a heating source term $Q_{US} = (\alpha_{np} p_{max}^2)/(\rho_b c_b)$, with α_{np} being the absorption coefficient of the brain at the considered frequency (59.04 $Np.m^{-1}$ at 15 MHz, calculated from $\alpha_{brain} = 0.21\ dB.cm^{-1}.MHz^{-y}$ and $y = 1.18$), the brain volumetric mass $\rho_{brain} = 1046\ kg.m^{-3}$, the brain sound speed $c_{brain} = 1546\ m.s^{-1}$ (Duck, Francis A., 1990; *ITIS Foundation DATABASE*), and p_{max} being the 3D maximum pressure field. This source term was then used in the resolution of a Penne's bioheat equation $\rho_{brain} C_{brain}.\partial T/\partial t = div(K_t.\nabla T) - \rho_{blood} C_{blood} P_{blood}(T - T_a) + Q$ in kWave, where C_{brain} is the blood specific heat capacity (3630 $J.kg^{-1}.C^{-1}$), K_t the brain thermal conductivity (0.51 $W.m^{-1}.C^{-1}$), ρ_{blood} the blood density 1050 kg/m^3, C_{blood} the blood specific heat capacity (3617 $J.kg^{-1}.C^{-1}$), P_{blood} the blood perfusion coefficient (9.7 $10^{-3} s^{-1}$), T_a the arterial temperature (37°C), and $Q = Q_{US} + \rho_{brain} \cdot \gamma_{brain}$ with γ_{brain} the heat generation of the brain tissue (11.37 $W.kg^{-1}$) (*ITIS Foundation DATABASE*; McIntosh and Anderson, 2010). The initial condition for the brain temperature was set to $T_0 = 37$°C. This simulation corresponds to a worst case scenario regarding the temperature rise given: 1) that the acoustic propagation is simulated in water only, with a lower attenuation coefficient (2.2 $10^{-3}\ dB.cm.MHz^{-2}$) than the brain (0.59 $dB.cm.MHz^{-1.27}$), even if a part of the propagation occurs within the brain. Therefore p_{max} maps are overestimated. 2) thermal absorption is simulated in brain tissue only, with a high absorption coefficient (0.21 $dB.cm.MHz^{-1.18}$) compared to water, even if a part of the maximum pressure field is actually located within the water of the acoustic coupling cone. Therefore Q_{US} is again slightly overestimated. We mapped the temperature in 3D and in time and looked for the point of maximal temperature rise (Figure E4 H-J).

Statistical analysis

Statistical analysis was carried out with Prism software (Prism 7, GraphPad). All values are expressed as means ± the standard error of the mean (SEM). The statistical tests performed are detailed in the figure legends. Data were analysed using an unpaired Welch's t-test (two-sided).

Data availability

The data that support the findings of this study are available from the corresponding author upon reasonable request.

Code availability

The custom Matlab codes are available from the corresponding author upon reasonable request.

ACKNOWLEDGEMENTS

The authors would like to thank J. Degardin, R. Goulet, C. Joffrois, M. Valet, M. Simonutti, M. Desrosiers, S. Fouquet, P. Annic, M. Celik for technical help and scientific advice. This work was supported by the European Re-

search Council (ERC) Synergy Grant Scheme (holistic evaluation of light and multiwave applications to high resolution imaging in ophthalmic translational research revisiting the helmholtzian synergies, ERC Grant Agreement 610110), by the Foundation Fighting Blindness, la fédération des aveugles de france, Optic 2000, Paris city, Région ile de France, and by French state funds managed by the Agence Nationale de la Recherche (ANR) within Programme Investissements d'Avenir, Laboratoire d'Excellence (LABEX) LIFESENSES (ANR-10-LABX-0065) and Institut Hospitalo-Universitaire FOReSIGHT (ANR-18-IAHU-0001).

AUTHOR CONTRIBUTIONS

S.C, C.D. designed the experiments, S.C.,M.P., G.L. carried out the experiments and analyzed the data, M.P., D.N., G.G., F.A., O.M., D.D. provided support on experiments and data analysis, S.P., M.T. , J.S. conceived the idea for this project and supervised the analysis of the data obtained. S.C., S.P., M.T., C.D, wrote the manuscript. All authors provided critical feedback about the research and manuscript.

COMPETING INTEREST DECLARATION

The authors have filled a patent for devices and methods for sonogenetic stimulation.

MATERIALS & CORRESPONDENCE

Correspondance and requests for materials should be addressed to sara.cadoni@inserm.fr or serge.picaud@inserm.fr.

REFERENCES

Akerman, Colin J., Darragh Smyth, and Ian D. Thompson (2002). "Visual experience before eye-opening and the development of the retinogeniculate pathway". In: *Neuron* 36.5, pp. 869–879.

Baron, Cecile, Jean François Aubry, Mickael Tanter, Stephen Meairs, and Mathias Fink (2009). "Simulation of Intracranial Acoustic Fields in Clinical Trials of Sonothrombolysis". In: *Ultrasound in Medicine and Biology* 35.7, pp. 1148–1158.

Beauchamp, Michael S., Denise Oswalt, Ping Sun, Brett L. Foster, John F. Magnotti, Soroush Niketeghad, Nader Pouratian, William H. Bosking, and Daniel Yoshor (2020). "Dynamic Stimulation of Visual Cortex Produces Form Vision in Sighted and Blind Humans". In: *Cell* 181.4, 774–783.e5.

Brindley, G. S. and W. S. Lewin (1968). "The sensations produced by electrical stimulation of the visual cortex". In: *The Journal of Physiology* 196.2, pp. 479–493.

Chaffiol, Antoine et al. (2017). "A New Promoter Allows Optogenetic Vision Restoration with Enhanced Sensitivity in Macaque Retina". In: *Molecular Therapy* 25.11, pp. 2546–2560.

Chernov, Mykyta M., Robert M. Friedman, Gang Chen, Gene R. Stoner, and Anna Wang Roe (2018). "Functionally specific optogenetic modulation in primate visual cortex". In: *Proceedings of the National Academy of Sciences of the United States of America* 115.41, pp. 10505–10510.

Choi, Vivian W., Aravind Asokan, Rebecca A. Haberman, and Richard Jude Samulski (2007). "Production of Recombinant Adeno-Associated Viral Vectors for In Vitro and In Vivo Use". In: *Current Protocols in Molecular Biology* 78.1, pp. 16.25.1–16.25.24.

Dalkara, Deniz, Leah C. Byrne, Ryan R. Klimczak, Meike Visel, Lu Yin, William H. Merigan, John G. Flannery, and David V. Schaffer (2013). "In

vivo-directed evolution of a new adeno-associated virus for therapeutic outer retinal gene delivery from the vitreous". In: *Science Translational Medicine* 5.189.

Deffieux, Thomas, Youliana Younan, Nicolas Wattiez, Mickael Tanter, Pierre Pouget, and Jean-François Aubry (2013). "Low-Intensity Focused Ultrasound Modulates Monkey Visuomotor Behavior". In: *Current Biology* 23.23, pp. 2430–2433.

Dobelle, Wm H. (2000). "Artificial vision for the blind by connecting a television camera to the visual cortex". In: *ASAIO Journal* 46.1, pp. 3–9.

Duck, Francis A., Author (1990). *Physical Properties of Tissues: A Comprehensive Reference Network*. Ed. by Academic Press. Vol. 36. London: Academic Press, pp. 459–466.

Ferrari, Ulisse, Stéphane Deny, Abhishek Sengupta, Romain Caplette, Francesco Trapani, José-Alain Sahel, Deniz Dalkara, Serge Picaud, Jens Duebel, and Olivier Marre (2020). "Towards optogenetic vision restoration with high resolution". In: *PLOS Computational Biology* 16.7. Ed. by Michiel van Wyk, e1007857.

Folloni, Davide, Lennart Verhagen, Rogier B. Mars, Elsa Fouragnan, Charlotte Constans, Jean François Aubry, Matthew F.S. Rushworth, and Jérôme Sallet (2019). "Manipulation of Subcortical and Deep Cortical Activity in the Primate Brain Using Transcranial Focused Ultrasound Stimulation". In: *Neuron* 101.6, 1109–1116.e5.

Guo, Hongsun, Mark Hamilton, Sarah J. Offutt, Cory D. Gloeckner, Tianqi Li, Yohan Kim, Wynn Legon, Jamu K. Alford, and Hubert H. Lim (2018). *Ultrasound Produces Extensive Brain Activation via a Cochlear Pathway*.

Hamill, Owen P. and Boris Martinac (2001). *Molecular basis of mechanotransduction in living cells*.

Huang, Yao-Shen et al. (2020). "Sonogenetic Modulation of Cellular Activities Using an Engineered Auditory-Sensing Protein". In:

ITIS Foundation DATABASE.

Ibsen, Stuart, Ada Tong, Carolyn Schutt, Sadik Esener, and Sreekanth H. Chalasani (2015). "Sonogenetics is a non-invasive approach to activating neurons in Caenorhabditis elegans". In: *Nature Communications* 6.1, p. 8264.

Jazayeri, Mehrdad, Zachary Lindbloom-Brown, and Gregory D. Horwitz (2012). "Saccadic eye movements evoked by optogenetic activation of primate V1". In: *Nature Neuroscience* 15.10, pp. 1368–1370.

Jensen, JΦrgen Arendt and Niels Bruun Svendsen (1992). "Calculation of Pressure Fields from Arbitrarily Shaped, Apodized, and Excited Ultrasound Transducers". In: *IEEE Transactions on Ultrasonics, Ferroelectrics, and Frequency Control* 39.2, pp. 262–267.

Jensen, Jørgen Arendt and Jørgen Arendt Jensen (1996). "FIELD: A Program for Simulating Ultrasound Systems". In: *10TH NORDICBALTIC CONFERENCE ON BIOMEDICAL IMAGING, VOL. 4, SUPPLEMENT 1, PART 1:351–353* 34, pp. 351–353.

Ju, Niansheng, Rundong Jiang, Stephen L. Macknik, Susana Martinez-Conde, and Shiming Tang (2018). "Long-term all-optical interrogation of cortical neurons in awake-behaving nonhuman primates". In: *PLOS Biology* 16.8. Ed. by Adam Kohn, e2005839.

Kim, Hyungmin, Alan Chiu, Stephanie D. Lee, Krisztina Fischer, and Seung-Schik Yoo (2014). "Focused Ultrasound-mediated Non-invasive Brain Stimulation: Examination of Sonication Parameters". In: *Brain Stimulation* 7.5, pp. 748–756.

Lee, Wonhye, Stephanie D. Lee, Michael Y. Park, Lori Foley, Erin Purcell-Estabrook, Hyungmin Kim, Krisztina Fischer, Lee-So Maeng, and Seung-Schik Yoo (2016). "Image-Guided Focused Ultrasound-Mediated Regional Brain Stimulation in Sheep". In: *Ultrasound in Medicine & Biology* 42.2, pp. 459–470.

Legon, Wynn, Priya Bansal, Roman Tyshynsky, Leo Ai, and Jerel K. Mueller (2018). "Transcranial focused ultrasound neuromodulation of the human primary motor cortex". In: *Scientific Reports* 8.1, p. 10007.

Legon, Wynn, Tomokazu F Sato, Alexander Opitz, Jerel Mueller, Aaron Barbour, Amanda Williams, and William J Tyler (2014). "Transcranial focused ultrasound modulates the activity of primary somatosensory cortex in humans". In: *Nature Neuroscience* 17.2, pp. 322–329.

McAlinden, Niall et al. (2019). "Multisite microLED optrode array for neural interfacing". In: *Neurophotonics* 6.03, p. 1.

McGregor, Juliette E., Tyler Godat, Kamal R. Dhakal, Keith Parkins, Jennifer M. Strazzeri, Brittany A. Bateman, William S. Fischer, David R. Williams, and William H. Merigan (2020). "Optogenetic restoration of retinal ganglion cell activity in the living primate". In: *Nature communications* 11.1, p. 1703.

McIntosh, Robert L. and Vitas Anderson (2010). *A comprehensive tissue properties database provided for the thermal assessment of a human at rest*.

Mehić, Edin, Julia M. Xu, Connor J. Caler, Nathaniel K. Coulson, Chet T. Moritz, and Pierre D. Mourad (2014). "Increased anatomical specificity of neuromodulation via modulated focused ultrasound". In: *PLoS ONE* 9.2.

Menz, M. D., O. Oralkan, P. T. Khuri-Yakub, and S. A. Baccus (2013). "Precise Neural Stimulation in the Retina Using Focused Ultrasound". In: *Journal of Neuroscience* 33.10, pp. 4550–4560.

Obidin, Nikita, Farita Tasnim, and Canan Dagdeviren (2020). "The Future of Neuroimplantable Devices: A Materials Science and Regulatory Perspective". In: *Advanced Materials* 32.15, p. 1901482.

Perozo, Eduardo (2006). *Gating prokaryotic mechanosensitive channels*.

Qiu, Zhihai, Shashwati Kala, Jinghui Guo, Minyi Yang, and Haoru Wang (2020). "Targeted Neurostimulation in Mouse Brains with Non-invasive Ultrasound". In:

Royer, D. and E. Dieulesaint (1986). "Optical probing of the mechanical impulse response of a transducer". In: *Applied Physics Letters* 49.17, pp. 1056–1058.

Sato, Tomokazu, Mikhail G. Shapiro, and Doris Y. Tsao (2018). "Ultrasonic Neuromodulation Causes Widespread Cortical Activation via an Indirect Auditory Mechanism". In: *Neuron* 98.5, 1031–1041.e5.

Soloperto, Alessandro, Anna Boccaccio, Andrea Contestabile, Monica Moroni, Grace I. Hallinan, Gemma Palazzolo, John Chad, Katrin Deinhardt, Dario Carugo, and Francesco Difato (2018a). "Mechano-sensitization of mammalian neuronal networks through expression of the bacterial large-conductance mechanosensitive ion channel". In: *Journal of Cell Science* 131.5, jcs210393.

Soloperto, Alessandro, Anna Boccaccio, Andrea Contestabile, Monica Moroni, Grace I. Hallinan, Gemma Palazzolo, John Chad, Katrin Deinhardt, Dario Carugo, and Francesco Difato (2018b). "Mechano-sensitization of mammalian neuronal networks through expression of the bacterial large-conductance mechanosensitive ion channel". In: *Journal of Cell Science* 131.5, jcs210393.

Sukharev (2001). "The gating mechanism of the large mechanosensitive channel MscL". In:

Sukharev, Sergei I., Paul Blount, Boris Martinac, Frederick R. Blattner, and Ching Kung (1994). "A large-conductance mechanosensitive channel in E. coli encoded by mscL alone". In: *Nature* 368.6468, pp. 265–268.

Tufail, Yusuf, Alexei Matyushov, Nathan Baldwin, Monica L. Tauchmann, Joseph Georges, Anna Yoshihiro, Stephen I. Helms Tillery, and William J. Tyler (2010). "Transcranial Pulsed Ultrasound Stimulates Intact Brain Circuits". In: *Neuron* 66.5, pp. 681–694.

Tufail, Yusuf, Anna Yoshihiro, Sandipan Pati, Monica M. Li, and William J. Tyler (2011). "Ultrasonic neuromodulation by brain stimulation with transcranial ultrasound". In: *Nature Protocols* 6.9, pp. 1453–1470.

Yang, Yaoheng et al. (2020). "Sonogenetics for noninvasive and cellular-level neuromodulation in rodent brain". In: *bioRxiv*, p. 2020.01.28.919910.

Ye, Jia et al. (2018). "Ultrasonic Control of Neural Activity through Activation of the Mechanosensitive Channel MscL". In: *Nano Letters* 18.7, pp. 4148–4155.

Ye, Patrick Peiyong, Julian R. Brown, and Kim Butts Pauly (2016). "Frequency dependence of ultrasound neurostimulation in the mouse brain". In: *Ultrasound in Medicine and Biology* 42.7, pp. 1512–1530.

Yger, Pierre et al. (2018). "A spike sorting toolbox for up to thousands of electrodes validated with ground truth recordings in vitro and in vivo". In: *eLife* 7.

Yoshimura, Kenjiro, Ann Batiza, Matt Schroeder, Paul Blount, and Ching Kung (1999). "Hydrophilicity of a Single Residue within MscL Correlates with Increased Channel Mechanosensitivity". In: *Biophysical Journal* 77.4, pp. 1960–1972.

Younan, Youliana, Thomas Deffieux, Benoit Larrat, Mathias Fink, Mickael Tanter, and Jean Francois Aubry (2013). "Influence of the pressure field distribution in transcranial ultrasonic neurostimulation". In: *Medical Physics* 40.8, pp. 1–10.

EXTENDED DATA FIGURES

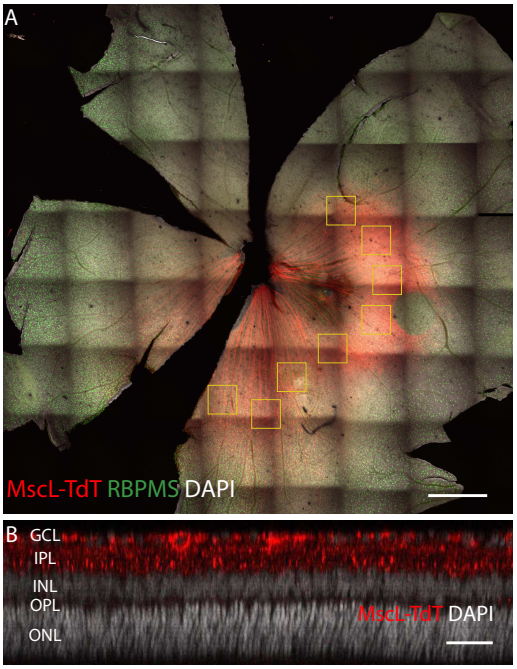

Figure E1 – Retinal expression of MscL. (A) Whole-mount retina expressing MscL WT (red) and labeled with the RGC-specific anti-RBPMS antibody (green), with DAPI staining of the nucleus (white). Yellow boxes represent the 8 zones selected for the counting of MscL- and RBPMS-positive cells. . (B) Optical section of a confocal stack showing MscL expression limited to the ganglion cell layer. The scale bars represent 1 mm in (A), 50 µm in (B).

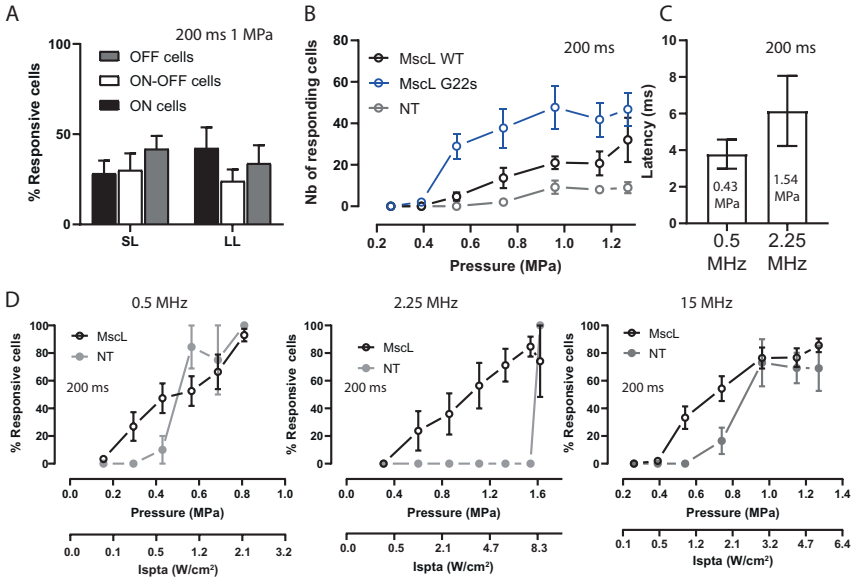

Figure E2 – Retinal sonogenetic response characteristics for US stimuli of different frequencies. (A) Classification of SL and LL responses in MscL (WT and G22S form) expressing RGCs to a 15 MHz stimulus (200 ms, 1 MPa), according to the responses to light stimulation, n=9 retinas. (B) Number of responding RGCs to a 200 ms 15 MHz stimulus of increasing acoustic pressure for MscL WT (n=3), MscL G22S (n=5) and NT (n=4) retinas. (C) Mean response latencies of SL cells for 0.5 and 2.25 MHz 200 ms long US stimuli (n=9 or 8 retinas, US pressure: 0.43, MPa for 0.5 MHz and 1.54 MPa for 2.25 MHz). (D) Percentage of cells responding to a 200 ms long US stimulus (normalized to the maximum number of responsive cells in the experiment) of increasing acoustic pressure for the three US frequencies tested. The lower x axis represents the corresponding acoustic intensity (Ispta). For all panels, error bars represent the SEM.

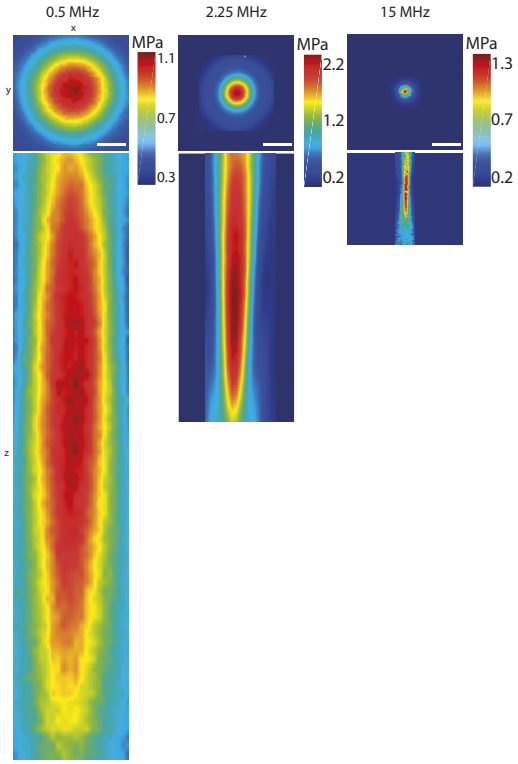

Figure E3 – US pressure fields for 0.5, 2.25 **and** 15 **MHz transducers, measured in water.** Color-coded pressure maps in the xy and xz planes, for 0.5 (A), 2.25 (B) and 15 (C) MHz. Scale bar represent 2 mm.

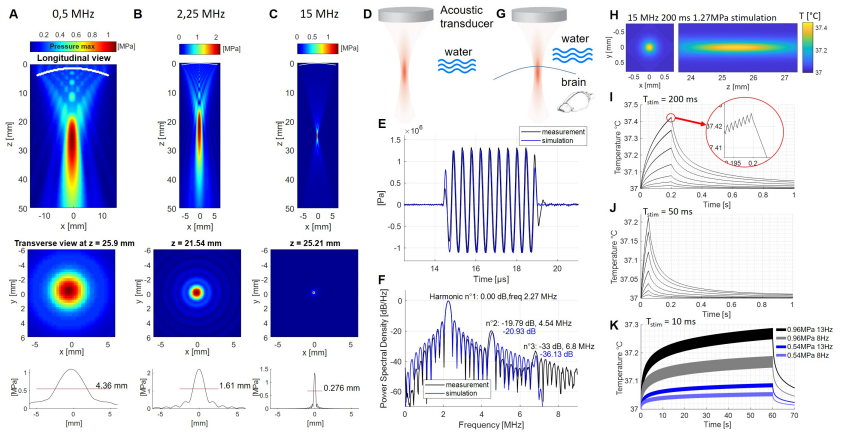

Figure E4 – Simulated acoustic fields and temperature increases. (A) Characterization of the radiated field for the 0.5 MHz transducer used in this study. (top) Longitudinal view of the maximal pressure for a monochromatic acoustic field radiated at 0.5 MHz by a 25.4 mm Ø, 31.75 mm focus transducer. Pressure maximum is reached at 25.9 mm, slightly nearer the focal point which is a documented effect 50. (middle) Transverse section of the maximal pressure field at depth z=25.9 mm. (bottom) One dimensional profile of this transverse section giving the full width at half maximum (FWHM) of the focal spot (4.36 mm at 0.5 MHz). (B) Same characterization for the 2.25 MHz 12.7′ Ø 25.4 mm focus transducer. (C) Same characterization for the 15 MHz 12.7′ Ø 25.4 mm focus transducer. Notice that the maximum pressure is reached very close to the geometrical focus (25.21 mm compared to 25.4 mm for the geometrical focus) for this configuration. FWHM of the focal spot is 0.276 mm. (D) Simulations are first conducted using an infinite propagation medium with same acoustic properties than water, to mimic the conditions obtained when calibrating the transducers in a water tank. (E) Comparison between a water tank measurement at focus (black) obtained with the 2.25 MHz transducer and reaching −1.11 MPa peak negative pressure, and a simulated waveform at focus (blue) reaching the same negative pressure. The two waveforms match very well (0.42% error) ensuring adequacy of our simulation setup and physical parameters. (F) Power spectral density of the measured (black) and simulated (blue) waveforms, showing that simulation enable to estimate the importance of the non-linear propagation. A second harmonic 20 dB below the fundamental indicates a factor 100 in terms of energy, meaning that absorption can be calculated in a linear approximation. (G) Thermal simulations are performed using a two-fold process corresponding to a worst-case scenario (see methods): propagation in a water medium, and thermal absorption in a brain mimicking medium. (H) 3D temperature map at the end of a 200 ms stimulation (at 15 MHz and 1.27 MPa). (I) Temperature rise at focus for a 15 MHz 200 ms stimulation with the 7 values of pressure used Fig 1I (0.26, 0.39, 0.54, 0.74, 0.96, 1.15, 1.27 MPa). A zoom on the increasing curve reveals the fluctuations due to the 1 kHz on-off cycles. (J) Temperature rise at focus for a 15 MHz 50 ms stimulation with the same 7 values of pressure. (K) Temperature rise at focus for 15 MHz 10ms stimulations (1 kHz modulation) at a repetition rate of 8 and 13 Hz (used in Figure 3O), for focus pressures of 0.96 MPa and 0.54 MPa. This shows that stimulation patterns compatible with video rate applications elicit very moderate thermal effect (max 0.3°C), emphasizing the safety of the technique.

Part III

Conclusions

3 DISCUSSION AND CONCLUSIONS

3.1 THE SONOGENETIC ACTUATOR CHOICE

The main aim of our work was to identify a suitable sonogenetic actuator for precise *in vivo* neural stimulation. To date, all attempts to achieve sonogenetic therapy *in vivo* were characterized by very low spatiotemporal resolution using Prestin protein (Huang et al., 2020; Wu et al., 2020), the TRPV1 ion channel (Yang et al., 2020) or the MscL G22S ion channel (Qiu et al., 2020). For the first two studies, the responses to US stimulation were attributed either to an indirect effect induced by US mechanical deformation on the actuator (Huang et al., 2020; Wu et al., 2020) or to US-induced tissue heating (Yang et al., 2020). On the other hand, the recent work of Qiu and coworkers demonstrated that the mechano-sensitive channel MscL G22S can efficiently sensitize neurons *in vivo* via the mechanical-deformation of cell membrane induced by US. However, even if this study presented the first proof-of-concept of MscL as a sonogenetic actuator for *in vivo* applications, no evidence about the spatio-temporal characteristics of the approach was provided.

We choose to investigate the MscL ion channel from *E. Coli* (in its WT form and G22S mutated form) as a potential actuator for sonogenetics because of its rapid kinetics, its biophysical mechanism of action, its small gene and its simple molecular structure. We here showed that sonogenetic therapy can be achieved with a high spatiotemporal precision on the isolated retina and in the *in vivo* cortex following MscL expression in the corresponding neurons. Our results confirmed previous findings of Qiu et. al that MscL-based sonogenetic therapy is effective on rodent brain, although it had been predicted that the use of this channel as a sonogenetic actuator would not be possible *in vivo* without the use of microbubbles (Maresca et al., 2018). We have shown, instead, that US activation of cortical neurons can be achieved without the boost of US-induced microbubble cavitation. Moreover we showed that MscL G22S expression leads to direct depolarization upon US stimulation *in vivo*. Moreover, *ex vivo*, this mutant form, G22S, of the MscL channel exhibited

a lower activation threshold compared to its WT form. Neurons expressing the MscL actuator were able to respond with a high temporal resolution, reflecting the fast mechanical gating properties of the MscL channel. Neurons responded to US frequencies from 0.5 MHz to 15 MHz showing that the required acoustic intensities were in a similar range for these different frequencies. In a previous study a mutated form of the same channel, MscL I92L, high frequency US stimulation was able to evoke responses in cultured neurons (Ye et al., 2018). These observations indicated that the US activation mechanism appeared to be virtually identical between our *in vivo* conditions and the previously reported *in vitro* conditions. Indeed the MscL channel opens rapidly when a mechanical stress is applied to the cell membrane (Sukharev, 2001). US-induced mechanical deformation of the cell membrane is therefore able to induce MscL channel opening when this deformation is over the threshold of channel gating. Moreover, 15 MHz stimulation has been found to be more effective in evoking a response in RGCs compared to lower US frequencies. This result suggests that acoustic radiation force might be responsible for cell membrane deformation and the consecutive ion channel opening as previously reported (Menz et al., 2017). This acoustic radiation force exerted on the tissue increases at higher acoustic frequencies because of the increased US absorption by the tissue. Further, our results indicate that stimulation efficiency at constant acoustic pressure was related to stimulus duration, suggesting thereby that the activation threshold is related not to the acoustic pressure but to the total energy delivered.

Therefore, our data are consistent with the notion that, as previously reported, the neuronal activation resulted from the mechano-sensitivity of the channel and is not related to US-induced temperature increase. Simulations of US-induced heating in our experimental conditions further supported this hypothesis. Indeed our stimulation protocol did not ledd to any significant tissue heating during the stimulation even at high stimulus repetition rates. Therefore, this evidences further suggests that the MscL-based sonogenetic approach will limit US-elicited side effects such as hemorrhages or tissue heating. This conclusion agrees with the fact that our acoustic parameters were lower than the safety limits defined by the FDA for US imaging (e. g. for a 20 ms US stimulus of 1.27 MPa the Ispta value is of 0.52 W/cm², FDA limit being of 0.72 W/cm²).

3.2 A SONOGENETIC ACTUATOR TO INCREASE SPATIOTEMPORAL RESOLUTION

The main aim of Sonogenetics is to specifically over-sensitize neurons to ultrasound and to increase the spatial and temporal precision that can be attempted compared to US stimulation only. Hereafter we discuss how this aim was attained with the MscL-based sonogenetic approach.

3.2.1 *MscL leads to high temporal resolution*

Neurons expressing the MscL actuator were able to respond with a rapid kinetics to US stimuli of short duration (up to 10 ms) and with high repetition rates (10 Hz) both in the isolated retina and *in vivo* in cortical neurons. These features reflect the fast mechanical gating properties of the MscL channel. Previous studies investigating sonogenetic actuators *in vitro* had already identified the MscL and the PIEZO1 channels as able to induce US responses with high temporal kinetics (Prieto et al., 2018; Ye et al., 2018). *In vivo*, Prestin and TRPV1 as sonogenetic actuators failed to achieve high temporal resolution. The TRPV1-induced responses were characterised by very long latencies and required long stimulus durations (> 4 s) (Yang et al., 2020). This is presumably due to the fact that the TRPV1-based approach requires the US-induced tissue heating to evoke a response. The temporal dynamics of temperature increase and decrease is of course longer than for US-induced mechanical deformation. For Prestin-based sonogenetics, the temporal dynamics has not yet been determinated (Huang et al., 2020; Wu et al., 2020). Similarly, the MscL has been shown recently to be able to sensitize neurons to US but its use to attempt high spatiotemporal precision was not proven *in vivo*. Our results show that MscL is able to induce direct and rapid depolarization of neurons when stimulated with US confirming previous *in vitro* results with the I92L mutant (Ye et al., 2018). The latency of the US evoked response varied from 12.2 ± 2.5 ms for RGCs in isolated retina to 7.57 ± 1.37 ms for cortical neurons *in vivo*. This temporal kinetics could be dependent on the expression rate of the channel on cell membrane, since the time to obtain cell depolarization might be dependent on the number and conductance of the active ion channels. However, it is likely that specific voltage-gated ion channels also influence this spike initiation in the respective cells. Therefore, response latency could be further reduced by

incrementing the expression rate of the channel on cell membrane. Moreover, a gain-of-function mutant of the MscL channel with faster gating kinetics could also be developed to further decrease the latency of the response.

3.2.2 *Choice of ultrasound frequency*

The choice of the ultrasonic frequency for US stimulation affects the spatial resolution of the neural response that can be attempted. Because of the physical properties of US waves travelling through a tissue, to achieve high spatial resolution high frequency US has to be used at the expense of the penetration ability and non-invasiveness (Figure 25). Moreover, at low frequencies exact targeting cannot be guaranteed because of the likely formation of standing waves[1]. This phenomenon generates reflected ultrasound waves with complex pressure fields outside the target area that are difficult to control because they are dependent on the curvature of the skull and the angle between the skull and the US probe (Baron et al., 2009). In rodent brain this phenomenon can even lead to reverberations in the entire braincase (Younan et al., 2013) and the likely stimulation of non-targeted structures such as the auditory pathway (Guo et al., 2018; Sato, Shapiro, and Tsao, 2018). On the other hand, higher US intensities might be required to effectively stimulate neurons at high US carrier frequencies (King et al., 2013; Ye, Brown, and Pauly, 2016) leading to potential side-effects such as tissue heating.

To be non-invasive and to avoid the use of high US intensities, most studies investigating US stimulation *in vivo* used sub-megahertz frequencies as outlined in Figure 26. All studies using US frequencies greater than 5 MHz concerned *in vitro* experimental preparations and used quite high intensity values (Kubanek et al., 2016; Menz et al., 2013; Menz et al., 2017; Prieto et al., 2018; Tyler et al., 2008), supporting the hypothesis that higher intensities are required for high frequency US stimulation. As a consequence, to our knowledge, high reso-

1 A standing or stationary wave derives from the combination of two waves moving in opposite directions and having the same amplitude and frequency. Standing waves originate from interference. For waves that are moving in opposite directions, interference produces an oscillating wave that is fixed in space (the nodes are the fixed positions) with an amplitude that is equal to the sum of the amplitudes of the single waves.

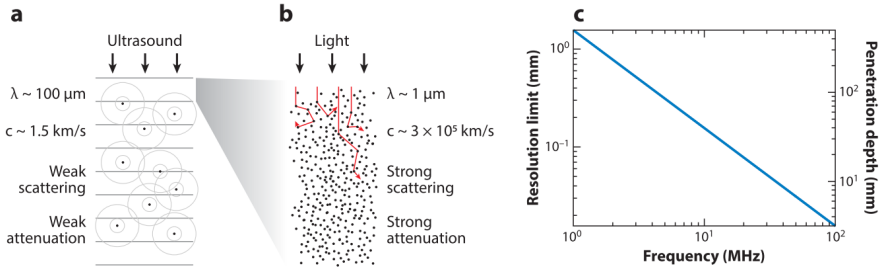

Figure 25: **Physical properties of ultrasound waves in biological tissues.** Physical properties of US (a) and light (b) travelling in a biological tissue. (c) Fundamental trade-off between ultrasound resolution and penetration depth as a function of frequency in brain tissue (penetration depth was assessed based on a 60 decibel round-trip attenuation). At an ultrasound frequency of 15 MHz, US can penetrate 2 cm into the brain with a 100 m resolution. Source: (Maresca et al., 2018)

lution US neuromodulation has not yet been attained *in vivo* and would be difficult to achieve without increasing the risk of potential side effects. Thus it would be difficult to apply US neuromodulation alone, without using a sonogenetic actuator, in all the applications requiring a precise and high throughput stimulation.

To date, all the studies investigating sonogenetic actuators showed that expressing them on the cell membrane induced an increased sensitivity to US compared to control preparations; however, the gain in spatial and temporal resolution remains to be assessed *in vivo* (see Table 2). Based on *in vitro* assessment, the PIEZO1 and MscL ion channels appear to be the most suitable actuators for precise sonogenetic stimulation because they were able to decrease the activation threshold and induce activation at high US frequencies, leading to high spatial resolution (Prieto et al., 2018; Ye et al., 2018). On the other hand, PIEZO1 appears to be less interesting for *in vivo* applications because its large gene cannot be easily packed into AAVs, the leading gene delivery vectors for the central nervous system. Our findings suggest that MscL G22S is able to increase the spatial resolution of US stimulation also *in vivo*. Indeed, neurons were able to respond to high frequency stimulation (15 MHz) with a limited acoustic intensity (I_{spta}: 0.52 W/cm² for 20 ms stimulation). Figure 26 illustrates that, in our experimental conditions, acoustic US intensity (red square) stays in the lower range of intensities

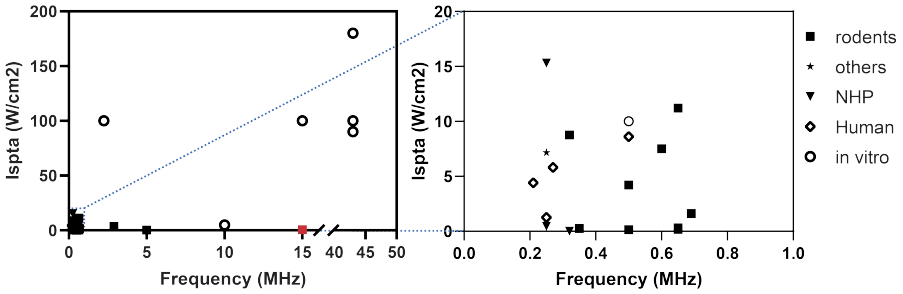

Figure 26: **US frequencies and intensities used in the literature for US neuromodulation.** The spatial peak temporal average US intensity (I_{spta}) and the corresponding US frequency are represented with a point for each of the reviewed studies listed in Table 1. The studies are grouped in*in vitro*, and *in vivo* preparations (and are further classified according to the organism that is targeted: human, non-human primates, rodents or others). On the right, a magnification for low frequency US (up to 1 MHz). The red square on the left panel represents the parameters that have been used for *in vivo* MscL-based sonogenetic stimulation in our work.

despite the high US frequency that we used. When comparing with previously investigated sonogenetic actuators for *in vivo* application, Prestin was not able to induce neural activation at US frequencies greater than 0.5 MHz (Huang et al., 2020; Wu et al., 2020) and both TRPV1 and MscL G22S channels were able to increase US sensitivity but high frequency US stimulation has not been investigated (Qiu et al., 2020; Yang et al., 2020).

3.3 APPLICATION FOR VISUAL RESTORATION

To date, the most promising neurostimulation technologies for vision restoration remain visual prostheses. Retinal implants are the mostly investigated visual prostheses because of the easy access to the retina. Several implants are already commercially available or in clinical trials (Cruz et al., 2016). However, such retinal prostheses are suitable only for those patients that are affected by photoreceptor degeneration. This approach is not suitable for patients that have lost the connection between the eye and higher visual centres in the brain. Direct stimulation of these higher visual centres has therefore been investigated (Brindley and Lewin, 1968). Cortical and intra-cortical electrode arrays have been developed to stimulate directly the primary visual cortex. This approach is very attractive because of the

straightforward and well-understood coding of the visual scene, the accessibility and the favourable magnification factor of the central visual field of the visual cortex. All these features render the visual cortex the main target for vision restoration besides the retina. Cortical electrode arrays are able to restore form vision in patients but suffer from low resolution due to the technological limitations of the stimulating electrodes (Beauchamp et al., 2020). In addition, loss of efficacy over time has been observed (Dobelle, 2000). Higher resolution with low currents can be achieved with more invasive penetrating electrodes reaching the deepest cortical layers (Tehovnik et al., 2005) but, again, long-term efficacy is not achieved (Fernandez et al., 2014). Moreover, a large portion of the early visual areas (V1, V2 and V3) is located in the medial surface of the occipital cortex. Implanting electrodes in these regions is problematic because of the risk of damaging the adjacent cortex and the difficult wireless transmission of the receiving and transmitting coils when they are orthogonal (Troyk, 2017). Vision restoration via direct optogenetic activation of the primary visual cortex seemed therefore a very promising approach that has been already tested on non-human primates (Jazayeri, Lindbloom-Brown, and Horwitz, 2012; Ju et al., 2018). Since the genetic photo-sensitization of neurons does not require electrodes, it is less invasive and offers potentially high resolution vision. In addition, this approach offers the ability to target specific cell populations. However, a major drawback is the high scattering of light into brain tissue, which prevents the efficient stimulation of deeper neuronal layers. Because of this scattering, the final volume of the brain that receives enough light is relatively superficial (Diester et al., 2011). To circumvent this problem and efficiently focus light into the brain, optical fibres can be implanted and the dura mater removed. Optic waveguides or optrodes have also been proposed to bring light deeper into the tissue, but the non-invasiveness of the approach is thereby lost (McAlinden et al., 2019). Deep cortical structures remain therefore difficult to target without increasing light intensities, which, however, might heat the more superficial tissue and affect normal neuronal physiology (Owen, Liu, and Kreitzer, 2019).

In this context, neurostimulation by means of US waves is considered a very promising strategy, because it can overcome certain limitations of the existing techniques. First of all it can be focused on deep cortical regions without major scattering and

attenuation as is the case for light stimulation in optogenetics (Figure 25). Secondly, it is able to modulate neuronal activity at higher resolution compared to other non-invasive techniques such as transcranial magnetic or current stimulation (Kime et al., 2018).
The presented sonogenetic approach can boost the sensitivity of neurons to US waves and lead to increased spatial and temporal resolution, a key feature for proper vision restoration. Besides direct cortical stimulation for vision restoration, the MscL-based sonogenetic strategy could also be applied in those cases where the optical window onto the retina is no longer available, i. e. diseases of the cornea that prevent the efficient transmission of light to the retina, necessary for optogenetics or photovoltaic retinal prostheses.
The MscL-based sonogenetic approach applied to vision restoration offer several major advantages:

- The achievement of high spatio-temporal resolution. As previously emphasised, this is a key element for vision restoration. Resolution could be further increased by boosting event more the expression rate of MscL in neurons. Indeed, it is likely that the latency of a sonogenetic-evoked response reflects the time required for MscL to depolarize the neuronal membrane potential to reach the action potential threshold, which is in turn governed by the number and conductance of active ion channels. Moreover, the expression rate could also influence the required activation threshold, allowing the use of even higher US carrier frequency, which would decrease further the size of focal beam and increase the spatial resolution of the approach. In comparison, the resolution of cortical prostheses is, nowadays, limited by technology. Previous *in vivo* studies demonstrated that form vision is possible with stimulating electrodes of $0.8 - 1$ mm diameter and with a spacing greater than 1 mm (Beauchamp et al., 2020; Dobelle, 2000). Our proposed sonogenetic approach offers a better spatial resolution.

- The safety of the approach. The safety of US waves in biomedical applications has been widely demonstrated both for imaging and for therapeutic applications. At the acoustic parameters used, no significant tissue heating is generated and US-induced cavitation is unlikely. Moreover, since the bacterial MscL responds exclusively to mechanical

stress, its over-expression in mammalian neurons is unlikely to generate negative effects on developed neurons, as previously reported (Soloperto et al., 2018).

- The tunability of the approach. Thanks to its simple submolecular structure, the MscL channel can be easily engineered to create gain-of-function mutants, e. g. a mutant that is ion selective, that opens at even lower pressure values or a fast gating mutant to increase frequency of US-evoked responses.

- The possibility of targeting hardly accessible regions of the visual cortex. Compared to cortical prostheses, US can also be focused on regions that are difficult to access with cortical implants because of the physical structure of the visual cortex. Cortical prostheses can comfortably access central receptive fields, which are located near the surface of the occipital lobe, but face difficulty when targeting regions corresponding to peripheral fields. The inter-hemispheric fissure represents an anatomical barrier for stimulating roughly 85% of V1 (Trobe, 2001) and convolutions on the surface of the brain can bury receptive fields. US waves can easily also target these hard-to-access regions.

The main limitation of the proposed approach remains that it cannot be considered non-invasive as it requires skull removal. It can be considered a distant stimulation procedure because the US transducer does not have to be in direct contact with the targeted tissue. Compared to intracortical prostheses and optogenetic therapy, this method remains still less invasive, as it does not require the removal of the dura mater.
Moreover, further studies are needed to generate an interface for coding visual information into US activation patterns onto the visual cortex at a video rate that would induce perception of the said stimuli by the subject. Indeed, even if we were able to record the direct response of cells following US stimulation, it still remains to be determined whether the induced cortical activity can encode a perception of the visual stimuli. Further behavioural tests will be needed to confirm this perception and our ability to generate form vision in a dynamic mode for navigation face recognition. Besides, an US stimulation array system needs to be developed to focus US stimuli simultaneously on different locations of the visual cortex at video rate to recreate a visual scene.

3.4 OTHER APPLICATIONS IN THE CENTRAL NERVOUS SYSTEM

Neuro-stimulation of the brain is a major challenge for neuroscience both in clinical practice and in fundamental research. In clinical practice, neurostimulation techniques are used for a wide range of neurological disorders and conditions: movement disorders, mental disorders, chronic pain, epilepsy, Parkinson's, Alzheimer's and deafness or blindness, through the aid of neural prostheses and brain-machine interfaces (Lebedev and Nicolelis, 2017; Lewis and Grandl, 2015). Neurostimulation of the brain is accomplished through either invasive (e. g. implanted or surface microelectrodes) or non-invasive means (e. g. transcranial magnetic or electrical simulation and ultrasound stimulation). Deep brain stimulation delivers electric currents to increase, suppress or distort neuronal activity through electrodes implanted deep into the brain. This approach has been successfully used in patients with essential tremor, dystonia or Parkinson's disease (Parihar et al., 2015; Perlmutter and Mink, 2006) but also for mental disorders. The main drawbacks of these electrode-based techniques is the quite invasive surgical procedure that can lead to complications: infections, neural immune system reactions and limited life of electrical components (Bronstein et al., 2011). Concerning non-invasive stimulation techniques, transcranial magnetic stimulation has been applied to the motor cortex to evoke movements or to the occipital cortex to produce phosphenes or scotomas (Hallett, 2000), or in patients suffering from major depressive disorders (Loo and Mitchell, 2005). Transcranial current stimulation cannot elicit action potentials like magnetic stimulation but can alter corticospinal excitability (Nitsche et al., 2008). Both techniques suffer from a limited spatial resolution with a radius of action (a few cm) such that it cannot target a specific brain region without stimulating the surrounding tissue.

In this context, sonogenetics opens a path toward a new type of brain-machine interface for all those clinical applications requiring cortical or sub-cortical stimulation with high spatio-temporal resolution. Sonogenetics could be applied to treat a large range of neurological diseases, e. g. it could be used to stimulate the auditory cortex to treat deafness, but also for handicap compensation. For instance, it could be used as an alternative to deep-brain stimulation to alleviate motor symptoms

in Parkinson's disease, thus offering an alternative to invasive bypass implantation surgeries. Moreover, this strategy could benefit from fast translatability from research to clinical applications because of the extensive medical reports already existing on US imaging and therapeutic US. In addition, AAVs-based gene therapy has also been applied successfully in several clinical trials for various conditions such as inherited blindness and neurodegenerative diseases. Because of all these features, sonogenetics represents to date a very promising approach for all applications requiring precise stimulation of the central nervous system.

BIBLIOGRAPHY

Ali, Robin R., Martin B. Reichel, Mahesh De Alwis, Naheed Kanuga, Christine Kinnon, Roland J. Levinsky, David M. Hunt, Shomi S. Bhattacharya, and Adrian J. Thrasher (1998). "Adeno-associated virus gene transfer to mouse retina". In: *Human Gene Therapy* 9.1, pp. 81–86.

Alloui, Abdelkrim et al. (2006). "TREK-1, a K+ channel involved in polymodal pain perception". In: *EMBO Journal* 25.11, pp. 2368–2376.

Ambati, Jayakrishna and Benjamin J. Fowler (2012). *Mechanisms of age-related macular degeneration*.

Árnadóttir, Jóhanna and Martin Chalfie (2010). "Eukaryotic Mechanosensitive Channels". In: *Annual Review of Biophysics* 39.1, pp. 111–137.

Auricchio, Alberto, Gary Kobinger, Vibha Anand, Markus Hildinger, Erin O' Connor, Albert M Maguire, James M Wilson, and Jean Bennett (2001). *Exchange of surface proteins impacts on viral vector cellular specificity and transduction characteristics: the retina as a model*. Tech. rep. 26, pp. 3075–3081.

Azhari, Haim (2010). *Basics of Biomedical Ultrasound for Engineers*. Hoboken, NJ, USA: John Wiley and Sons.

Baden, Tom, Philipp Berens, Katrin Franke, Miroslav Román Rosón, Matthias Bethge, and Thomas Euler (2016). "The functional diversity of retinal ganglion cells in the mouse". In: *Nature* 529.7586, pp. 345–350.

Bair, Wyeth and Christof Koch (1996). "Temporal Precision of Spike Trains in Extrastriate Cortex of the Behaving Macaque Monkey". In: *Neural Computation* 8.6, pp. 1185–1202.

Bang, Hyoweon, Yangmi Kim, and Donghee Kim (2000). "TREK-2, a new member of the mechanosensitive tandem-pore K+ channel family". In: *Journal of Biological Chemistry* 275.23, pp. 17412–17419.

Baron, Cecile, Jean François Aubry, Mickael Tanter, Stephen Meairs, and Mathias Fink (2009). "Simulation of Intracranial Acoustic Fields in Clinical Trials of Sonothrombolysis". In: *Ultrasound in Medicine and Biology* 35.7, pp. 1148–1158.

Beauchamp, Michael S., Denise Oswalt, Ping Sun, Brett L. Foster, John F. Magnotti, Soroush Niketeghad, Nader Pouratian, William H. Bosking, and Daniel Yoshor (2020). "Dy-

namic Stimulation of Visual Cortex Produces Form Vision in Sighted and Blind Humans". In: *Cell* 181.4, 774–783.e5.

Bi, Anding, Jinjuan Cui, Yu Ping Ma, Elena Olshevskaya, Mingliang Pu, Alexander M. Dizhoor, and Zhuo Hua Pan (2006). "Ectopic Expression of a Microbial-Type Rhodopsin Restores Visual Responses in Mice with Photoreceptor Degeneration". In: *Neuron* 50.1, pp. 23–33.

Blackmore, Joseph, Shamit Shrivastava, Jerome Sallet, Chris R. Butler, and Robin O. Cleveland (2019). "Ultrasound Neuromodulation: A Review of Results, Mechanisms and Safety". In: *Ultrasound in Medicine & Biology*.

Blicher, Andreas, Katarzyna Wodzinska, Matthias Fidorra, Mathias Winterhalter, and Thomas Heimburg (2009). "The temperature dependence of lipid membrane permeability, its quantized nature, and the influence of anesthetics". In: *Biophysical Journal* 96.11, pp. 4581–4591.

Blount, P., S. I. Sukharev, M. J. Schroeder, S. K. Nagle, and C. Kung (1996). "Single residue substitutions that change the gating properties of a mechanosensitive channel in Escherichia coli." In: *Proceedings of the National Academy of Sciences* 93.21, pp. 11652–11657.

Boye, Shannon E., Sanford L. Boye, Alfred S. Lewin, and William W. Hauswirth (2013). *A comprehensive review of retinal gene therapy*.

Brindley, G. S. and W. S. Lewin (1968). "The sensations produced by electrical stimulation of the visual cortex". In: *The Journal of Physiology* 196.2, pp. 479–493.

Bronstein, Jeff M. et al. (2011). *Deep brain stimulation for Parkinson disease an expert consensus and review of key issues*.

Brown, Paul K. and George Wald (1963). "Visual pigments in human and monkey retinas". In: *Nature* 200.4901, pp. 37–43.

Busskamp, V., S. Picaud, J. A. Sahel, and B. Roska (2012). *Optogenetic therapy for retinitis pigmentosa*.

Busskamp, Volker et al. (2010). *Genetic reactivation of cone photoreceptors restores visual responses in retinitis pigmentosa*.

Carattino, Marcelo D., Shaohu Sheng, and Thomas R. Kleyman (2004). "Epithelial Na+ Channels Are Activated by Laminar Shear Stress". In: *Journal of Biological Chemistry* 279.6, pp. 4120–4126.

Cesare, P., A. Moriondo, V. Vellani, and P. A. Mcnaughton (1999). "Ion channels gated by heat". In: *Proceedings of the National Academy of Sciences of the United States of America* 96.14, pp. 7658–7663.

Chaffiol, Antoine et al. (2017). "A New Promoter Allows Optogenetic Vision Restoration with Enhanced Sensitivity in Macaque Retina". In: *Molecular Therapy* 25.11, pp. 2546–2560.

Chang, G., R. H. Spencer, A. T. Lee, M. T. Barclay, and D. C. Rees (1998). "Structure of the MscL Homolog from Mycobacterium tuberculosis: A Gated Mechanosensitive Ion Channel". In: *Science* 282.5397, pp. 2220–2226.

Choi, Vivian W., Douglas M. McCarty, and R. Jude Samulski (2006). "Host Cell DNA Repair Pathways in Adeno-Associated Viral Genome Processing". In: *Journal of Virology* 80.21, pp. 10346–10356.

Cobbold, Richard S. C. (2007). *Foundations of biomedical ultrasound*. Oxford University Press, p. 802.

Constans, Charlotte, Thomas Deffieux, Pierre Pouget, Mickael Tanter, and Jean Francois Aubry (2017). "A 200-1380-kHz Quadrifrequency Focused Ultrasound Transducer for Neurostimulation in Rodents and Primates: Transcranial in Vitro Calibration and Numerical Study of the Influence of Skull Cavity". In: *IEEE Transactions on Ultrasonics, Ferroelectrics, and Frequency Control* 64.4, pp. 717–724.

Coste, Bertrand, Jayanti Mathur, Manuela Schmidt, Taryn J. Earley, Sanjeev Ranade, Matt J. Petrus, Adrienne E. Dubin, and Ardem Patapoutian (2010). "Piezo1 and Piezo2 are essential components of distinct mechanically activated cation channels". In: *Science* 330.6000, pp. 55–60.

Cruz, Lyndon da et al. (2016). "Five-Year Safety and Performance Results from the Argus II Retinal Prosthesis System Clinical Trial". In: *Ophthalmology* 123.10, pp. 2248–2254.

Curcio, Christine A., Kenneth R. Sloan, Orin Packer, Anita E. Hendrickson, and Robert E. Kalina (1987). "Distribution of cones in human and monkey retina: Individual variability and radial asymmetry". In: *Science* 236.4801, pp. 579–582.

Curie, Jacques and Pierre Curie (1880). "Développement par compression de l'électricité polaire dans les cristaux hémièdres à faces inclinées". In: *Bulletin de la Société minéralogique de France* 3.4, pp. 90–93.

Curley, M.G. (1993). "Soft tissue temperature rise caused by scanned, diagnostic ultrasound". In: *IEEE Transactions on Ultrasonics, Ferroelectrics and Frequency Control* 40.1, pp. 59–66.

Dalecki, Diane (2004). "Mechanical Bioeffects of Ultrasound". In: *Annual Review of Biomedical Engineering* 6.1, pp. 229–248.

Dalkara, Deniz, Leah C. Byrne, Ryan R. Klimczak, Meike Visel, Lu Yin, William H. Merigan, John G. Flannery, and David V. Schaffer (2013). "In vivo-directed evolution of a new adeno-associated virus for therapeutic outer retinal gene delivery from the vitreous". In: *Science Translational Medicine* 5.189.

Dallapiazza, Robert F., Kelsie F. Timbie, Stephen Holmberg, Jeremy Gatesman, M. Beatriz Lopes, Richard J. Price, G. Wilson Miller, and W. Jeffrey Elias (2018). "Noninvasive neuromodulation and thalamic mapping with low-intensity focused ultrasound". In: *Journal of Neurosurgery* 128.3, pp. 875–884.

Dayan, Eran, Nitzan Censor, Ethan R Buch, Marco Sandrini, and Leonardo G Cohen (2013). "Noninvasive brain stimulation: from physiology to network dynamics and back HHS Public Access". In: *Nat Neurosci* 16.7, pp. 838–844.

Deffieux, Thomas, Youliana Younan, Nicolas Wattiez, Mickael Tanter, Pierre Pouget, and Jean-François Aubry (2013). "Low-Intensity Focused Ultrasound Modulates Monkey Visuomotor Behavior". In: *Current Biology* 23.23, pp. 2430–2433.

Delmas, Patrick and Bertrand Coste (2013). *XMechano-gated ion channels in sensory systems*.

Demb, Jonathan B. and Joshua H. Singer (2015). "Functional Circuitry of the Retina". In: *Annual Review of Vision Science* 1.1, pp. 263–289.

Diester, Ilka, Matthew T. Kaufman, Murtaza Mogri, Ramin Pashaie, Werapong Goo, Ofer Yizhar, Charu Ramakrishnan, Karl Deisseroth, and Krishna V. Shenoy (2011). "An optogenetic toolbox designed for primates". In: *Nature Neuroscience* 14.3, pp. 387–397.

Dobelle, Wm H. (2000). "Artificial vision for the blind by connecting a television camera to the visual cortex". In: *ASAIO Journal* 46.1, pp. 3–9.

Dong, Biao, Hiroyuki Nakai, and Weidong Xiao (2010). "Characterization of genome integrity for oversized recombinant AAV vector". In: *Molecular Therapy* 18.1, pp. 87–92.

Dowling, John E. (1987). *The Retina: An Approachable Part of the Brain*. The Belknap Press of Harvard University.

Duc, C., N. Farman, C. M. Canessa, J. P. Bonvalet, and B. C. Rossier (1994). "Cell-specific expression of epithelial sodium channel α, β, and γ subunits in aldosterone-responsive epithelia from the rat: Localization by in situ hybridization and immunocytochemistry". In: *Journal of Cell Biology* 127.6 II, pp. 1907–1921.

Duh, Elia J., Jennifer K. Sun, and Alan W. Stitt (2017). *Diabetic retinopathy: current understanding, mechanisms, and treatment strategies*.

Dussik, Karl Theo (1942). "Über die Möglichkeit, hochfrequente mechanische Schwingungen als diagnostisches Hilfsmittel zu verwerten". In: *Zeitschrift für die gesamte Neurologie und Psychiatrie* 174.1, pp. 153–168.

FDA (2008). "Information for Manufacturers Seeking Marketing Clearance of Diagnostic Ultrasound Systems and Transducers". In: pp. 1–64.

Fenno, Lief, Ofer Yizhar, and Karl Deisseroth (2011). "The Development and Application of Optogenetics". In: *Annual Review of Neuroscience* 34.1, pp. 389–412.

Fernandez, Eduardo, Bradley Greger, Paul A. House, Ignacio Aranda, Carlos Botella, Julio Albisua, Cristina Soto-Sanchez, Arantxa Alfaro, and Richard A. Normann (2014). "Acute human brain responses to intracortical microelectrode arrays: challenges and future prospects". In: *Frontiers in Neuroengineering* 7.JUL, p. 24.

Fernández, Eduardo and Richard A. Normann (2017). "CORTIVIS Approach for an Intracortical Visual Prostheses". In: *Artificial Vision*. Springer International Publishing, pp. 191–201.

Fillafer, Christian and Matthias F. Schneider (2016). "On the excitation of action potentials by protons and its potential implications for cholinergic transmission". In: *Protoplasma* 253.2, pp. 357–365.

Fink, Michel, Fabrice Duprat, Florian Lesage, Roberte Reyes, Georges Romey, Catherine Heurteaux, and Michel Lazdunski (1996). "Cloning, functional expression brain localization of a novel unconventional outward rectifier K+ channel". In: *EMBO Journal* 15.24, pp. 6854–6862.

Folloni, Davide, Lennart Verhagen, Rogier B. Mars, Elsa Fouragnan, Charlotte Constans, Jean François Aubry, Matthew F.S. Rushworth, and Jérôme Sallet (2019). "Manipulation of Subcortical and Deep Cortical Activity in the Primate Brain Using Transcranial Focused Ultrasound Stimulation". In: *Neuron* 101.6, 1109–1116.e5.

Fry, F. J., H. W. Ades, and W. J. Fry (1958). "Production of reversible changes in the central nervous system by ultrasound". In: *Science* 127.3289, pp. 83–84.

Garafalo, Alexandra V., Artur V. Cideciyan, Elise Héon, Rebecca Sheplock, Alexander Pearson, Caberry WeiYang Yu, Alexander Sumaroka, Gustavo D. Aguirre, and Samuel G.

Jacobson (2020). *Progress in treating inherited retinal diseases: Early subretinal gene therapy clinical trials and candidates for future initiatives*.

Garry, Ambroise, Berengere Fromy, Nicolas Blondeau, Daniel Henrion, Frederic Brau, Pierre Gounon, Nicolas Guy, Catherine Heurteaux, Michel Lazdunski, and Jean Louis Saumet (2007). "Altered acetylcholine, bradykinin and cutaneous pressure-induced vasodilation in mice lacking the TREK1 potassium channel: The endothelial link". In: *EMBO Reports* 8.4, pp. 354–359.

Gislin, Dagnelie and Margalit Eyal (2004). "THE VISUAL SYSTEM AS A NEUROPROSTHESIS SUBSTRATE: ANATOMY, PHYSIOLOGY, FUNCTION". In: *Neuroprosthetics: Theory and Practice*, pp. 235–259.

Goodman, Miriam B., Glen G. Ernstrom, Dattananda S. Chelur, Robert O'Hagan, C. Andrea Yao, and Martin Chalfie (2002). "MEC-2 regulates C. elegans DEG/ENaC channels needed for mechanosensation". In: *Nature* 415.6875, pp. 1039–1042.

Guharay, F. and F. Sachs (1984). "Stretch-activated single ion channel currents in tissue-cultured embryonic chick skeletal muscle." In: *The Journal of Physiology* 352.1, pp. 685–701.

Guo, Hongsun, Mark Hamilton, Sarah J. Offutt, Cory D. Gloeckner, Tianqi Li, Yohan Kim, Wynn Legon, Jamu K. Alford, and Hubert H. Lim (2018). *Ultrasound Produces Extensive Brain Activation via a Cochlear Pathway*.

Haar, Gail ter (2011). "Ultrasonic imaging: safety considerations". In: *Interface Focus* 1.4, pp. 686–697.

Hallett, Mark (2000). *Transcranial magnetic stimulation and the human brain*.

Hamill, Owen P. and Boris Martinac (2001). *Molecular basis of mechanotransduction in living cells*.

Hangiandreou, Nicholas J (2003). "IMAGING & THERAPEUTIC TECHNOLOGY AAPM/RSNA Physics Tutorial for Residents: Topics in US B-mode US: Basic Concepts and New Technology 1". In: *RadioGraphics* 23, pp. 1019–1033.

Haswell, Elizabeth S., Rob Philipps, and Douglas C. Rees (2011). "Mechanosensitive channels: what can they do and how do they do it?" In: *Structure* 19.10, pp. 1356–1369.

Herrera, E. and C. A. Mason (2007). *The evolution of crossed and uncrossed retinal pathways in mammals*.

Hodgkin, A. L. and A. F. Huxley (1952). "A quantitative description of membrane current and its application to conduction

and excitation in nerve". In: *The Journal of Physiology* 117.4, pp. 500–544.

Horton, Jonathan C. and William F. Hoyt (1991). "The Representation of the Visual Field in Human Striate Cortex: A Revision of the Classic Holmes Map". In: *Archives of Ophthalmology* 109.6, pp. 816–824.

Huang, Mingxia and Martin Chalfie (1994). "Gene interactions affecting mechanosensory transduction in Caenorhabditis elegans". In: *Nature* 367.6462, pp. 467–470.

Huang, Yao-Shen et al. (2020). "Sonogenetic Modulation of Cellular Activities Using an Engineered Auditory-Sensing Protein". In:

Hubel, D. H. and T. N. Wiesel (1962). "Receptive fields, binocular interaction and functional architecture in the cat's visual cortex". In: *The Journal of Physiology* 160.1, pp. 106–154.

Hudry, Eloise and Luk H Vandenberghe (2019). "Therapeutic AAV Gene Transfer to the Nervous System: A Clinical Reality". In: *Neuron* 101, pp. 839–862.

Ibsen, Stuart, Ada Tong, Carolyn Schutt, Sadik Esener, and Sreekanth H. Chalasani (2015). "Sonogenetics is a non-invasive approach to activating neurons in Caenorhabditis elegans". In: *Nature Communications* 6.1, p. 8264.

Inoue, I., Y. Kobatake, and I. Tasaki (1973). "Excitability, instability and phase transitions in squid axon membrane under internal perfusion with dilute salt solutions". In: *BBA - Biomembranes* 307.3, pp. 471–477.

Jazayeri, Mehrdad, Zachary Lindbloom-Brown, and Gregory D. Horwitz (2012). "Saccadic eye movements evoked by optogenetic activation of primate V1". In: *Nature Neuroscience* 15.10, pp. 1368–1370.

Ju, Niansheng, Rundong Jiang, Stephen L. Macknik, Susana Martinez-Conde, and Shiming Tang (2018). "Long-term all-optical interrogation of cortical neurons in awake-behaving nonhuman primates". In: *PLOS Biology* 16.8. Ed. by Adam Kohn, e2005839.

Julian, F. J. and D. E. Goldman (1962). "The effects of mechanical stimulation on some electrical properties of axons". In: *The Journal of general physiology* 46.2, pp. 297–313.

Kim, Hyungmin, Alan Chiu, Stephanie D. Lee, Krisztina Fischer, and Seung-Schik Yoo (2014). "Focused Ultrasound-mediated Non-invasive Brain Stimulation: Examination of Sonication Parameters". In: *Brain Stimulation* 7.5, pp. 748–756.

Kim, Hyungmin, Michael Y. Park, Stephanie D. Lee, Wonhye Lee, Alan Chiu, and Seung Schik Yoo (2015). "Suppression of EEG visual-evoked potentials in rats through neuromodulatory focused ultrasound". In: *NeuroReport* 26.4, pp. 211–215.

Kim, Hyungmin, Seyed Javid Taghados, Krisztina Fischer, Lee So Maeng, Shinsuk Park, and Seung Schik Yoo (2012). "Noninvasive Transcranial Stimulation of Rat Abducens Nerve by Focused Ultrasound". In: *Ultrasound in Medicine and Biology* 38.9, pp. 1568–1575.

Kime, S, C Simon-Shane, Q Sabatier, F Galluppi, and R Benosman (2018). "High Temporal Sub-millisecond Time Resolution Stimulation Increases Performances of Retina Prosthetic Vision". In: *bioRxiv*, p. 442269.

Kime, Sihem, Francesco Galluppi, Xavier Lagorce, Ryad B. Benosman, and Jean Lorenceau (2016). "Psychophysical Assessment of Perceptual Performance with Varying Display Frame Rates". In: *Journal of Display Technology* 12.11, pp. 1372–1382.

King, Randy L., Julian R. Brown, William T. Newsome, and Kim Butts Pauly (2013). "Effective parameters for ultrasound-induced in vivo neurostimulation". In: *Ultrasound in Medicine and Biology* 39.2, pp. 312–331.

Krasovitski, Boris, Victor Frenkel, Shy Shoham, and Eitan Kimmel (2011). "Intramembrane cavitation as a unifying mechanism for ultrasound-induced bioeffects". In: *Proceedings of the National Academy of Sciences of the United States of America* 108.8, pp. 3258–3263.

Kubanek, Jan (2018). "Neuromodulation with transcranial focused ultrasound". In: *Neurosurgical Focus* 44.2, E14.

Kubanek, Jan, Jingyi Shi, Jon Marsh, Di Chen, Cheri Deng, and Jianmin Cui (2016). "Ultrasound modulates ion channel currents". In: *Scientific Reports* 6.1, p. 24170.

Kung, Ching (2005). "A possible unifying principle for mechanosensation". In: *Nature* 436.7051, pp. 647–654.

Kung, Ching, Boris Martinac, and Sergei Sukharev (2010). "Mechanosensitive Channels in Microbes". In: *Annual Review of Microbiology* 64.1, pp. 313–329.

Kwom, Young H., John H. Fingprt, Markus H. Kuehn, and Wallace L.M. Alward (2009). *Primary open-angle glaucoma*.

Lagali, Pamela S., David Balya, Gautam B. Awatramani, Thomas A. Münch, Douglas S. Kim, Volker Busskamp, Constance L. Cepko, and Botond Roska (2008). "Light-activated channels

targeted to ON bipolar cells restore visual function in retinal degeneration". In: *Nature Neuroscience* 11.6, pp. 667–675.

Larsson, Matz L. (2015). "Binocular vision, the optic chiasm, and their associations with vertebrate motor behavior". In: *Frontiers in Ecology and Evolution* 3.JUL.

Lebedev, Mikhail A. and Miguel A.L. Nicolelis (2017). "Brain-machine interfaces: From basic science to neuroprostheses and neurorehabilitation". In: *Physiological Reviews* 97.2, pp. 767–837.

Lee, J. C. F., J. C. Callaway, and R. C. Foehring (2005). "Effects of Temperature on Calcium Transients and Ca ²⁺ -Dependent Afterhyperpolarizations in Neocortical Pyramidal Neurons". In: *Journal of Neurophysiology* 93.4, pp. 2012–2020.

Lee, Wonhye, Phillip Croce, Ryan W. Margolin, Amanda Cammalleri, Kyungho Yoon, and Seung Schik Yoo (2018). "Transcranial focused ultrasound stimulation of motor cortical areas in freely-moving awake rats". In: *BMC Neuroscience* 19.1, p. 57.

Lee, Wonhye, Hyungmin Kim, Yujin Jung, In Uk Song, Yong An Chung, and Seung Schik Yoo (2015). "Image-guided transcranial focused ultrasound stimulates human primary somatosensory cortex". In: *Scientific Reports* 5.1, pp. 1–10.

Lee, Wonhye, Stephanie D. Lee, Michael Y. Park, Lori Foley, Erin Purcell-Estabrook, Hyungmin Kim, Krisztina Fischer, Lee-So Maeng, and Seung-Schik Yoo (2016). "Image-Guided Focused Ultrasound-Mediated Regional Brain Stimulation in Sheep". In: *Ultrasound in Medicine & Biology* 42.2, pp. 459–470.

Legon, Wynn, Priya Bansal, Roman Tyshynsky, Leo Ai, and Jerel K. Mueller (2018). "Transcranial focused ultrasound neuromodulation of the human primary motor cortex". In: *Scientific Reports* 8.1, p. 10007.

Legon, Wynn, Tomokazu F Sato, Alexander Opitz, Jerel Mueller, Aaron Barbour, Amanda Williams, and William J Tyler (2014). "Transcranial focused ultrasound modulates the activity of primary somatosensory cortex in humans". In: *Nature Neuroscience* 17.2, pp. 322–329.

Lesage, Florian, Cécile Terrenoire, Georges Romey, and Michel Lazdunski (2000). "Human TREK2, a 2P Domain Mechano-sensitive K+ Channel with Multiple Regulations by Polyunsaturated Fatty Acids, Lysophospholipids, and Gs, Gi, and

Gq Protein-coupled Receptors". In: *Journal of Biological Chemistry* 275.37, pp. 28398–28405.

Lewis, Amanda H. and Jörg Grandl (2015). "Mechanical sensitivity of Piezo1 ion channels can be tuned by cellular membrane tension". In: *eLife* 4.December2015, pp. 1–17.

Li, Fenfang, Chen Yang, Fang Yuan, Defei Liao, Thomas Li, Farshid Guilak, and Pei Zhong (2018). "Dynamics and mechanisms of intracellular calcium waves elicited by tandem bubble-induced jetting flow". In: *Proceedings of the National Academy of Sciences of the United States of America* 115.3, E353–E362.

Li, Guo Feng et al. (2016). "Improved Anatomical Specificity of Non-invasive Neuro-stimulation by High Frequency (5 MHz) Ultrasound". In: *Scientific Reports* 6, pp. 1–11.

Loo, Colleen K. and Philip B. Mitchell (2005). *A review of the efficacy of transcranial magnetic stimulation (TMS) treatment for depression, and current and future strategies to optimize efficacy*.

Lund, Jennifer S. (1973). "Organization of neurons in the visual cortex, area 17, of the monkey (Macaca mulatta)". In: *Journal of Comparative Neurology* 147.4, pp. 455–495.

Maingret, François, Michel Fosset, Florian Lesage, Michel Lazdunski, and Eric Honoré (1999). "TRAAK is a mammalian neuronal mechano-gated K+ channel". In: *Journal of Biological Chemistry* 274.3, pp. 1381–1387.

Maresca, David, Anupama Lakshmanan, Mohamad Abedi, Avinoam Bar-Zion, Arash Farhadi, George J. Lu, Jerzy O. Szablowski, Di Wu, Sangjin Yoo, and Mikhail G. Shapiro (2018). "Biomolecular Ultrasound and Sonogenetics". In: *Annual Review of Chemical and Biomolecular Engineering* 9.1, pp. 229–252.

Marg, E. and G. Dierssen (1965). "Reported visual percepts from stimulation of the human brain with microelectrodes during therapeutic surgery." In: *Confinia neurologica* 26.2, pp. 57–75.

Masland, Richard H (2012). "The neuronal organization of the retina." In: *Neuron* 76.2, pp. 266–80.

Maurer, Joshua A. and Dennis A. Dougherty (2003). "Generation and evaluation of a large mutational library from the Escherichia coli mechanosensitive channel of large conductance, MscL. Implications for channel gating and evolutionary design". In: *Journal of Biological Chemistry* 278.23, pp. 21076–21082.

Mazoue, H, P Chauchard, and R G Busnel (1953). "[Nervous excitation with high frequency ultrasonics]." In: *Journal de physiologie* 45.1, pp. 179–82.

McAlinden, Niall et al. (2019). "Multisite microLED optrode array for neural interfacing". In: *Neurophotonics* 6.03, p. 1.

Mehić, Edin, Julia M. Xu, Connor J. Caler, Nathaniel K. Coulson, Chet T. Moritz, and Pierre D. Mourad (2014). "Increased anatomical specificity of neuromodulation via modulated focused ultrasound". In: *PLoS ONE* 9.2.

Menz, M. D., O. Oralkan, P. T. Khuri-Yakub, and S. A. Baccus (2013). "Precise Neural Stimulation in the Retina Using Focused Ultrasound". In: *Journal of Neuroscience* 33.10, pp. 4550–4560.

Menz, Mike, Patrick Ye, Kamyar Firouzi, Kim Butts Pauly, Pierre Khuri-Yakub, and Stephen Baccus (2017). "Physical mechanisms of ultrasonic neurostimulation in the in vitro retina". In: *bioRxiv*.

Morris, Catherine E. (2012). "Why are so many ion channels mechanosensitive?" In: *Cell Physiology Source Book*. Elsevier Inc., pp. 493–505.

Nash, Benjamin M, Dale C Wright, John R Grigg, Bruce Bennetts, and Robyn V Jamieson (2015). "Retinal dystrophies, genomic applications in diagnosis and prospects for therapy." In: *Translational pediatrics* 4.2, pp. 139–13963.

Newman, Eric A. and Kathleen R. Zahs (1998). "Modulation of neuronal activity by glial cells in the retina". In: *Journal of Neuroscience* 18.11, pp. 4022–4028.

Nitsche, Michael A. et al. (2008). *Transcranial direct current stimulation: State of the art 2008*.

Nyborg, Wesley Le Mars (1965). "Acoustic Streaming". In: *Physical Acoustics*. Vol. 2. Academic Press, pp. 265–331.

O'Brien Jr., William D (2007). "Ultrasound-biophysics mechanisms." In: *Progress in biophysics and molecular biology* 93.1-3, pp. 212–55.

O'Brien, W R and D S Ellis (1999). "Evaluation of the unscanned soft-tissue thermal index." In: *IEEE transactions on ultrasonics, ferroelectrics, and frequency control* 46.6, pp. 1459–76.

Oga, Tomofumi, Tsuguhisa Okamoto, and Ichiro Fujita (2016). "Basal dendrites of layer-III pyramidal neurons do not scale with changes in cortical magnification factor in macaque primary visual cortex". In: *Frontiers in Neural Circuits* 10.SEP.

Owen, Scott F., Max H. Liu, and Anatol C. Kreitzer (2019). "Thermal constraints on in vivo optogenetic manipulations". In: *Nature Neuroscience* 22.7, pp. 1061–1065.

Palanker, Daniel, Yannick Le Mer, Saddek Mohand-Said, Mahiul Muqit, and Jose A. Sahel (2020). "Photovoltaic Restoration of Central Vision in Atrophic Age-Related Macular Degeneration". In: *Ophthalmology*. Vol. 127. 8. Elsevier Inc., pp. 1097–1104.

Panametrics-NDT™ (2006). *Ultrasonic transducers technical notes*.

Panetsos, Fivos, Abel Sanchez-Jimenez, Elena Diaz De Cerio, Idoia Diaz-Guemes, and Francisco M. Sanchez (2011). "Consistent phosphenes generated by electrical microstimulation of the visual thalamus. An experimental approach for thalamic visual neuroprostheses". In: *Frontiers in Neuroscience* JUL.

Parihar, Raminder, Ron Alterman, Efstathios Papavassiliou, Daniel Tarsy, and Ludy C Shih (2015). "Comparison of VIM and STN DBS for Parkinsonian Resting and Postural/Action Tremor." In: *Tremor and other hyperkinetic movements (New York, N.Y.)* 5, p. 321.

Pasquinelli, Cristina, Lars G Hanson, Hartwig R Siebner, Hyunjoo J Lee, and Axel Thielscher (2019). "Safety of transcranial focused ultrasound stimulation: A systematic review of the state of knowledge from both human and animal studies". In: *Brain Stimulation* 12, pp. 1367–1380.

Patel, A. J., E. Honoré, F. Maingret, F Lesage, M. Fink, F. Duprat, and M. Lazdunski (1998). "A mammalian two pore domain mechano-gated S-like K+ channel." In: *Embo J.* 17.15, pp. 4283–4290.

Pearson, R. A. et al. (2016). "Donor and host photoreceptors engage in material transfer following transplantation of postmitotic photoreceptor precursors". In: *Nature Communications* 7.1, pp. 1–15.

Perlmutter, Joel S. and Jonathan W. Mink (2006). "DEEP BRAIN STIMULATION". In: *Annual Review of Neuroscience* 29.1, pp. 229–257.

Perozo, Eduardo (2006). *Gating prokaryotic mechanosensitive channels*.

Perozo, Eduardo, Anna Kloda, D. Marien Cortes, and Boris Martinac (2002). "Physical principles underlying the transduction of bilayer deformation forces during mechanosensitive channel gating". In: *Nature Structural Biology* 9.9, pp. 696–703.

Petrov, Alexander G. (2002). *Flexoelectricity of model and living membranes*.

Pinton, Gianmarco, Jean Francois Aubry, Mathias Fink, and Mickael Tanter (2012). "Numerical prediction of frequency dependent 3D maps of mechanical index thresholds in ultrasonic brain therapy". In: *Medical Physics* 39.1, pp. 455–467.

Plaksin, Michael, Shy Shoham, and Eitan Kimmel (2014). "Intramembrane cavitation as a predictive bio-piezoelectric mechanism for ultrasonic brain stimulation". In: *Physical Review X* 4.1, pp. 1–28.

Polanía, Rafael, Michael A. Nitsche, and Christian C. Ruff (2018). *Studying and modifying brain function with non-invasive brain stimulation*.

Polyak, Stephen T. (1957). *The Vertebrate Visual System*.

Powell, Sara Kathleen, Ricardo Rivera-Soto, and Steven J. Gray (2015). "Viral expression cassette elements to enhance transgene target specificity and expression in gene therapy". In: *Discovery Medicine* 19.102, pp. 49–57.

Prasad, Sashank and Steven L. Galetta (2011). *Anatomy and physiology of the afferent visual system*. Vol. 102. Handb Clin Neurol, pp. 3–19.

Prieto, Martin Loynaz, Kamyar Firouzi, Butrus T. Khuri-Yakub, and Merritt Maduke (2018). "Activation of Piezo1 but Not NaV1.2 Channels by Ultrasound at 43MHz". In: *Ultrasound in Medicine and Biology* 44.6, pp. 1217–1232.

Prieto, Martin Loynaz, Ömer Oralkan, Butrus T. Khuri-Yakub, and Merritt C. Maduke (2013). "Dynamic Response of Model Lipid Membranes to Ultrasonic Radiation Force". In: *PLoS ONE* 8.10, p. 77115.

Purves, Dale, George J Augustine, David Fitzpatrick, Lawrence C Katz, Anthony-Samuel LaMantia, James O McNamara, and S Mark Williams (2001). "Phototransduction". In:

Qiu, Zhihai, Shashwati Kala, Jinghui Guo, Minyi Yang, and Haoru Wang (2020). "Targeted Neurostimulation in Mouse Brains with Non-invasive Ultrasound". In:

Qiu, Zhihai et al. (2019). "The Mechanosensitive Ion Channel Piezo1 Significantly Mediates In Vitro Ultrasonic Stimulation of Neurons". In: *iScience* 21, pp. 448–457.

Rabinowitz, Joseph E., Fabienne Rolling, Chengwen Li, Hervè Conrath, Weidong Xiao, Xiao Xiao, and R. Jude Samulski (2002). "Cross-Packaging of a Single Adeno-Associated Virus (AAV) Type 2 Vector Genome into Multiple AAV Serotypes

Enables Transduction with Broad Specificity". In: *Journal of Virology* 76.2, pp. 791–801.

Rodieck, Robert W. (1998). *The First Steps in Seeing*. Vol. 1.

Rosholm, Kadla R., Matthew A. B. Baker, Pietro Ridone, Yoshitaka Nakayama, Paul R. Rohde, Luis G. Cuello, Lawrence K. Lee, and Boris Martinac (2017). "Activation of the mechanosensitive ion channel MscL by mechanical stimulation of supported Droplet-Hydrogel bilayers". In: *Scientific Reports* 7.1, p. 45180.

Roska, Botond and José Alain Sahel (2018). "Restoring vision". In: *Nature* 557.7705, pp. 359–367.

Rudenko, O. V., A. P. Sarvazyan, and S. Y. Emelianov (1996). "Acoustic radiation force and streaming induced by focused nonlinear ultrasound in a dissipative medium". In: *The Journal of the Acoustical Society of America* 99.5, pp. 2791–2798.

Sato, Tomokazu, Mikhail G. Shapiro, and Doris Y. Tsao (2018). "Ultrasonic Neuromodulation Causes Widespread Cortical Activation via an Indirect Auditory Mechanism". In: *Neuron* 98.5, 1031–1041.e5.

Schön, Christian, Martin Biel, and Stylianos Michalakis (2015). "Retinal gene delivery by adeno-associated virus (AAV) vectors: Strategies and applications". In: *European Journal of Pharmaceutics and Biopharmaceutics* 95, pp. 343–352.

Schultze, Max (1886). "Zur Anatomie und Physiologie der Spinalganglien". In: *Archiv für mikroskopische Anatomie* 2.1, pp. 175–286.

Schwartz, Steven D. et al. (2015). "Human embryonic stem cell-derived retinal pigment epithelium in patients with age-related macular degeneration and Stargardt's macular dystrophy: Follow-up of two open-label phase 1/2 studies". In: *The Lancet* 385.9967, pp. 509–516.

Shapiro, Mikhail G., Kazuaki Homma, Sebastian Villarreal, Claus Peter Richter, and Francisco Bezanilla (2012). "Infrared light excites cells by changing their electrical capacitance". In: *Nature Communications* 3.1, pp. 1–11.

Solomon, Samuel G. and Peter Lennie (2007). *The machinery of colour vision*.

Soloperto, Alessandro, Anna Boccaccio, Andrea Contestabile, Monica Moroni, Grace I. Hallinan, Gemma Palazzolo, John Chad, Katrin Deinhardt, Dario Carugo, and Francesco Difato (2018). "Mechano-sensitization of mammalian neuronal networks through expression of the bacterial large-conductance

mechanosensitive ion channel". In: *Journal of Cell Science* 131.5, jcs210393.

Spyropoulos, C. S. (1957). "Response of single nerve fibers at different hydrostatic pressures". In: *The American journal of physiology* 189.1, pp. 214–218.

Strotmann, Rainer, Christian Harteneck, Karin Nunnenmacher, Günter Schultz, and Tim D. Plant (2000). "OTRPC4, a nonselective cation channel that confers sensivity to extracellular osmolarity". In: *Nature Cell Biology* 2.10, pp. 695–702.

Sukharev (2001). "The gating mechanism of the large mechanosensitive channel MscL". In:

Sukharev, Sergei 1, Boris Martinac, Vadim Y Arshavsky, and Ching Kung (1993). *Two Types of Mechanosensitive Channels in the Escherichia coli Cell Envelope: Solubilization and Functional Reconstitution*. Tech. rep., pp. 177–183.

Sukharev, Sergei I., Paul Blount, Boris Martinac, Frederick R. Blattner, and Ching Kung (1994). "A large-conductance mechanosensitive channel in E. coli encoded by mscL alone". In: *Nature* 368.6468, pp. 265–268.

Sukharev, Sergei I., Paul Blount, Boris Martinac, Kung, and Ching (1997). " MECHANOSENSITIVE CHANNELS OF ESCHERICHIA COLI :The MscL Gene, Protein, and Activities ". In: *Annual Review of Physiology* 59.1, pp. 633–657.

Sukharev, Sergei I., Wade J. Sigurdson, Ching Kung, and Frederick Sachs (1999). "Energetic and spatial parameters for gating of the bacterial large conductance mechanosensitive channel, MscL". In: *Journal of General Physiology* 113.4, pp. 525–539.

Sukharev, Sergei (2002). "Purification of the small mechanosensitive channel of Escherichia coli (MscS): The subunit structure, conduction, and gating characteristics in liposomes". In: *Biophysical Journal* 83.1, pp. 290–298.

Sukharev, Sergei and David P. Corey (2004). *Mechanosensitive channels: multiplicity of families and gating paradigms.*

Summaries of Genes and Loci Causing Retinal Diseases, https://sph.uth.edu/retnet/sum-dis.htm.

Szabo, Thomas L. (2004). *Diagnostic Ultrasound Imaging: Inside Out: Second Edition*. Elsevier Inc., pp. 1–549.

Taylor, Graham J., Frederick A. Heberle, Jason S. Seinfeld, John Katsaras, C. Patrick Collier, and Stephen A. Sarles (2017). "Capacitive Detection of Low-Enthalpy, Higher-Order Phase Transitions in Synthetic and Natural Composition Lipid Membranes". In: *Langmuir* 33.38, pp. 10016–10026.

Tehovnik, E. J., W. M. Slocum, C. E. Carvey, and P. H. Schiller (2005). *Phosphene induction and the generation of saccadic eye movements by striate cortex*.

Tehovnik, Edward J. and Warren M. Slocum (2007). *Phosphene induction by microstimulation of macaque V1*.

Tong, Frank (2003). "Cognitive neuroscience: Primary visual cortex and visual awareness". In: *Nature Reviews Neuroscience* 4.3, pp. 219–229.

Tovée, Martin J. (2008). *An introduction to the visual system*. Cambridge University Press.

Trobe, D. Jonathan (2001). *The Neurology of Vision*. Oxford University Press.

Troyk, Philip R. (2017). "The Intracortical Visual Prosthesis Project". In: *Artificial Vision*. Springer International Publishing, pp. 203–214.

Tufail, Yusuf, Alexei Matyushov, Nathan Baldwin, Monica L. Tauchmann, Joseph Georges, Anna Yoshihiro, Stephen I. Helms Tillery, and William J. Tyler (2010). "Transcranial Pulsed Ultrasound Stimulates Intact Brain Circuits". In: *Neuron* 66.5, pp. 681–694.

Tufail, Yusuf, Anna Yoshihiro, Sandipan Pati, Monica M. Li, and William J. Tyler (2011). "Ultrasonic neuromodulation by brain stimulation with transcranial ultrasound". In: *Nature Protocols* 6.9, pp. 1453–1470.

Tyler, William J. (2011). "Noninvasive neuromodulation with ultrasound? A continuum mechanics hypothesis". In: *Neuroscientist* 17.1, pp. 25–36.

Tyler, William J., Yusuf Tufail, Michael Finsterwald, Monica L. Tauchmann, Emily J. Olson, and Cassondra Majestic (2008). "Remote Excitation of Neuronal Circuits Using Low-Intensity, Low-Frequency Ultrasound". In: *PLoS ONE* 3.10. Ed. by Hiromu Tanimoto, e3511.

Velling, V. A. and S. P. Shklyaruk (1988). "Modulation of the functional state of the brain with the aid of focused ultrasonic action". In: *Neuroscience and Behavioral Physiology* 18.5, pp. 369–375.

Verhagen, Lennart et al. (2019). "Offline impact of transcranial focused ultrasound on cortical activation in primates". In: *eLife* 8, pp. 1–28.

Watakabe, Akiya, Masanari Ohtsuka, Masaharu Kinoshita, Masafumi Takaji, Kaoru Isa, Hiroaki Mizukami, Keiya Ozawa, Tadashi Isa, and Tetsuo Yamamori (2015). "Comparative analyses of adeno-associated viral vector serotypes 1, 2, 5,

8 and 9 in marmoset, mouse and macaque cerebral cortex". In: *Neuroscience Research* 93, pp. 144–157.

Welkozitz, W. and W. J. Fry (1956). "Effects of High Intensity Sound on Electrical Conduction in Muscle". In: *Journal of cellular and comparative physiology* 48.3, pp. 435–457.

Woo, Joseph (2002). *A short history of the development of ultrasound in obstetrics and gynecology*. Tech. rep., pp. 1–25.

Wu, Chun Yao, Ching Hsiang Fan, Nai Hua Chiu, Yi Ju Ho, Yu Chun Lin, and Chih Kuang Yeh (2020). "Targeted delivery of engineered auditory sensing protein for ultrasound neuromodulation in the brain". In: *Theranostics* 10.8, pp. 3546–3561.

Wunderlich, B., C. Leirer, A. L. Idzko, U. F. Keyser, A. Wixforth, V. M. Myles, T. Heimburg, and M. F. Schneider (2009). "Phase-state dependent current fluctuations in pure lipid membranes". In: *Biophysical Journal* 96.11, pp. 4592–4597.

Yang, Pai Feng, M. Anthony Phipps, Allen T. Newton, Vandiver Chaplin, John C. Gore, Charles F. Caskey, and Li Min Chen (2018). "Neuromodulation of sensory networks in monkey brain by focused ultrasound with MRI guidance and detection". In: *Scientific Reports* 8.1, pp. 1–9.

Yang, Po Song, Hyungmin Kim, Wonhye Lee, Mark Bohlke, Shinsuk Park, Timothy J. Maher, and Seung-Schik Yoo (2012). "Transcranial Focused Ultrasound to the Thalamus Is Associated with Reduced Extracellular GABA Levels in Rats". In: *Neuropsychobiology* 65.3, pp. 153–160.

Yang, Yaoheng et al. (2020). "Sonogenetics for noninvasive and cellular-level neuromodulation in rodent brain". In: *bioRxiv*, p. 2020.01.28.919910.

Ye, Jia et al. (2018). "Ultrasonic Control of Neural Activity through Activation of the Mechanosensitive Channel MscL". In: *Nano Letters* 18.7, pp. 4148–4155.

Ye, Patrick Peiyong, Julian R. Brown, and Kim Butts Pauly (2016). "Frequency dependence of ultrasound neurostimulation in the mouse brain". In: *Ultrasound in Medicine and Biology* 42.7, pp. 1512–1530.

Yoo, Seung Schik, Alexander Bystritsky, Jong Hwan Lee, Yongzhi Zhang, Krisztina Fischer, Byoung Kyong Min, Nathan J. McDannold, Alvaro Pascual-Leone, and Ferenc A. Jolesz (2011). "Focused ultrasound modulates region-specific brain activity". In: *NeuroImage* 56.3, pp. 1267–1275.

Yoshimura, Kenjiro, Ann Batiza, Matt Schroeder, Paul Blount, and Ching Kung (1999). "Hydrophilicity of a Single Residue

within MscL Correlates with Increased Channel Mechanosensitivity". In: *Biophysical Journal* 77.4, pp. 1960–1972.

Younan, Youliana, Thomas Deffieux, Benoit Larrat, Mathias Fink, Mickael Tanter, and Jean Francois Aubry (2013). "Influence of the pressure field distribution in transcranial ultrasonic neurostimulation". In: *Medical Physics* 40.8, pp. 1–10.

Yue, Lan, James D. Weiland, Botond Roska, and Mark S. Humayun (2016). *Retinal stimulation strategies to restore vision: Fundamentals and systems*.

Zagzebski, James A. (1996). *Essencials of Ultrasound Physics*, p. 220.

Zhang, Xu Feng, Jun Chen, Connie R. Faltynek, Robert B. Moreland, and Torben R. Neelands (2008). "Transient receptor potential A1 mediates an osmotically activated ion channel". In: *European Journal of Neuroscience* 27.3, pp. 605–611.